Identification of Cellular Interaction Partners of Human Papillomavirus Minor Capsid Protein L2

Dissertation

Submitted to the Combined Faculties for
the Natural Sciences and for Mathematics of the
Ruperto-Carola University of Heidelberg, Germany

for the degree of
Doctor of Natural Sciences

presented by

Caroline Odenwald, M.Sc.

August 2015

Dissertation

submitted to the Combined Faculties for

the Natural Sciences and for Mathematics of the

Ruperto-Carola University of Heidelberg, Germany

for the degree of

Doctor of Natural Sciences

presented by

Caroline Odenwald, M.SC.

Born in Heidelberg, Germany

Oral-examination:: .....

Identification of Cellular Interaction Partners of Human Papillomavirus Minor Capsid Protein L2

Referees: **Prof. Dr. Martin Müller**

PD Dr. Dirk Nettelbeck

Thesis Declaration

Declaration according to §8 of the doctoral degree regulations

I hereby declare that I have written the submitted dissertation independently and have not used other sources and materials than those particularly indicated.

Further, I declare that I have not applied to be examined at any other institution, nor have I presented this dissertation to any other faculty, nor have I used this dissertation in any form in another examination.

Heidelberg, Caroline Odenwald

Acknowledgments

I would like to express my gratitude to all of those who supported me in any conceivable way during my time as a PhD student.

Above all I would like to thank Prof. Dr. Martin Müller for giving me the opportunity to accomplish my PhD thesis in his lab and for providing this very interesting and challenging project. Further I would like to thank Prof. Dr. Müller for the excellent supervision and always providing scientific input and advice.

I thank PD Dr. Dirk Nettelbeck for being my second examiner and his support and scientific advice during my TAC meetings.

I would also like to thank PD Dr. Suat Özbek and Dr. Steeve Boulant for agreeing to participate in my thesis evaluation committee.

I am thankful to Dr. Dirk Grimm who joined my TAC committee and always participated with good scientific discussion and advice.

Special thanks, also goes to Dr. Damir Krunic who supported me a lot, teaching me how to handle the fluorescence microscopes and always being willing to help with all the questions and problems I had. Furthermore I would like to thank Dr. Martina Schnölzer and Dr. Tore Kempf for the MS analysis of my samples and the supporting advice on the sample preparation.

I like to thank all current and former lab members of F035 for the nice working atmosphere, the helpful discussions and their unconfined readiness to help with every problem and also mental support in hard times. In this respect special thanks goes to Dr. Ivonne Rubio, Dr. Anna Sacher, Dr. Lis Ribeiro, Dr. Frank Burkart, Dr. Somayeh Pouyanfard, Qingxin Chen, Xueer Zao, Liesa-Marie Schreiber, Katharina Henrich, Michael Bartolff-Kopp, Federica Savini, Irene Daverio, Almira Henic, Tobias Schulze. The time in the lab was a great experience and I became acquainted with a lot of very nice people and new friend.

In particular, I like to thank Dr. Hanna Seitz who supported me through my whole PhD with very good scientific input and help whenever it was needed but rather became a very good and close friend. I am more than grateful that I had the privilege to meet her and I am very happy that our friendship persists even across the continents.

I also want to give a special thanks to Petra Galmbacher who was always willing to support me in the lab and was always a good interlocutor concerning scientific but also personal topics. She was a really great and entertaining bench neighbor and I will for sure miss the time standing next to her.

I am grateful to all the colleagues on the 2nd floor of the ATV for all the kindness, support, scientific discussion and valuable input in and outside of the Monday Seminars over the last years. In this respect a special thanks goes to the assi room crew, Dr. Angelika Michel, Dr. Daniela Höfler, Lea Schoeder, Juliane Schröter, Dr. Axel Szabowski. I will really miss the time with you, especially the great conversations about every conceivable topic concerning science, future or whatever was worth to discuss.

I like to thank Madeleine Sporleder, Susanne Latzko and Diana Sandel for always having an open ear and becoming really good friends.

I want to express gratitude and deepest respect for my parents, Gisela and Hans-Jürgen Odenwald for the continuous support and appreciation of my work but rather for the fact that they are always there being the greatest support I can imagine throughout my life.

My sister and her husband, Katrin and Christoph Teusch, I want to thank for being my best and most trusted friends. I am really thankful for them being my “rock in the surf” and that I can always count on them. Additionally, I want to thank my two gorgeous nieces, Clara Sophie and Charlotte Marie, which I love more than I could have ever expected, for giving me the necessary distraction whenever I saw them.

My friends I thank for their support and consideration, especially during the time of writing and for not being offended by never-returned phone calls. I am grateful to have friends like this, always willing to listen to my problems and concerns but also participating in the joyful moments making my life much better at all times.

Finally, I like to thank everybody who supported me in the execution of my PhD and thus accounted for the success of this thesis.

Table of Contents

Summary

The human papillomavirus (HPV) belongs to the family of *Papillomaviridae* with more than 200 members, including HPVs but also papillomaviruses (PV) infecting for example cattle or rodents. Due to the causative association of HPV infection with the development of cervical cancer intensive investigation on HPV has been conducted over the last decades. Therefore, many aspects on the viral structure, infection as well as the transforming properties especially of the high risk HPV types have already been deciphered. In the course of these investigations, the HPV minor capsid protein L2 has been identified as an important player in the establishment of viral infection. Even though, the protein is dispensable for capsid formation, it has been demonstrated to have several functions crucial for e.g. DNA encapsidation, viral entry and the delivery of the viral genome to the host cell nucleus. However, the exact function of L2 during some of these processes is still unknown and under continuous investigation. In this context, many functional domains of the L2 protein have been identified especially in the highly conserved N-terminus of the protein however the function of the remaining parts is still unrevealed. Regarding the importance of the L2 protein for viral infection further investigation on potential functions still represents a promising field of research.

The objective of this thesis was the identification of novel cellular interaction partners of L2. To this end, three independent experimental approaches were established, allowing the co-purification of interacting proteins. A) Tandem affinity purification (TAP) a two-step purification method based on the overexpression of HPV16 L2 as fusion protein with the TAP tag. B) Immunoprecipitation (IP) of HPV16 L2 from pseudovirus (PsV) infected cells, mimicking the natural infection pathway of HPV16. C) Peptide pull down of cellular proteins using immobilized HPV16 L2 epitopes which are targets for neutralizing antibodies. For identification of the co-purified interaction candidates the samples derived from the different experimental approaches were analyzed by mass spectrometry (MS). Based on the results, the insulin receptor substrate 4 (IRS4), the 14-3-3 zeta/delta (YWHAZ), the exportin-2 (CSE1L) as well as the calpain 2 (CAPN2) and the cullin-associated and neddylation-dissociated 1 (CAND1) proteins were selected as most promising candidates for functional studies. These five proteins were validated as L2 binding partners by Co-IP and immunofluorescence (IF) after overexpression. An inhibitory effect on HPV16 L2 PsV transduction of the downregulation of protein expression was demonstrated for IRS4, YWHAZ and CSE1L. In contrast, knockdown of CAPN2 and CAND1 had neither inhibitory nor enhancing influence on PsV transduction. While the obtained data suggests a role of IRS4, YWHAZ and CSE1L during the infection process of HPV16, interaction with CAPN2 and CAND1, respectively is supposed to be important in a different step of the viral life cycle.

Zusammenfassung

Der Humane Papillomvirus (HPV) gehört zur Familie der *Papillomaviridae*, die mehr als 200 verschiedene Typen umfasst. Darunter befinden sich neben den HPV unter anderem auch Papillomviren (PV), die Rinder oder Nagetiere infizieren. Auf Grund der Assoziation zwischen HPV Infektion und der Entstehung von Zervixkarzinomen fand in den letzten Jahrzehnten eine intensive HPV Forschung statt. Viele Aspekte, wie die Struktur, der Infektionsvorgang und der Mechanismus der Zelltransformation durch HPV wurden dadurch aufgedeckt. In diesem Zusammenhang wurde auch gezeigt, dass das L2 Strukturprotein wichtige Funktionen bei verschiedenen Schritten des viralen Lebenszyklus erfüllt. Obwohl das L2 Protein für den Aufbau des Kapsids nicht essentiell ist, wurde eine wichtige Funktion bei der Verpackung des viralen Genoms, dem Eintritt in die Zelle, sowie dem Transport durch die Zelle nachgewiesen. Die Mechansimen wurden jedoch noch nicht im Detail erforscht. Es konnten aber schon diverse funktionelle Domänen des L2 Proteins identifiziert werden, speziell solche, die sich im konservierten Amino-Terminus befinden.

Das Ziel der vorliegenden Arbeit war es daher neue, zelluläre Interaktionspartner von L2 zu identifizieren, um dadurch weiteren Einblick in die Funktionen des Proteins zu gewinnen. Um dieses Ziel zu erreichen, wurden drei unabhängige Methoden etabliert. A) Die Tandem Affinitäts Reinigung (TAP), welche auf der Expression des HPV16 L2 als Fusionsprotein mit dem TAP-Tag basiert. B) Co-Immunopräzipitation von L2 aus Pseudovirus-infizierten Zellen, welche den natürlichen Infektionsverlauf von HPV nachahmt. C) Peptid-Pull-Down, bei dem HPV16 L2 Epitope immobilisiert wurden um interagierende, zelluläre Protein zu isolieren. Um die gereinigten Proteine zu identifizieren wurden die verschiedenen Proben im Massenspektrometer (MS) analysiert. Als vielversprechende Kandidaten wurden Insulin Rezeptor Substrat 4 (IRS4), 14-3-3 zeta/delta, Exportin-2 (CSE1L), sowie Calpain 2 (CAPN2) und Cullin-assoziierte und Neddylations-dissoziierte 1 (CAND1) ausgewählt. Eine Interaktion dieser fünf Proteine mit L2 konnte durch Co-IP und Immunfluoreszenz Analysen validiert werden. Des Weiteren konnte ein inhibierender Einfluss auf die Transduktion durch PsV nach Herunterregulierung der Proteinexpression für die Interaktionspartner IRS4, YWHAZ und CSE1L festgestellt werden. Für CAPN2, sowie CAND1 konnte weder eine Inhibierung noch eine Verstärkung der Transduktionseffizienz von PsV beobachtet werden. Auf Grund der vorliegenden Daten wird daher vermutet, das IRS4, YWHAZ und CSE1L womöglich eine Rolle während des Infektionsprozesses spielen, während CAPN2, sowie CAND1 möglicherweise eine andere, noch unbekannte Funktion im HPV Lebenszyklus spielen.

1. Introduction

1.1. Human Papillomavirus (HPV)

The human papillomavirus (HPV) belong to the taxonomic family of *Papillomaviridae* and represents a group of non-enveloped dsDNA viruses with a genome size of ~8kb. The *Papillomaviridae* are highly diverse, occurring in most mammals and birds. Among the family of *Papillomaviridae*, more than 200 human PV (HPV) types have been isolated and characterized so far and been divided in different genera.

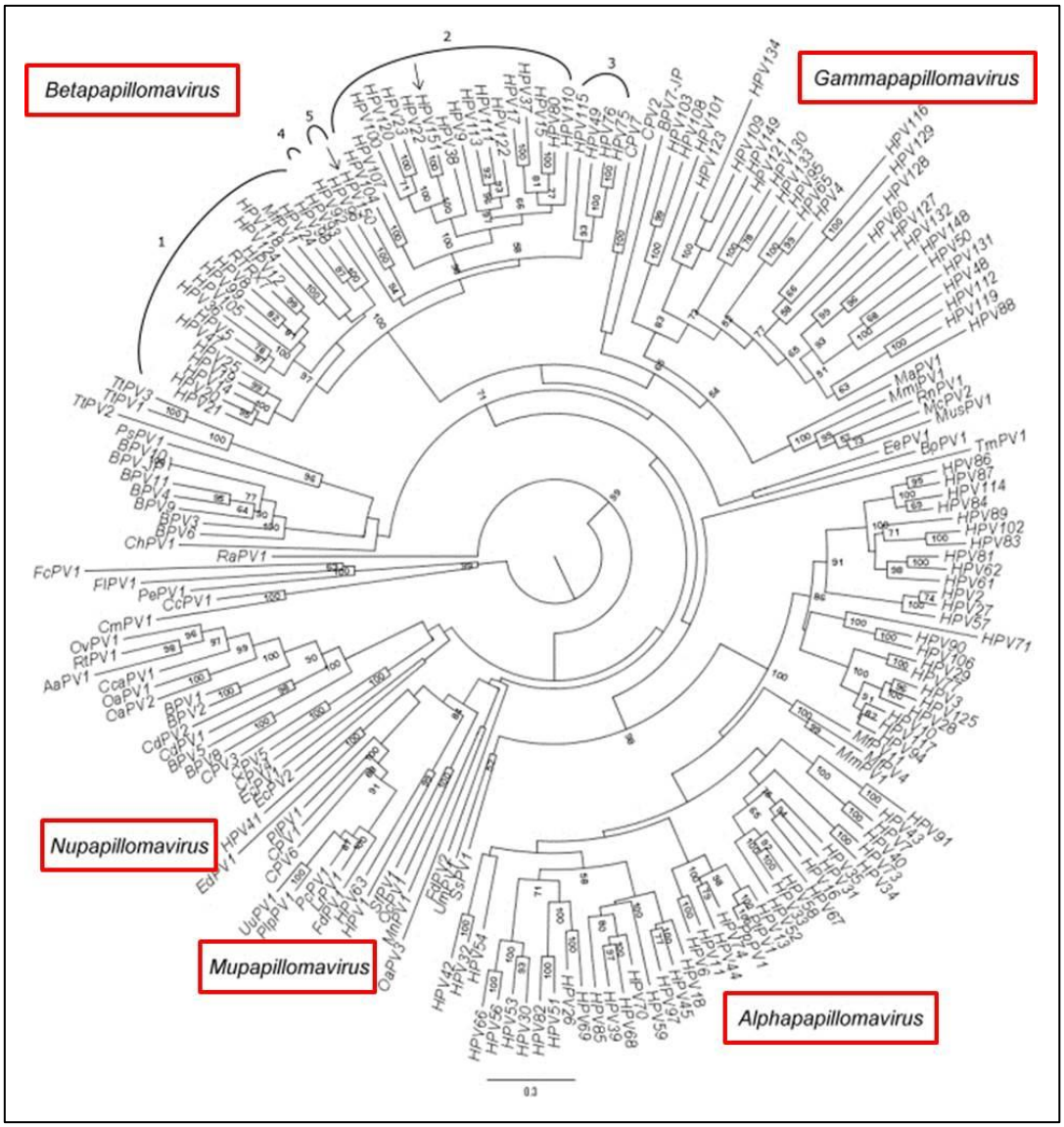

Figure 1Phylogenetic tree of 200 PV types. Classification of 200 papillomaviruses based on the homology of the L1 protein. The species of Betapapillomaviruses are indicated by the outer semi circles. Human papillomaviruses (HPV), alpha, beta, gamma, mu and nu are highlighted with red boxes. The remaining genera (pi, omicron, xi, lambda, kappa, lota, theta, eta, zeta, epsilon and delta) comprise the animal PVs are not specifically indicated. PVs are defined with the corresponding number at the associated branches [1].

HPVs of the alpha genus are known to infect mucosal but also cutaneous epithelial cells of the genital and upper respiratory tract as well as the skin. Within the alpha genus, low risk types, e.g. HPV6 and HPV11, can cause benign genital warts, whereas the high risk types (e.g. HPV16 and HPV18) are causatively associated to cervical cancer [2-4]. HPVs of the β-genus are exclusively infecting the cutaneous epithelial and are suggested to play a role in the formation of Non-Melanoma Skin Cancer (NMSC). The remaining genera (gamma, mu and nu) have been associated to the development of cutaneous papillomas and warts [5]. Until now, 17 different high risk types have been described in the alpha genus of HPV, namely HPV 16, 18, 26, 31, 33, 35, 39, 45, 51, 52, 53, 56, 59, 66, 68, 73 and 82. Within these high risk HPVs, HPV16 and HPV18 have the highest, transformation potential causing 50% and 20% of cervical cancer cases, respectively [6, 7]. Cervical cancer is a major burden worldwide and represents the fourth most frequent cancer in women (http://globocan.iarc.fr/old/FactSheets/ cancers/cervix-new.asp). During their life time most sexually active women get infected with mucosal HPV types, though most of the infections stay asymptomatic and can be cleared by the immune system. Only in a minority of infected women, the infection will progress to low and/or high grade cervical interepithelial neoplasia (CIN). However, even high grade CIN lesion can still regress and infection can be cleared whereas only a few will further progress to cervical carcinoma [8].

The HPV genome contains 8 open reading frames (ORFs), encoding for three regulatory proteins (E1, E2 and E4), two structural proteins (L1 and L2) and three oncoproteins (E5, E6 and E7), which are regulated by the long control region (LCR), located between the ORFs L1 and E6 [9].

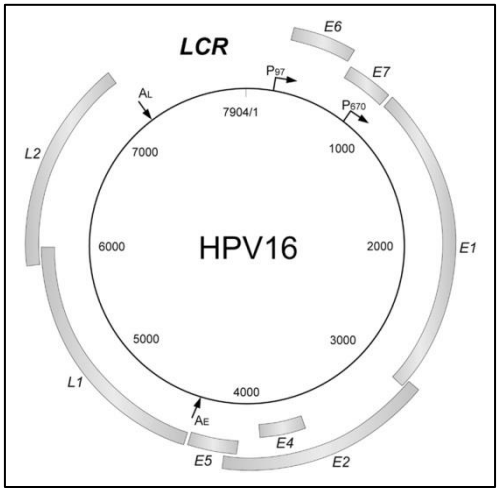

Figure 2 Organization of the HPV16 genome. HPV16 has a genome size of about 8kb and contains 8 open reading frames (ORF). It encodes for three regulatory proteins, E1 and E2 controlling for example transcription of viral genes and genome amplification and three structural proteins L1, L2 and E4. L1 and L2 are essential for capsid assembly and encapsidation of the viral genome. Moreover, the genome contains three oncoproteins, E5, E6 and E7 which play a major role during viral infection and cancer progression of the infected cells. Figure adopted from [10].

HPV-driven cervical cancer is characterized by a high expression level of the oncoproteins E6 and E7 as well as integration of the episomal HPV genome into the host genome [11]. It has been demonstrated that E6 and E7 play a major role in the development of HPV associated cancer, since they are directly involved in the transformation process. The E6 protein targets p53, a transcription factor regulating cell cycle arrest and apoptosis, for proteasomal degradation [12, 13]. And E7 regulates cell cycle division by binding to hypo-phosphorylated pRB [14, 15]. Binding of E7 with pRB disrupts pRB-E2F interaction, leading the infected cells to progression into S-phase[16] . Therefore, high expression levels of E6 and E7 increase the chance for infected cells to progress to CIN and cervical cancer [17, 18].

1.2. The HPV Capsid

The viral DNA is encased by a non-enveloped icosahedral capsid of about 50-60nm, composed of 72 capsomers of five L1 molecules each. In general, the capsid is formed by the major capsid protein L1 while the minor capsid protein L2 is finally incorporated into the L1 capsid structure. It has been demonstrated that L1, in absence of L2, is able to spontaneously self-assemble and form virus-like particles (VLPs) with similar morphology to native virions [4, 19]. The virus-like particles are produced either by expressing L1 alone or together with L2. In both systems the capsids possess the correct size (~55nm) and density in the gradient, comparable to native virions [19].

HPV capsid structure and localization of the L2 molecules

Stabilization of the viral capsid is achieved by maturation of the previously immature and still flexible virion. In the mature capsid state, the L1 molecules are cross-linked by disulfide bonds between neighboring L1 molecules [20]. The bonds have been demonstrated to be essential for the stabilization of the viral capsid [21]. The L1 pentamers form a knobby exterior surface and the N- and C-termini of L1 form the floor between the knobs. Furthermore it has been demonstrated that flexible C-terminal arms play a major role in the formation of the disulfide bonds between neighboring pentamers. In the mature capsid, each L1 molecule participates either in disulfide-linked dimers or ring-shaped trimers [22, 23]. For capsid assembly of L1/L2 capsids, L2 translocates into the nucleus, mainly into the PML bodies, before L1 pentamers are recruited, initiating the assembly of the viral capsid [24]. It was postulated that co-expression of L1 and L2 leads to 10-100fold higher capsid yields compared to L1 only expression, leading to the suggestion that L2 might also be involved in capsid stabilization [19]. Further analysis of L2 within the viral capsid revealed a diversity of different PsV preparations to have more than the previously suggested 12 L2 molecules [25, 26]. Buck et al. (2008) could show an average of 36 L2 molecules incorporated into PsV capsids and revealed up to 72 L2 binding sites within the L1 pentameric capsid structure. Furthermore Cryo-EM analyses (Figure 3) could demonstrate that L2 is mainly located around the base of the capsomer lumen in close apposition of neighboring L2 molecules. The predicted contact between neighboring L2 molecules was further shown to be specific in the assembled capsids [27]. The interaction of the L2 protein with the L1 capsomers is suggested to be found in the central cavity of the L1 pentamers and non-covalent [28]. The analysis of potential interaction domains of HPV11 L2 revealed a single domain within amino acid 396 and 439 to participate in L1 interaction. In the corresponding domain, conserved proline residues have been identified which were found to be conserved in a variety of HPV types. This hydrophobic stretch seems to play a major role in anchoring the L2 protein in the capsid [24].

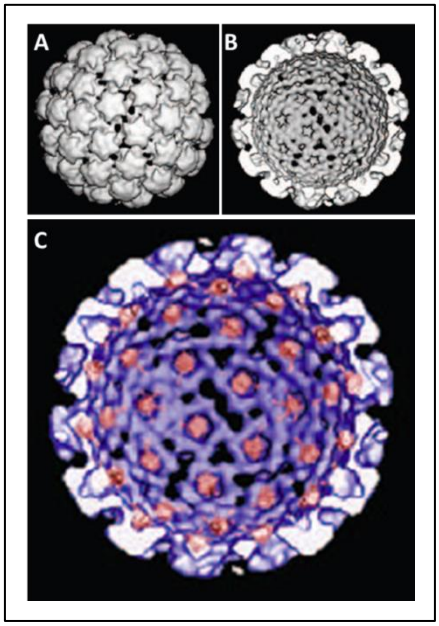

Figure 3 Computerized reconstruction of a HPV16 L1+L2 capsid. Reconstruction of the capsids was generated based on results from the Cryo-EM analysis after capsid preparation in 293TT cells and maturation overnight. A Exterior surface of the L1+L2 capsid with the knobby structure formed by the L1 pentamers. B View of the interior capsid. C Interior view of the capsid, showing the L2 densities in red detected in the Cryo-EM. Figure adopted from [27].

The L2 protein is known to be mainly hidden within the viral capsid although the precise localization within the capsid is still unknown. However, several groups could identify different regions to be accessible when L2 is incorporated into the L1 capsid. For example, the region between amino acid 1-120 of HPV16 seems to be available for binding [29-31]. A recently proposed model of PV infection suggests several conformational changes within the viral capsid during the entry process. Some L2 regions might get accessible upon a distinct conformational change, which alters the availability of L2 on the surface of the capsid. Gambhira et al. described an epitope at amino acid 17-36 which has been demonstrated to get available for antibody binding after binding to the ECM, followed by furin cleavage of the very N-terminal part of L2 [26, 32, 33]. Whereas, Richards et al. as well as Yang et al. described two epitopes (aa 100-120 and aa 13-31) to be constitutively exposed on the surface of PV capsids [31, 34].

Prophylactic HPV vaccines based on the structural proteins L1 and L2

To date, there are two HPV vaccines available on the market and both are L1 VLP-based vaccines to prevent HPV infection with the most prominent high risk types, HPV16 and HPV18. While Cervarix®(GlaxoSmithKline) is a bivalent vaccine, composed of HPV16 L1 and HPV18 L1 VLPs, Gardasil® (Merck) is a quadrivalent vaccine and covers protection against two additional HPV types (HPV6 and HPV11). Though L1-based vaccines induce high titers of neutralizing antibodies, the protection is limited strictly to the distinct types included in the formulation of the vaccine [35]. In order to generate a second generation vaccine, several HPV L2 peptides have been demonstrated to

induce cross-protection against a high number of HPV types [30, 36-39]. Especially highly conserved N-terminal L2 epitopes represent the targets for neutralizing and cross-neutralizing antibodies [30]. However, the mechanism of neutralization and the function of these epitopes for viral infection have not been revealed so far. Their ability to elicit (cross-) neutralizing antibody responses might be an evidence for an essential role in during the infection process. Binding of neutralizing antibodies to these epitopes is suggested to inhibit a crucial function which might be crucial e.g. for the interaction with a specific cellular interaction partner.

1.3. Minor Capsid Protein L2

L2 has been described to have important functions in several processes of DNA encapsidation and viral infection. The L2 protein is highly conserved between different papillomavirus types and is known to fulfill comparable functions in the PVs. Even though the protein is under 500 amino acids and therefore should have a molecular size of around 55 kDa in SDS-PAGE, it has been observed that the protein runs at a molecular weight of 64-78 kDa. This phenomenon could not be explained until now, since the only post-translational modification known is the SUMOylation at lysine 35 [40-42]. Little is known about the higher order structure of papillomavirus L2 proteins. The highly conserved N-terminal part of L2 was shown to contain two cysteine residues (C22 and C28) that are 100% conserved across the *Papillomaviridae.* These cysteines are able to generate intra-molecular disulfide hairpin loops that seem crucial for PV infectivity. Experiments targeting C22 and C28 demonstrated that exchanging either one lead to a loss of infectivity of the corresponding PV [43, 44].

1.3.1. The role of L2 in capsid assembly and genome encapsidation

Assembly of the viral capsid

Within the nucleus L2 is recruited to the PML bodies, facilitated by a specific region at amino acid 390-420 [45, 46]. Furthermore it has been shown that PML localization of L2 leads to an accumulation of L1 and DAXX in the PML bodies. This process might play a role in the assembly of viral capsids [47, 48]. Also other viral proteins were detected to accumulate in the PML bodies, for example the viral E2 protein. Since E2 has not been identified to be important for viral assembly but rather for transcription and replication, recruitment of E2 is supposed to induce replication of the viral genome [25, 49]. Beside viral proteins, several cellular proteins have been demonstrated to co-localize and interact with L2 in the PML bodies. Among other proteins, transcriptional regulators, like PATZ and TBX2 and 3 have been identified. Especially PATZ was previously suggested to be an important protein, regulating gene transcription and cell differentiation during formation of papillomas [50, 51].

Encapsidation of the viral genome

The minor capsid protein L2 is also known to play an important role in the encapsidation of the viral genome. L2 has been shown to recruit other viral proteins to the ND-10 of the host nucleus. In the ND-10, or PML bodies, L2 co-localizes with L1, the viral DNA and E2 and is supposed to organize the encapsidation of DNA and the assembly of the L1/L2 viral capsid [45, 52]. Conserved regions at the N- and C-terminus of the L2 protein have been described to have DNA binding activity, consisting of positively charged basic amino acids [53, 54]. L2 is crucial for encapsidation of the viral genome of

different PV types [53, 55-57]. Deleting one of the two regions of L2 did not lead to inhibition of DNA encapsidation but rendered the particles non-infectious. Since the regions, described to have DNA binding activity, overlap with the nuclear localization signals (NLS) at the N- and C-terminus of L2, results gained from the deletion of both regions remain controversial [58-61]. The DNA binding activity of L2 is not sequence specific but rather depends on ionic interaction due to the affinity of negatively charged DNA and the positively charged amino acid regions of L2 [61].

1.3.2. HPV entry – from the cell surface to the nucleus

Binding to heparan sulfate proteoglycans (HSPG)

The published data about the viral cell binding and entry process are still debated and based on the use of L1 and L1/L2 VLPs or PsV. To date, binding and cell entry of PV have not been completely revealed, however there are models of the entry process under discussion [33, 62]. The general opinion about the binding of HPV to the surface coincides about the initial binding to heparan sulfate proteoglycans (HSPGs) either on the cell surface or at the extracellular matrix [33, 63, 64]. HSPGs are reported to have different activities in a variety of biological process amongst others these proteins serve as attachment receptors for viral and bacterial pathogens [65, 66]. In keratinocytes, the target cells of PVs, the most prominent HSPG is known to be syndecan-1. This protein consists of a core transmembrane domain (TM) as well as an ectodomain containing between 3 and 5 HS chains. Syndecan-1 was described to be highly expressed during wound healing, correlating with the necessity of epithelial micro lesions for efficient, natural PV infection [67]. In addition to syndecan-1, several HSPGs have also been described as potential binding receptors of different PVs [68, 69]. The binding to HSPGs is based on two specific lysine residues in the L1 protein which are located at position 278 and 361 of the HPV16 L1 protein [70, 71]. Additionally, modifications, for example sulfation of the HSPG receptor seem to have a crucial effect on HPV (especially HPV16 and HPV33) binding [72]. The binding of L1 to the corresponding HSPGs leads to a conformational change in the L1 protein. This event is supposed to play a role in the transfer of virions to a potential secondary receptor facilitating viral entry [73].

Exposure of the HPV L2 N-terminus and furin cleavage

In the common binding models, the viral L2 protein, mainly hidden within the capsid, is suggested to expose the N-terminal part following the conformational changes in the L1 protein and the interaction of L2 with cyclophillin B (CyPB) [34, 74, 75]. CyPB is a peptidyl-prolyl cis-/trans-isomerase, known to associate with syndecan-1 after secretion to the extracellular space [76, 77]. After exposure of the L2 N-terminus the protein is cleaved at amino acid 12 by a furin protein convertase, removing the N-terminal located NLS [33, 34, 63, 73]. In addition, furin cleavage seems to be crucial

for infectivity of different PV types. The furin cleavage motif is highly conserved and several PV types show decreased infection potential after exposure to furin inhibitors [34]. Moreover, distinct point mutations of the furin cleavage site led to the production of infection deficient particles. Further analysis of these non-infectious particles showed proper incorporation of L2 and viral DNA during the capsid assembly. Whereas the following steps, like cell surface binding as well as uncoating of the viral DNA, have been demonstrated to be not affected by these mutations. However, Richards et al. could show an accumulation of the L2/viral genome complex in the endosomal compartment. The same results could be observed using furin inhibitors. Cleavage by furin protein convertase therefore seems to be crucial to facilitate the endosomal escape of the L2/viral genome complex and further transport to the nucleus [34].

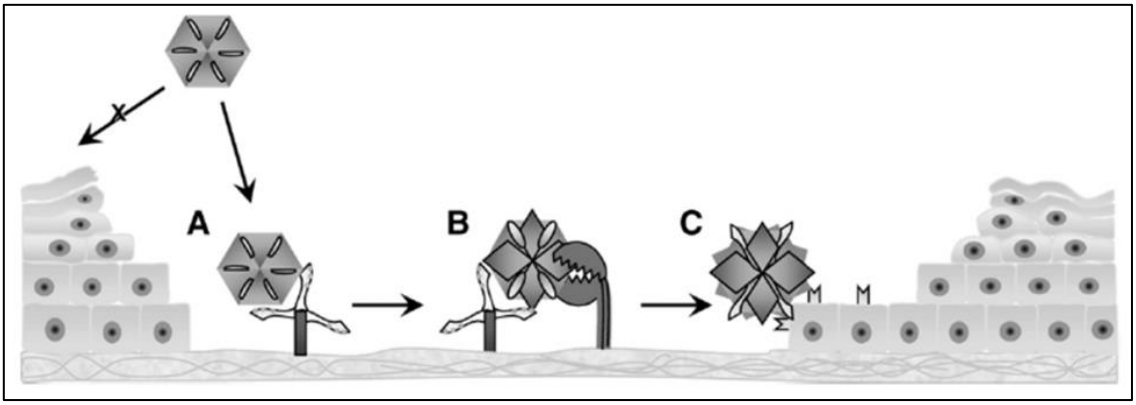

Figure 4 HPV surface interaction, conformational changes and binding to the target cell. A HPVs are transferred to the basement membrane through micro-lesions and bind to the HSPGs. **B** This binding induces a conformational change in the viral L1 capsid protein which leads to the exposure of the L2 N-terminus. The furin cleavage site then gets susceptible for the protein convertase which releases aa 1-12. **C** After a second conformational change in the capsid, the virion is transferred to the target cell and binds to a still unknown secondary receptor from where the particle is internalized. Figure adopted from [78].

Furthermore, CyPB is suggested to have additional functions after virus internalization, specifically during dissociation of L1 and the L2/viral genome complex [79]. Since furin cleavage also induces a second conformational change of the capsid and exposes additional epitopes of L2, another hypothesis suggests L2 to bind to the still unknown secondary receptor at the surface of the target cell. This suggestion is supported by the identification of two independent L2 epitopes (aa 13-31 and aa 108-120) targeted by neutralizing antibodies. The epitope aa 13-31 has been shown to bind the cell surface and further contains the highly conserved cysteines (C22 and C28) which are both essential for viral infection [31, 37, 43]. In addition, the L2 epitope aa 108-120 has also been reported to bind epithelial cells and show high conservation between different types [37]. The involvement of a secondary receptor for viral entry is further based on the observation that HSPGs and CyPB do not induce endocytosis. These findings strongly support the existence of a secondary receptor or a co-receptor initiating the internalization of the viral capsids into the host cell [74, 80].

Cellular factors involved in the uptake of HPV

Several publications describe α_6-integrin as a promising secondary receptor candidate because of the known interactions between integrins, tetraspanins, HSPGs, CyPB and intracellular signaling pathways [64, 69, 81]. Additionally, HPV16 PsV have been shown to interact with a HSPG/growth factor (GF) complex inducing signaling cascades through the corresponding growth factor receptors (GFR). In this context, the PsV are suggested to be covered by HSPG/GF complexes allowing the binding to the GFR. One example is the induction of the PI3K/Akt/mTOR signaling pathway by activation of the EGFR after binding of HPV16 PsV [62, 82]. The function of L2 during the binding and internalization of the virus is still under discussion. While some data clearly show a better infectivity of PsV with a high average of L2 incorporation, binding of HPV33 VLPs on HeLa cells have been described to be comparable for L1 and L1/L2 VLPs [27, 83, 84]. In 2012, Woodham and colleagues identified annexin A2 as an interaction partner of the L2 surface binding epitope 108-126, therefore revealing an additional candidate for receptor binding of L2 [85]. The Ca^{2+}- and phospholipid binding protein annexin A2 consists of two A2 monomers together with a S100A10 dimer in a heterotetrameric complex [86]. The complex is known to be involved in several processes like endo- and exocytosis, cell adhesion, membrane fusion as well as binding, uptake and trafficking of a variety of viruses [87, 88]. For example, annexin A2 is a receptor for cytomegalovirus (CMV), facilitating CMV infection together with a variety of additional molecules, including HSPGs, integrins and EGFR [89, 90]. The use of a complex set of molecules for viral entry would correlate with the slow and asynchronous uptake of HPV because of many rate limiting steps as conformational changes, furin cleavage and recruitment of a multitude of surface molecules [80, 91, 92]. Though the process of PV internalization could not be completely revealed to date, some of the common pathways have already been excluded. The endocytosis of HPV16 could be demonstrated to be clathrin-, caveolae-, lipid raft-, flotillin-, cholesterol- and dynamin- independent. However, actin polymerization seems to be crucial for HPV16 infection in contrast to Rho-like GTPase activity. The ligand-induced uptake of HPV16 might be a new pathway which is closely related to micropinocytosis, depending on multiple factors like EGFR, PKC, PI3K and maybe other tyrosine and/or serine/threonine kinases [92, 93].

Internalization and trafficking of the Viral Particles

Different PV types have been reported to use variable cellular pathways during the internalization process [93-95]. Beside the different PV types, another variable factor for the selection of the internalization pathway might be the cell type or the PV genome used in the distinct experiment. Whereas L1 only VLPs were shown to enter immune cells via a clathrin-mediated or caveolae-dependent pathway, L1/L2 VLPs are internalized by clathrin- and caveolae-independent mechanisms [96, 97]. This observation leads to the suggestion that L2 might affect directly the selected

internalization pathway of the corresponding PV. Studies using Langerhans cells demonstrated maturation of L1 VLP-infected cells while L1/L2 VLP treated cells did not enter the maturation process [98]. Consistent to these findings, L2 might have another crucial function in escaping the immune system which might be due to the selection of an alternative uptake pathway [98]. Infection of epithelial cells, the natural target of PVs, led to uptake of the virions and transfer to early endosomes followed by transition to late endosomes, an acidification-dependent process [93].

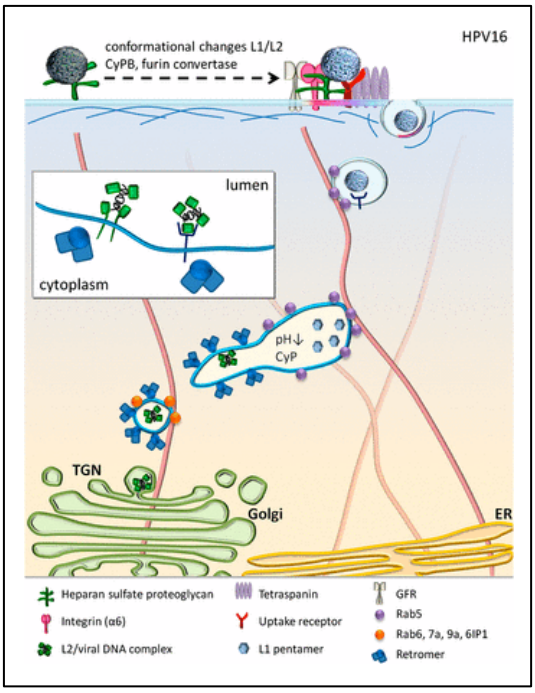

Figure 5 Intracellular trafficking of HPV16. After binding of the virus to the cell surface and the corresponding conformational changes in the capsid, the virus is internalized probably by a micropinocytosis related process. During internalization the virion is suggested to interaction with different factors, like integrin α6, tetraspanin, GFR and an unknown uptake receptor. Actin polymerization leads to the release of the HPV16 containing endocytic vesicle into the cytoplasm of the target cell. Acidification of the endosome and interaction with CyPB further lead to the disassembly of L1 from the L2/viral DNA complex. Several cellular factors, e.g. Rab 7b and Rab 9a, are suggested to play a role in the transition of the L2/viral DNA complex to the trans Golgi network (TGN) from where the complex is further transported to the nucleus. However, the process of TGN to nucleus trafficking is still unrevealed. Figure adopted from [99].

Several host cell proteins have been identified, permitting entry and transport of the virions. In PV infection CyPB might fulfill two distinct functions during the internalization of the virions. First of all, it is supposed to induce the previously described conformational change in the PV capsid, allowing furin cleavage [75]. Secondly, CyPB might facilitate the uncoating of the viral DNA in the late endosomes, leading to the dissociation of L1 and L2/viral genome complex [79]. While the L2/viral genome complex has been reported to escape the late endosome and travel through the trans Golgi network (TGN) after dissociation from L1, L1 remains in the late endosomes [100, 101]. In context of the described pathway, Day and colleagues described the furin cleavage to be crucial for the PV for entry to the TGN and further passage of the L2/viral genome complex. The TGN has been reported to be an essential subcellular compartment for transfer of the L2/viral genome complex to the nucleus

[102].This data was demonstrated by the dependence of HPV16 infection on Rab7b and Rab9a GTPases, which are known to be necessary for the transport of cargos between different cellular compartments. Rab7b and Rab9a have been published to be directly involved in transition of cargo proteins from the late endosome to the TGN [103]. Other compartments, like the caveosomes and the endoplasmatic reticulum (ER) have also been described to be important for intracellular trafficking of different PV (BPV1, HPV31 and HPV16) [104-106].

Endosomal escape of the L2/viral genome complex

After encapsidation of the viral DNA, the L2/viral genome complex needs to escape the endosomal compartment and further travel to the host cell nucleus. Especially the mechanism leading to the endosomal escape is under continuous investigation and not completely understood to date. Kamper at al., identified a hydrophobic and basic cluster at the C-terminus of HPV33 L2 which is supposed to be able to invade cellular membranes and potentially destabilize the endosomal membrane. Further investigations on this L2 region by mutation experiments showed an impaired infectivity of the corresponding virus. In this context, the L2/DNA complex was observed to be retained in the late endosomes instead of being transported to the nucleus [107]. Another region of L2 which might be involved in the endosomal escape of the L2/DNA complex has been described to be a transmembrane-like domain at aa 45-67 including several GxxxG motifs [108]. The corresponding GxxxG motifs are highly conserved between different PV types which might point to an important function of the specific domain. Furthermore, the authors found the structure of this area to be alpha-helical with the GxxxG motifs on opposite faces of the helix. This localization allows the self-association of motifs either homo- or heterotypically. This process might form higher order structures, therefore allowing the penetration of the endosomal membrane. This suggestion is strongly supported by experiments using altered GxxxG motifs, leading impaired endosomal escape of the L2/DNA complex [108].

A cellular protein, identified to play a role in the endosomal compartment, is sorting nexin 17 (SNX17), a cytosolic adapter protein involved in endosomal recycling. L2 sequences of several types show a conserved SNX17 binding site at around amino acid 245-257. Publications from 2012 and 2013 demonstrated that knockdown of SNX17 or mutation of the potential SNX17 binding site in L2, induced retention of L2 in the late endosome followed by lysosomal degradation [109, 110]. SNX17 is strongly connected to the sorting process of cargo proteins within the endosomal network. SNX17 protects integrins from lysosomal degradation by targeting the intergrins towards a recycling pathway [111, 112]. Recently, L2 has been reported to interact with SNX27, which belongs to the same protein family as SNX17 [113]. SNX27 is known to at least indirectly interact with the retromer complex [114]. SNX27 might be involved in the association of L2 with the retromer complex which

has previously been reported by Popa et al. [115]. Association of L2 with the retromer complex was described to mediate the endosomal escape and transport of the L2/viral genome complex to the TGN [115].

In addition, the dependence of the L2/viral DNA transport on the Rab GTPases might also point to the trafficking of L2/viral DNA through the TGN to nucleus. Along this line an interaction of L2 with the dynein light chain Tctex1, described to be localized in the Golgi and the interphase nuclei was reported [116-118]. Though the final steps of L2/viral genome transport to the nucleus have not been revealed, the findings might confirm the hypothesis of L2/viral DNA nuclear entry during mitosis and nuclear envelope breakdown. In this context, the Tctex1 might be involved in the transition of the L2/viral DNA complex from the Golgi to the kinetochores of mitotic cells [117, 118]. However, the details of TGN to nucleus transition of the L2/viral genome complex are still under constant research and need to be further elucidated.

Nuclear Entry of the L2/viral genome complex

The L2 protein sequence is known to contain two NLS however the mechanism of nuclear entry is not completely understood by now. Pyeon et al. claim that entry of the host cell into mitosis and the nuclear breakdown are crucial events for L2 nuclear entry. According to the publication from 2009, L2 does not enter the host cell nucleus through the nuclear pores mediated by the NLS sequence of L2 [119]. Besides, a nuclear retention signal at amino acid 296-316 has been described, which seems to be important for viral infection. In context of a nuclear entry during nuclear breakdown, these regions are suggested to facilitate association of L2/viral genome with the nuclear matrix during metaphase [120].

1.4. Objective

The HPV minor capsid protein L2 has been reported to be crucial for infectious viral entry and a variety of processes during the viral life cycle of several HPVs. Even though some functional domains, especially in the highly conserved N-terminus of L2, have already been described (Figure 6), there are still many regions in the protein sequence that might play a role in the infection process or during formation of new virions after infection.

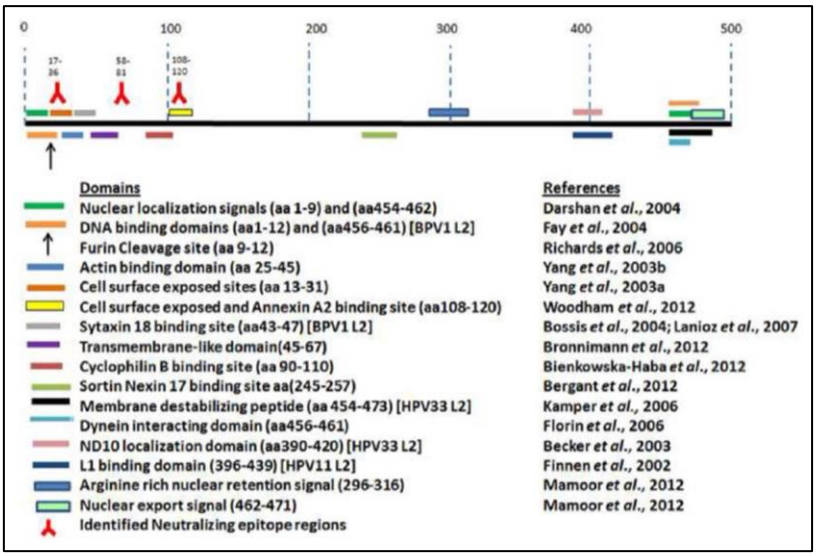

Figure 6 Summary of described L2 functional domains and epitopes for binding of neutralizing antibodies. Functional domains of the PV L2 protein are highlighted with the colored bars, like described in the caption. The furin cleavage site is marked by a black arrow, whereas the epitopes for neutralizing antibodies are indicated by the red antibody symbol. Figure adopted from [121].

The objective of the PhD project is the analysis of unrevealed HPV L2 domains to get further insight into the functional role of L2. Therefore, the aim of my thesis is the identification and validation of cellular proteins interacting with the HPV16 minor capsid protein L2. The **first approach** (Figure 7, A Tandem Affinity Purification (TAP)) focused on the identification of specific interaction candidates after overexpression of a tagged HPV16 L2 protein. The tandem-affinity purification (TAP) was used to co-purify interacting cellular proteins together with a TAP-tag containing HPV16 L2 fusion protein, followed by mass spectrometry (MS) analysis to identify co-purified proteins. In a **second approach** (Figure 7, B Co-Immunoprecipitation (Co-IP)), HPV16 L2 and its potential interaction partners were (co-)purified by immunoprecipitation (IP), from cells previously infected with HPV16 PsV. L2-specific and L1-specific antibodies were used for precipitation and the co-purified set of proteins was further analyzed by MS. Based on the identification of (cross-) neutralizing epitopes (aa 20-38, aa 28-42 and aa 64-81) at the N-terminal part of HPV16 L2 [30], the **third approach** (Figure 7, C Peptide Pull Down (PPD)) of the thesis relied on the immobilization of the corresponding epitopes and the identification of potential interaction partners by pull-down from cellular extracts. This approach should provide

further insight into the function of the specific epitopes within the L2 protein and their role during viral infection.

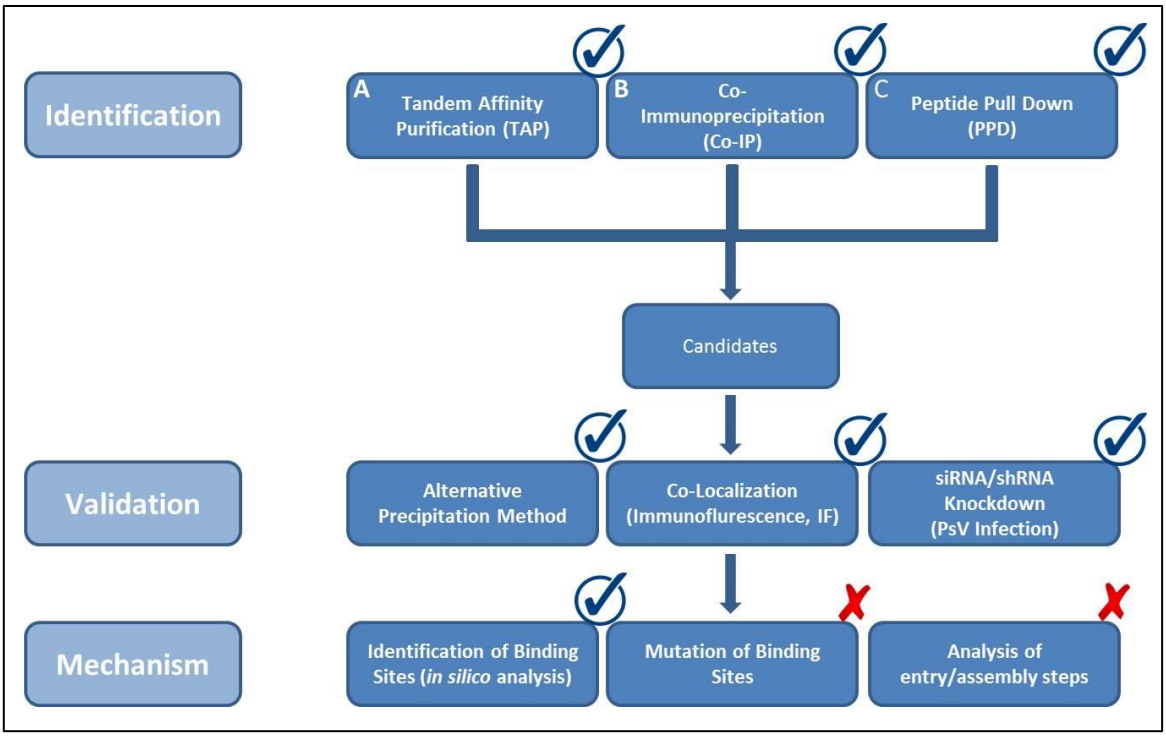

Figure 7 Overview of the PhD thesis workflow. Potential interaction candidates of HPV16 L2 were identified, using three independent approaches. A Tandem Affinity Purification, based on the overexpression of a TAP-tagged HPV16 L2 protein and the co-puification of interacting proteins. B Co-immunoprecipitation (IP) of HPV16 capsids from cells infected with HPV16 PsV and co-purification of potential binding partners. C Peptide Pull Down (PPD), focusing on three biotinylated HPV16 L2 epitopes, immobilized on avidin beads and further used for pull-down of interacting proteins from cell extracts. To validate potential candidates, the candidates were overexpressed and analyzed in either an alternative precipitation method for binding to L2 or immunofluorescence (IF) for co-localization with L2. Additionally, the candidates were down regulated by siRNA or shRNA and transduction efficiency of HPV16 PsV was analyzed. Potential binding sites were identified by *in silico* analysis using the eukaryotic linear motif (ELM) online tool. Further investigations on the mechanism have not been executed during the experimental phase of the PhD thesis.

Identified interaction candidates were further validated for their ability to physically bind HPV16 L2 by alternative precipitation methods and co-localization by immunofluorescence. In addition, HPV16 PsV transduction was analyzed after downregulation of the expression levels of distinct candidates by siRNA and shRNA, respectively. In order to identify potential interaction sites of the validated candidates, L2 protein sequences of different low and high risk HPV types were analyzed using the eukaryotic linear motif (ELM) online tool for *in silico* analysis. Further investigations on the mechanism of the corresponding interactions, like the mutation of identified binding sites and the analysis of specific steps of the viral life cycle, have not been executed during the thesis.

2. Material

2.1. Biological Material

2.1.1. Prokaryotic Cells

Strain	Genotyp	Company
E.coli MegaX DH10α^{TM} T1^{R}	F– mcrA Δ(mrr-hsdRMS-mcrBC) Φ80lacZΔM15 ΔlacX74 recA1 endA1 araD139 Δ(ara leu)7697 galU galK λ– rpsL nupG tonA	Invitrogen
E.coli Solo Pack Gold Competent Cells	Tetr Δ(mcrA)183 Δ(mcrCB-hsdSMR-mrr)173 endA1 supE44 thi-1 recA1 gyrA96 relA1 lac Hte [FÅL proAB lacIqZΔM15 Tn10 (TetR)Amy CamR]	Stratagene, Agilent Technologies
E.coli Rosetta^{TM}	F- ompT hsdSB(rB- mB-) gal dcm (DE3) pRARE2 (CamR)	Merck4Biosciences
E.coli SURE (Stop Unwanted Rearrangement Events) Competent Bacteria	e14-(McrA-) Δ(mcrCB-hsdSMR-mrr)171 endA1 gyrA96 thi-1 supE44 relA1 lac recB recJ sbcC umuC::Tn5 (KanR) uvrC [F´ proAB lacIqZΔM15 Tn10 (Tetr)]	Stratagene, Agilent Technologies

2.1.2. Eukaryotic Cells

Cell Line	Description
HaCaT	Keratinocyte cell line derived from adult human skin. Spontaneously transformed and immortal cell line. Described as aneuploid. Culture medium: supplemented DMEM
HEK 293	Human embryonic kidney cells derived from a healthy aborted human embryo and transformed with E1A/B of Adenovirus 5. Described as hypotriploid. Culture medium: supplemented DMEM
HEK 293TT	HEK 293 cells stably expressing two copies of the Simian virus (SV) 40 large T-antigen. Cultured under selective conditions using 62,5µM Hygromycin B. Culture medium: supplemented DMEM
HeLa	Immortal cell line derived from HPV18 positive human cervical carcinoma of Henrietta Lacks. The cells are hypertriploid ($3n^{+}$). Culture medium: supplemented DMEM
HeLa T	HeLa cells stably expressing one copy of the Simian virus (SV) 40 large T-antigen. Cultured under selective conditions using 125µM Hygromycin B. Culture medium: supplemented DMEM
Phoenix	Phoenix cells are derived from HEK 293T cells. Constructs capable of producing gag-pol as well as envelope proteins were introduced into the 293T cells. Therefore the cells stably express lentiviral packaging proteins and can be used for Lentivirus production. Culture medium: high glucose DMEM, supplemented with 10% FCS, 1% P/S, 1% glutamine and 10µg/ml ciprofloxacin

2.1.3. Pseudoviruses (PSV)

HPV type	Reporter	Plasmid	Source
HPV16	Gaussia Luciferase, GFP	#988 #1998	N. Thönes/M. Müller
HPV18	Gaussia Luciferase, GFP	#1165 #1166 #1998	J. Schiller/M. Müller
HPV31	Gaussia Luciferase, GFP	#1698 #1998	J. Schiller/C. Buck/M. Müller
HPV45	Gaussia Luciferase, GFP	#2271 #2273 #1998	I. Rubio/M. Müller

2.1.4. Adeno-associated Viruses (AAV)

AAV type	Reporter	Plasmid	Source
AAV2	Gaussia Luciferase, ssDNA	#2772 #1814 #3193	A. Sacher/M. Müller
AAV2	Gaussia Luciferase, scDNA	#2772 #1814 #2485	A. Sacher/M. Müller

2.1.5. Lentiviruses

shRNA	Packaging Plasmids	Source
#3311 pLKO.1 SHC002 shRNA ctrl.	#3294 #3295 #3296	This thesis
#3312 pLKO.1 SHC003 GFP turbo	#3294 #3295 #3296	This thesis
#3344 IRS4_2 shRNA	#3294 #3295 #3296	This thesis
#3345 YWHAZ_1 shRNA	#3294 #3295 #3296	This thesis
#3347 CSE1L_1 shRNA	#3294 #3295 #3296	This thesis
#3348 SPOP_1 shRNA	#3294 #3295 #3296	This thesis

2.2. Media and Supplements

2.2.1. Procaryotic Cells

Designation	Composition
Agar Plates	98,5% LB medium (v/v) 1.5% bacto-agar (w/v) autoclaved antibiotics added when < 40°C
Luria Broth (LB) medium	1% Trypton (w/v) 0.5% Yeast Extract (w/v) 0.5% NaCl (w/v) in H_2O, pH 7.5 autoclaved
Antibiotics	Ampicilin (Amp): 100mg/ml Kanamycin (Kan): 25mg/ml Zeocin (Zeo): 100mg/ml

2.2.2. Eukaryotic Cells

Media	Company
Dulbecco´s Modified Eagle Medium (DMEM)	Sigma-Aldrich, Deisenhofen, Germany

Supplements	Concentration	Company
FCS		PAN Biotec, Aidenbach, Germany
L-glutamin (200mM)	200mM	Genaxxon, Ulm, Germany
Penicillin/Streptomycin (10.000 units/ml Pen and 10.000µg/ml Strep)	10.000U/ml	Gibco Life Technologies, Paisley, UK

2.3. Molecular Cloning

2.3.1. Oligonucleotides for Cloning of HPV16L2 Fragments for TAP

As template DNA for the PCR of the following HPV16L2 fragments, #893 pUF3 containing the humanized HPV16L2 full-length sequence were used.

BamHI restriction sites were added to the primer sequences, to allow cloning of the amplified DNA sequences into the destination vector #2175 pZOME1_C. To improve translation of the HPV16L2 fragments, the Kozak sequences was included into the forward primer sequences of HPV16L2_Fr2 (aa 129-334) and HPV16L2_Fr3 (aa 262-473).

Designation	Sequence 5´-3´
HPV16L2_Fr1 (aa 1-193)F	CTTTGGATCCGCCACCATGAGGCACAAG
HPV16L2_Fr1 (aa 1-193)R	CTTTGGATCCGTAGTTGTGGGTGCTGATGG
HPV16L2_Fr2 (aa 129-334)F	ATTTGGATCCGCCACCATGGACGTGAGCGGCTTCAGCATCACC
HPV16L2_Fr2 (aa 129-334)R	CTTTGGATCCGGTGCTCAGGTCGTAGTAGTAGTG
HPV16L2_Fr3 (aa 262-473)F	CTTTGGATCCGCCACCATGGACGTGGACAACACCCTGTACTTC
HPV16L2_Fr3 (aa 262-473)R	ATTTGGATCCCGCGGCCAGGCTCACG

highlighted in blue, BamHI restriction site
highlighted in green, Kozak sequence

2.3.2. Oligonucleotides for siRNA knockdown

Designation	Taget Sequence	Order # (Qiagen, Hilden, Germany)
Hs-SNX17_1 Flexi tube siRNA	CTGGCCCTCGATGCCAAAT	SI00107877
Hs-SNX17_2 Flexi tube siRNA	CAGCGAGACTTTCAACAGT	SI00107884
Hs-SNX17_3 Flexi tube siRNA	CTCCGCCTACGTGGCCTAT	SI00107891
Hs-SNX17_5 Flexi tube siRNA	TACATGCAAGCTGTTCGGC	SI03108378
Hs-IRS4_3 Flexi tube siRNA	GAGGGTGACTACATTGAAG	SI00053494
Hs-IRS4_5 Flexi tube siRNA	GCGGCGCGTGATCACCCTA	SI02631398
Hs-IRS4_6 Flexi tube siRNA	CAGCTCTAGTGACTACGTC	SI03068226

Hs-IRS4_7 Flexi tube siRNA	CAGGCGCTACTTCGTGCTC	SI03070620
Hs-YWHAZ_3 Flexi tube siRNA	CAGGTTTATGTTACTTCTA	SI00764813
Hs-YWHAZ_6 Flexi tube siRNA	Sequence not provided	SI04135663
Hs-YWHAZ_7 Flexi tube siRNA	Sequence not provided	SI04295375
Hs-YWHAZ_8 Flexi tube siRNA	Sequence not provided	SI04330900
Hs-CSE1L_2 Flexi tube siRNA	CTGACGGTATCAAATATAT	SI00025298
Hs-CSE1L_3 Flexi tube siRNA	Sequence not provided	SI00025305
Hs-CSE1L_4 Flexi tube siRNA	CAAATGAACTTGTAAACCT	SI00025312
Hs-CSE1L_7 Flexi tube siRNA	CAGGATAATGTTATCAAAG	SI02654015
Hs-CAPN2_4 Flexi tube siRNA	CTGGAACACTATAGACCCA	SI00338114
Hs-CAPN2_5 Flexi tube siRNA	CACCAGCGATACCTACAAG	SI03057306
Hs-CAPN2_6 Flexi tube siRNA	CTCGGAGGCCATCACGTTT	SI03091648
Hs-CAPN2_8 Flexi tube siRNA	Sequence not provided	SI05168996
Hs-SPOP_2 Flexi tube siRNA	CAGGCTCACAAGGCTATCT	SI00732214
Hs-SPOP_6 Flexi tube siRNA	Sequence not provided	SI04137630
Hs-SPOP_8 Flexi tube siRNA	Sequence not provided	SI04327155
AllStars negative control siRNA	Sequence not provided	SI03650318

2.3.3. Oligonucleotides for shRNA knockdown

All oligonucleotides listed, were ordered and produced at MWG Eurofins in Ebersberg, Germany.

Designation	**Sequence 5´-3´**
IRS4_1 fwd	CCGGGCGGAGCCACCCTTCTATAAACTGCAGTTTATAGAAGGGTGGCTCCGCTTTTTG
IRS4_1 rev	AATTCAAAAAGCGGAGCCACCCTTCTATAAACTGCAGTTTATAGAAGGGTGGCTCCGC
IRS4_2 fwd	CCGGCTGAGTGCTGTATGGATATTTCTGCAGAAATATCCATACAGCACTCAGTTTTTG
IRS4_2 rev	AATTCAAAAACTGAGTGCTGTATGGATATTTCTGCAGAAATATCCATACAGCACTCAG
YWHAZ_1 fwd	CCGGGCAGAGAGCAAAGTCTTCTATCTGCAGATAGAAGACTTTGCTCTCTGC-TTTTTG
YWHAZ_1 rev	AATTCAAAAAGCAGAGAGCAAAGTCTTCTATCTGCAGATAGAAGACTTTGCTCTCTGC
YWHAZ_2 fwd	CCGGGCTCGAGAATACAGAGAGAAACTGCAGTTTCTCTCTGTATTCTCGAGCTTTTTG
YWHAZ_2 rev	AATTCAAAAAGCTCGAGAATACAGAGAGAAACTGCAGTTTCTCTCTGTATTCTCGAGC
CSE1L_1 fwd	CCGGCGCTGACAAGTATCTGTGAAACTGCAGTTTCACAGATACTTGTCAGCGTTTTTG
CSE1L_1 rev	AATTCAAAAACGCTGACAAGTATCTGTGAAACTGCAGTTTCACAGATACTTGTCAGCG
CSE1L_2 fwd	CCGGGCATGGAATTACACAAGCAAACTGCAGTTTGCTTGTGTAATTCCATGCTTTTTG
CSE1L_2 rev	AATTCAAAAAGCATGGAATTACACAAGCAAACTGCAGTTTGCTTGTGTAATTCCATGC
SPOP_1 fwd	CCGGCACAAGGCTATCTTAGCAGCTCTGCAGAGCTGCTAAGATAGCCTTGTGTTTTTG
SPOP_1 rev	AATTCAAAAACACAAGGCTATCTTAGCAGCTCTGCAGAGCTGCTAAGATAGCCTTGTG
SPOP_2 fwd	CCGGCTCCTACATGTGGACCATCAACTGCAGTTGATGGTCCACATGTAGGAGTTTTTG
SPOP_2 rev	AATTCAAAAACTCCTACATGTGGACCATCAACTGCAGTTGATGGTCCACATGTAGGAG

2.3.4. Plasmids

Designation	Description	Reference
#3	Bluescript KS empty	M. Müller
#893	pUF3 with HPV16L2	M. Müller
#988	pCDNA 4.0 TO with HPV16 L1 and L2 (IRES)	M. Müller
#1998	pGF with Gaussia luciferase and GFP	C. Buck
#2175	pZOME1-C eukaryotic vector for TAP	M. Müller
#2459	pZOME1-C with HPV16L2 TAP-tag	H. Seitz
#2800	pZOME1-C with HPV16L2_Fr1 (aa 1-193)	This thesis
#2801	pZOME1-C with HPV16L2_Fr3 (aa 262-473)	This thesis
#2873	pZOME1-C with HPV16L2_Fr2 (aa 130-334)	This thesis
#2957	pDEST15 E.coli expression vector (GST-Tag) Gateway compatible	GPCF, DKFZ
#2958	pDEST Mammalian expression vector (N-terminal Myc), Gateway compatible	GPCF, DKFZ
#2959	pDEST Mammalian expression vector (N-terminal Flag), Gateway compatible	GPCF, DKFZ
#2960	pDEST Mammalian expression vector (w/o tag), Gateway compatible	GPCF, DKFZ
#3136	CSE1L cDNA (closed) in pENTR221, Gateway compatible	GPCF, DKFZ
#3137	Skp1 cDNA (closed) in pENTR221, Gateway compatible	GPCF, DKFZ
#3138	YWHAZ cDNA (closed) in pENTR221, Gateway compatible	GPCF, DKFZ
#3139	HNRNPK cDNA (closed) in pENTR221, Gateway compatible	GPCF, DKFZ
#3140	PSMD12 cDNA (closed) in pENTR221, Gateway compatible	GPCF, DKFZ
#3142	PSMD12 in pDEST w/o tag (#3140 in 2960)	This thesis
#3143	Skp1 in pDEST w/o tag (#3137 in 2960)	This thesis
#3144	CSE1L in pDEST w/o tag (#3136 in 2960)	This thesis
#3145	YWHAZ in pDEST w/o tag (#3138 in 2960)	This thesis
#3146	HNRNPK in pDEST w/o tag (#3139 in 2960)	This thesis
#3147	N-GST-PSMD12 in pDEST (#3140 in 2957)	This thesis
#3148	N-GST-CSE1L in pDEST (#3136 in 2957)	This thesis
#3149	N-GST-HNRNPK in pDEST (#3139 in 2957)	This thesis
#3150	N-Flag-PSMD12 in pDEST (#3140 in 2959)	This thesis
#3151	N-Flag-Skp1 in pDEST (#3137 in 2959)	This thesis
#3152	N-Flag-CSE1L in pDEST (#3136 in 2959)	This thesis
#3153	N-Flag-YWHAZ in pDEST (#3138 in 2959)	This thesis
#3154	N-Flag-HNRNPK in pDEST (#3139 in 2959)	This thesis
#3155	N-Myc-PSMD12 in pDEST (#3140 in 2958)	This thesis
#3156	N-Myc-CSE1L in pDEST (#3136 in 2958)	This thesis
#3157	N-Myc-YWHAZ in pDEST (#3138 in 2958)	This thesis

#3158	N-Myc-HNRNPK in pDEST (#3139 in 2958)	This thesis
#3159	N-Myc-Skp1 in pDEST (#3137 in 2958)	This thesis
#3185	eEF1A1 cDNA (closed) in pENTR221, Gateway compatible	GPCF, DKFZ
#3186	IRS4 cDNA (closed) in pENTR223, Gateway compatible	GPCF, DKFZ
#3188	N-Myc-IRS4 in pDEST (#3186 in #2958)	This thesis
#3189	N-Myc-eEF1A1 in pDEST (#3185 in #2958)	This thesis
#3190	N-Flag-eEF1A1 in pDEST (#3185 in #2959)	This thesis
#3191	N-Flag-IRS4 in pDEST (#3186 in #2959)	This thesis
#3199	N-GST-HNRNPK in pDEST (#3139 in #2957)	This thesis
#3200	N-GST-CSE1L in pDEST (#3139 in #2957)	This thesis
#3265	SNX17-GFP	Dr. Lawrence Banks
#3266	SNX-Flag	Dr. Lawrence Banks
#3294	pMDLg/pRRE (Gag/Pol)	Addgene, Plasmid #12251
#3295	pRSV-Rev (Rev)	Addgene, Plasmid #12253
#3296	pMD2.G (VSV G)	Addgene, Plasmid #12259
#3311	pLKo.1 SHC002 shRNA ctrl. (non-mammalian shRNA control)	Sigma-Aldrich, Deisenhofen, Germany
#3312	pLKO.1 SHC003 GFP turbo (positive control)	Sigma-Aldrich, Deisenhofen, Germany
#3310	pLKO.1 TRC control	Addgene, Plasmid #10879
#3343	IRS4_1 shRNA in pLKO.1 TRC control	This thesis
#3344	IRS4_2 shRNA in pLKO.1 TRC control	This thesis
#3345	YWHAZ_1 shRNA pLKO.1 TRC control	This thesis
#3347	CSE1L_1 shRNA pLKO.1 TRC control	This thesis
#3348	SPOP_1 shRNA pLKO.1 TRC control	This thesis

2.3.5. Enzymes

Designation	**Company**
Calf intestine alkaline phosphatase (CIP)	New England Biolabs, Frankfurt, Germany
KOD HiFi Polymerase	Novagen/Merck, Darmstadt, Germany
Quick Ligase	New England Biolabs, Frankfurt, Germany
Restriction enzymes	New England Biolabs, Frankfurt, Germany
RNAse	Roche, Mannheim, Germany
T4 DNA Ligase	New England Biolabs, Frankfurt, Germany

2.3.6. Buffers and Solutions for DNA Purification and Analysis

2.3.6.1. Purification of plasmid DNA

Designation	Composition
Alkali lysis buffer	200mM NaOH 1% SDS (w/v) in H_2O
Chloroform-isoamyl alcohol mix (CIA)	Chloroform-isoamyl alcohol mix 24:1
Glucose buffer	50mM glucose 10mM EDTA 25mM Tris HCl in H_2O, pH 8.0
Phenol mix	Phenol-CIA mix 1:1 100µg hydroxyquinoline per 100ml
Sodium acetate	3M sodium acetate in H_2O, pH 5.2
1x TE buffer	10mM Tris 1mM EDTA in H_2O, pH 8.0

2.3.6.2. Agarose Gel Electrophoresis

Designation	Composition/Company
1% agarose gel	1% agarose (w/v) 1x TAE buffer 0.006% ethidium bromid (v/v)
Ethidium bromide	Roth, Karlsruhe, Germany
Lambda/HindII marker	New England Biolabs, Frankfurt, Germany
6x loading buffer	New England Biolabs, Frankfurt, Germany
1x TAE buffer	40mM Tris 5.71% acetic acid (v/v) 10% 500mM EDTA, pH 8.0 (v/v) in H_2O
Quick-Load™ 100bp DNA ladder	New England Biolabs, Frankfurt, Germany

2.4. Buffers and Solutions for Protein Analysis

2.4.1. SDS-polyacrylamid gels

Designation	Composition
12.5% separation gel for 5 mini gels	18.75ml 30% acrylamide solution 16.88ml 1M Tris/HCl buffer, pH 8.8 8.48ml H_2O 450µl 10% SDS 450µl 10% APS 22.5µl TEMED
3% stacking gel for 5 mini gels	1.5ml 30% acrylamide solution 1.95ml 1M Tris/HCl buffer, pH 6.8 11.25ml H_2O 150µl 10% SDS 150µl 10% APS 22.5µl TEMED

2.4.2. Electrophoresis

Designation	Composition
3x protein loading buffer	30% glycerol 6% SDS 15% β-mercaptoethanol 0.003% bromphenol blue 187.5mM Tris in H_2O, pH 6.8
1x TGS buffer (running buffer)	2.5mM Tris 1.45% glycine 0.1% SDS in H_2O, pH 8.3
Tris buffer pH 6.8	1M Tris/HCl 0.03% bromphenol blue in H_2O, pH 6.8
Tris buffer pH 8.8	1M Tris/HCl in H_2O, pH 8.8

2.4.3. Western Blot Analysis

Designation	Composition
Blocking buffer	5% skim milk in PBS-T
1x EMBL buffer	48mM Tris 39mM glycine 1.3mM SDS 20% methanol in H_2O, pH 8.2
1x PBS-T	0.3% Tween 20 (v/v) in 1x PBS

2.5. Immunological Methods

2.5.1. Antibodies

Designation	Description	Reference
14-3-3 ζ (C-16): sc-1019	Polyclonal rabbit antibody detecting human YWHAZ. Reactive in ELISA, WB, IF, IP and IHC(P).	Santa Cruz Biotechnology, Heidelberg, Germany
Actin (C4)	Mouse monoclonal antibody detecting human actin. The detected epitope lies between amino acid 18-40. Reactive in WB, IF and IHC.	MP Biomedicals, Solon, USA
AlexaFlour488 (anti-mouse)	Goat-anti-mouse coupled with AlexaFlour 488	Life Technologies, Darmstadt, Germany
AlexaFlour488 (anti-rabbit)	Goat-anti-rabbit coupled with AlexaFlour 488	Life Technologies, Darmstadt, Germany
AlexaFlour594 (anti-mouse)	Goat-anti-mouse coupled with AlexaFlour 594	Life Technologies, Darmstadt, Germany
AlexaFlour 594 (anti-rabbit)	Goat-anti-rabbit coupled with AlexaFlour 594	Life Technologies, Darmstadt, Germany
Calpain 2 (CAPN2)	Mouse monoclonal, used as hybridoma supernatant. Reactive in ELISA, WB and IF.	This thesis
CAS (H-2): sc-271537	Mouse monoclonal antibody detecting human CSE1L. Raised against amino acid 672-971. Reactive in ELISA, WB, IF and IP.	Santa Cruz Biotechnology, Heidelberg, Germany
DAGPO	Donkey-anti-goat coupled with HRP	Santa Cruz Biotechnology, Heidelberg, Germany
GAMPO	Goat-anti-mouse coupled with HRP	Dianova, Hamburg, Germany
GARPO	Goat-anti-rabbit coupled with HRP	Dianova, Hamburg, Germany
Anti-IRS4 06-771	Polyclonal rabbit antibody detecting human IRS4. Raised against amino acid 1240-1257. Reactive in WB and IP.	Merck Millipore, Darmstadt, Germany
K1L2	Mouse monoclonal antibody detecting amino acid 74-77 of HPV16 L2. Reactive in ELISA, WB, and IF.	I. Rubio/M.Müller
K4L2	Mouse monoclonal antibody, detecting amino acid 21-31 of HPV16 L2. Reactive in ELISA, WB, and IF.	I. Rubio/M.Müller
K8L2	Mouse monoclonal antibody, detecting amino acid 32-38 of HPV16 L2. Reactive in ELISA, WB, and IF.	I. Rubio/M.Müller
K18L2	Mouse monoclonal antibody, detecting amino acid 22-30 of HPV16 L2. Reactive in ELISA, WB, and IF.	I. Rubio/M.Müller
MD2H11	Mouse monoclonal antibody, recognizing HPV16 L1 in WB, ELISA and IF	M. Durchdewald/ M.Müller
Myc hybridoma	9E10 mouse monoclonal antibody, raised against myc. Used as hybridoma snt. Reactive in WB and IF.	
Myc (9E10)	Mouse monoclonal antibody detecting the epitope EQKLISEEDL of human c-myc.	New England Biolabs, Frankfurt, Germany
Myc (71D10)	Rabbit monoclonal antibody detecting the epitope EQKLISEEDL of human c-myc.	Cell Signaling Technology, Leiden, Netherlands
Serum #7	Polyclonal serum derived from a rabbit immunized with HPV16 L2-GST.	M. Müller

SNX17 (H-10): sc-166957	Mouse monoclonal antibody detecting SNX17, amino acid 270-470. Reactive in ELISA, WB, IF and IP.	Santa Cruz Biotechnology, Heidelberg, Germany
SPOP (B-8): sc-377206	Mouse monoclonal antibody detecting human SPOP. Raised against amino acid 351-374. Reactive in ELISA, WB, IF and IP.	Santa Cruz Biotechnology, Heidelberg, Germany
SPOP (C-14): sc-66649	Goat polyclonal antibody detecting an epitope at the C-terminus of human SPOP. Reactive in ELISA, WB, IF and IP.	Santa Cruz Biotechnology, Heidelberg, Germany

2.5.2. Immunoprecipitation (IP) from PSV Infected Cells

2.5.2.1. Buffers and Solutions

Designation	**Composition**
Acetate buffer	100mM NaAc 500mM NaCl In H_2O, pH 4.0
Blocking buffer	100mM Tris/HCl in H_2O, pH 8.0
Coupling buffer	100mM $NaHCO_3$ 500mM NaCl in H_2O, pH 8.3
EBC lysis buffer	50mM Tris/HCl pH 8.0 120mM NaCl 0.5% NP-40 1x protease inhibitor tablet (Roche) per 7ml in H_2O
3x Loading buffer w/o β-mercapthoethanol	30% glycerol 6% SDS 0.003% bromphenol blue 187.5mM Tris in H_2O, pH 6.8
NET-N buffer	20mM Tris/HCl, pH 8.0 100mM NaCl 1mM EDTA 1% NP-40

2.5.2.2. Beads

Designation	**Company**
CNBr Activated Sepharose® 4 Fast Flow	GE Healthcare, Buckinghamshire, UK

2.5.3. Immunoprecipitation (IP) of Overexpressed Proteins

2.5.3.1. Buffers and Solutions

Designation	Composition
Non-denaturing lysis buffer (NDLB)	20mM Tris-HCl, pH 8.0 137mM NaCl 10% glycerol 1% NP-40 2mM EDTA 1x protease inhibitor tablet (Roche) per 7ml in H_2O
NET-N buffer	20mM Tris-HCl, pH 8.0 100mM NaCl 1mM EDTA 1% NP-40

2.5.3.2. Beads

Designation	Company
GammaBind™ Plus Sepharose™	GE Healthcare, Buckinghamshire, UK

2.5.4. Immunofluorescence (IF)

Designation	Composition/Company
Blocking Solution	1% BSA (w/v) in 1x PBS
DAPI	100mg/ml in 1x PBS
Fixation Solution	2% PFA (w/v) in 1x PBS
Mounting medium	Dianova, Hamburg, Germany
Permeabilization Solution	0.2% TritonX-100 (v/v) in 1x PBS
Quenching Solution	50mM Ammoniumchloride in 1x PBS

2.5.5. Enzyme-linked Immunosorbant Assay (ELISA)

2.5.5.1. Buffers and Solutions

Designation	Composition
ABTS	10mg/ml 2,2´-azino-bis (3-ethyl-benzothiazoline-6-sulfonate) in H_2O
Blocking buffer	2% Casein (w/v) in 1xPBS
Coating buffer	2,5µg/ml Streptavidin in H_2O
ELISA substrate buffer	100mM NaOAc 50mM NaH_2PO_4 in H_2O, pH 4.2
Streptavidin (1mg/ml)	250µg/ml streptavidin in H_2O
Substrate solution (volume per plate)	9,5ml ELISA substrate buffer 0.5ml ABTS 4µ H_2O_2

2.5.5.2. Peptides

Designation	Sequence	Company
HPV16L2 aa20-38	Biotin-KTCKQAGTCPPDIIPKVEG	PSL GmbH, Heidelberg, Germany
HPV16L2 aa28-42	Biotin-CPPDIIPKVEGKTIA	PSL GmbH, Heidelberg, Germany
HPV16L2 64-82	Biotin-SGTGGRTGYIPLGTRPPT	PSL GmbH, Heidelberg, Germany

2.6. Tandem-Affinity Purification (TAP)

2.6.1. Buffers and Solutions

Designation	Composition
Calmodulin binding buffer	10mM Tris-HCl, pH 8.0 150mM NaCl 1mM MgOAc 1mM Imidazole 0.1% NP-40 2mM $CaCl_2$ 10mM β-mercaptoethanol (to be added freshly) in H_2O
Calmodulin elution buffer	50mM NH_4HCO_3, pH 8.0 25mM EGTA in H_2O
Calmodulin wash buffer	50mM NH_4HCO_3, pH 8.0 75mM NaCl 1mM MgOAc 1mM Imidazole 2mM $CaCl_2$ in H_2O

Lysis Buffer	10% glycerol 50mM Tris-HCl, pH 8.0 100mM KCl 0.1% NP-40 2mM DTT (to be added freshly) 1x protease inhibitor tablet (Roche) per reaction in H_2O
TEV-buffer	10mM Tris-HCl, pH 8.0 150mM NaCl 0.1% NP-40 0.5mM EDTA 1mM DTT (to be added freshly) in H_2O

2.6.2. Beads

Designation	**Company**
Calmodulin Seoharose 4B	GE Healthcare, Buckinghamshire, UK
IgG Sepharose™ 6 Fast Flow	GE Healthcare, Buckinghamshire, UK

2.7. Peptide Pull Down (PPD)

2.7.1. Buffers and Solutions

Designation	**Composition**
EBC lysis buffer	50mM Tris/HCl pH 8.0 120mM NaCl 0.5% NP-40 1x protease inhibitor tablet (Roche) per 7ml in H_2O
Glycine	100mM glycine pH 2.8 in H_2O
PBS	137mM NaCl 2,7mM KCl 4,3mM Na_2HPO_4 1,47mM KH_2Po_4 pH 7.4 in H_2O
Sodium azide	10% sodium azide (w/v) in H_2O
TritonX-100	20% TritonX-100 (v/v) in H_2O

2.7.2. Beads

Designation	**Company**
Pierce™ Avidin Agarose	Thermo Scientific, Schwerte, Germany

2.7.3. Peptides

Designation	Sequence	Company
HPV16L2 aa20-38	Biotin-KTCKQAGTCPPDIIPKVEG	PSL GmbH, Heidelberg, Germany
HPV16L2 aa28-42	Biotin-CPPDIIPKVEGKTIA	PSL GmbH, Heidelberg, Germany
HPV16L2 64-82	Biotin-SGTGGRTGYIPLGTRPPT	PSL GmbH, Heidelberg, Germany

2.8. Pseudovirus Production

2.8.1. Material

Designation	Company
Benzonase (100.000 U/ml)	Merck, Darmstadt, Germany
Brij58	Sigma-Aldrich, Taufkirchen, Germany
1x DPBS	Gibco Life Technologies, Paisley, UK
OptiPrep™ (60% w/v)	Sigma-Aldrich, Taufkirchen, Germany
RNase A/T1 mix	Fermentas Thermo Scientific, St.Leon-Rot, Germany
Turbofect™ transfection reagent	Fermentas Thermo Scienific, St.Leon-Rot, Germany

2.8.2. Buffers and Solutions

Designation	Composition/Company
Brij58	10% Brij58 (w/v) in H_2O
Lysis buffer	140µl DPBS 9µl 10% Brij58 1µl RNase A/T1 mix
NaCl	5M NaCl in H_2O

2.9. Lentivirus Production

2.9.1. Buffers and Solutions

Designation	Composition/Company
Polyethylenimine (PEI) transfection reagent	1mg/ml PEI in H_2O, pH 7.0-7.4 Polyscience Inc., Eppelheim, Germany
1x Phosphate buffered saline (PBS)	137mM NaCl 27mM KCl 10mM Na_2HPO_4 1.8mM KH_2PO_4

2.10. Chemicals

All chemicals were of analytical grade or better and purchased from one of the following companies.

Company	Location
Applichem	Darmstadt, Germany
Fulka	Neu-Ulm, Germany
Gibco BRL	Eggenstein, Germany
Life Technologies	Karlsruhe, Germany
Fisher-Scientific	Schwerte, Germany
Merck	Darmstadt, Germany
Roche Diagnostics	Mannheim, Germany
Roth	Karlsruhe, Germany
Serva	Heidelberg, Germany
Sigma-Aldrich	Munich, Germany

2.11. Kits

Designation	Company
Chemiluniscence Kit PicoDetect	Applichem, Darmstadt, Germany
Gaussia Glow-juice BIG Kit	PJK, Kleinbittersdorf, Germany
Qiagen MaxiPrep Kit	Qiagen, Hilden, Germany
QIAprep Spin Miniprep Kit	Qiagen, Hilden, Germany
QIAquick Gel Extraction Kit	Qiagen, Hilden, Germany
QIAquick PCR Purification Kit	Qiagen, Hilden, Germany
StrataClone Blunt PCR Cloning Kit	Stratagene Agilent Technologies, La Jolla, USA

2.12. Laboratory Equipment

2.12.1. Electrical Equipment

Designation	Company
1420 Multilabel Counter Viktor	Perkin Elmar, Norwalk, USA
800 W microwave	Bosch, Gerlingen-Schillerhohe, Germany
Bacterial culture shaker	Informs AG, Bottmingen, Switzerland
Beckmann XL70 Ultracentrifuge	Beckmann Coulter, Krefeld, Germany
Bio GARD cell culture hood	The Baker Company, Sanford, USA
C1000™ Touch Thermal Cycler	BioRad, Munich, Germany
Combimag Red/RET magnetic stirrer	IKA, Staufen, Germany
Developing Machine AgfaCurix60	Agfa, Munich, Germany
Duomax 1030 shaker	Heidolph, Kelheim, Germany
EconoPump	BioRad, Munich, Germany

Electrophoresis chamber	Carl Roth GmbH, Karlsruhe, Germany
Electrophoresis gel slides	Carl Roth GmbH, Karlsruhe, Germany
Electrophoresis power supply ST 606 T	Gibco BRL, Eggenstein, Germany
Electrophoresis power supply ST PS 305	Gibco BRL, Eggenstein, Germany
F12-6x500 Rotor	Thermo Scientific, Waltham, USA
Function Line incubator	Heraeus, Hanau, Germany
Gel Doc EZ Imager	BioRad, Munich, Germany
GFC water bath	Grant Instruments, Cambridge, UK
Horizontal Gel Electrophoresis Horizon 11.14	Gibco BRL, Eggenstein, Germany
Ice maker	Hoshizaki, Willich-Munchheide, Germany
Impulse Sealer	RNS Corp, Taipei, Taiwan
Incubator Innova 4230	New Brunswick Scientific, Edison, USA
Integra pipetboy	Integra Bioscience GmbH, Fernwald, Germany
Labotect CO_2 incubator	Labotect, Göttingen, Germany
Leica DMIL microscope	Leica Microsystems, Wetzlar, Germany
Liebherr Comfort	Liebherr, Biberach, Germany
Liebherr MedLine	Liebherr, Biberach, Germany
Liebherr Premium	Liebherr, Biberach, Germany
Liebherr ProfiLine	Liebherr, Biberach, Germany
Megafuge 1.0	Heraeus, Hanau, Germany
Megafuge 1 S-R	Heraeus, Hanau, Germany
MicroPulser™ Electroporator	BioRad, Munich, Germany
Microscope for cell culture	Diavert Leitz, Wetzlar, Germany
Microscope for cell culture	Wilorat S Helmut Hund, Wetzlar, Germany
MilliQ ultra-pure water unit	Millipore Merck, Darmstadt, Germany
MR 2000/2002 magnetic stirrer	Heidolph, Kelheim, Germany
Multifuge 1 S-R	Heraeus, Hanau, Germany
Multiskan GO (ELISA reader)	Thermo Scientific, Waltham, USA
Nanodrop spectrophotometer	PegLab, Erlangen, Germany
Neubauer Counting Chamber	Neolab Migge, Heidelberg, Germany
Nitrogen tank Chrono	Messer, Krefeld, Germany
pH meter	Sartorius, Göttingen, Germany
Polyacrylamid Gel Electrophoresis Chamber	Hoefer, San Francisco, USA
PreCision 50-1200µl (multichannel)	Biozym, Hessisch-Oldendorf, Germany
Refrigerated Sorvall RC6+ centrifuge	Thermo Scientific, Waltham, USA
Refrigerated tabletop centrifuge 5417R	Eppendorf, Hamburg, Germany
Refrigerators and freezers	Liebherr, Ochsenhausen, Germany
Research Pro 1200 (multichannel)	Eppendorf, Hamburg, Germany
Research Pro 300 (multichannel)	Eppendorf, Hamburg, Germany
Sanyo CO_2 icubator	Sanyo/Panasonic Healthcare
Sartorius Scale	Sartorius, Göttingen, Germany

Sterile GARDR III Advance cell culture hood	The Baker Company, Sanford, USA
SW32-Ti	Beckman Coulter, Krefeld, Germany
SW41-Ti	Beckman Coulter, Krefeld, Germany
Tabletop centrifuge 5415 C	Eppendorf, Hamburg, Germany
Test-tube rotator	Snijders Scientific, Tilburg, Netherlands
TH-604	Thermo Scientific, Waltham, USA
Thermomixer 5436	Eppendorf, Hamburg, Germany
Thermomixer comfort	Eppendorf, Hamburg, Germany
Transblot SD chamber	BioRad, Munich, Germany
UC water bath	Julabo, Seelbach, Germany
Ultracentrifuge SorvallR Discovery 90 SE	Sorvall Hitachi, Newton, USA
Ultra-low freezer	Eppendorf Inc., Ensfield, USA
Varifuge RF	Heraeus, Hanau, Germany
Vibramax-VXR	IKA, Staufen, Germany
Vortex Genie 2™	Bender and Hobein, Ismaning, Germany
Western Blot Transfer Chamber	BioRad, Munich, Germany
Western Blot Exposition Cassette	Kodak, Stuttgart, Germany
Zeiss Cell Observer	Zeiss, Jena, Germany

2.12.2. Common use Equipment

Designation	**Company**
1,5 ml and 2 ml reaction tubes	Eppendorf, Hamburg, Germany
15 ml reaction tubes	TPP Trasadingen, Switzerland
50 ml reaction tubes	Greiner, Frickenhausen, Germany
25cm2, 75cm2 and 150cm2 tissue culture flasks	TPP Trasadingen, Switzerland
6, 10 and 15 cm cell culture plates	Greiner, Frickenhausen, Germany
6-, 12-, 24-, 48 and 96-well tissue culture plates	TPP Trasadingen, Switzerland
96-well LIA plate	Greiner, Frickenhausen, Germany
96-well plates polysorb	Nunc, Roskilde, Denmark
Amersham HyperfilmTM ECL	GE Healthcare, Buckinghamshire, UK
Bottle top filter	Costar, Coning, USA
Cell scraper	Sarstedt, Nümbrecht, Germany
Coverglasses 15mm	Carl Roth GmbH, Karlsruhe, Germany
Cryotubes, 2 ml	Carl Roth GmbH, Karlsruhe, Germany
Electroporation cuvettes (25 x 2 mm)	Peqlab, Erlangen, Germany
Examination gloves Blossom	Mexpo International Inc., USA
Examination gloves XCEED^{TM} Nitril	Starlab, Ahrensburg, Germany
Nitrocellulose membrane	GE Healthcare, Buckinghamshire, UK
Objekt slide	
One-time use filter, 0.2/0.4µm	Renner, Dannstadt, Germany

Parafilm “M”	American National Can, Chicago, USA
Petri dishes	Greiner, Frickenhausen, Germany
Pipettes (1000, 200, 20, 10 and 2µl)	Gilson Middleton, USA
Pipette Tipps (200µl, 10µl)	NerbePlus, Winsen/Luhe, Germany
Pipette Tipps (1000µl, 200µl)	Greiner, Frickenhausen, Germany
Pipette Tips (10µl)	Sorenson™ Bioscience, Salt Lake City, USA
Syringes and needles	BD Franklin Lakes, USA
Ultracentrifuge tubes Herolab 13.2ml PA	Beranek, Weinheim, Germany
Ultra-Centrifuge Tubes SW32	Beranek Laborgeräte, Weinheim, Germany
Whatman filter paper 3MM	Schleicher & Schuell, Dassel, Germany

2.13. Software

Designation	**Company**
Adobe CS4/CS6	Adobe, San Jose, USA
Clone Manager 9.0	Scientific Educational Software, Cary, USA
Eucaryotic Linear Motif Resource for functional Sites in Proteins (ELM)	www.elm.eu.org/
Endnote X5	Thomson Reuter, New York, USA
Fiji win64	
Graphpad Prism 5.0	GraphPad Software, La Jolla, USA
Microsoft Office 2003, 2010	Microsoft, Redmont, USA
Microsoft Windows XP/8	Microsoft, Redmont, USA
String 9.0 database	www.string-db.org
Wallac 1420 Workstation	Perkin Elmer, Norwalk, USA
ZEN Black	Zeiss, Jena, Germany

3. Methods

3.1. Cultivation and Manipulation of Prokaryotic Cells

3.1.1. Cultivation and Storage of Bacteria

The cultivation of bacteria was performed either in liquid LB medium or on agar plates, containing selective antibiotics. After transformation (4.1.3) of the bacteria, 20-150µl bacterial culture were plated on Agar plates containing the corresponding antibiotics and incubated at 37°C o/n. Each colony formed, originated from a single transformed bacterial cell. Therefore, one colony represents a single bacterial clone and each cell within this colony contains identical plasmid DNA. For the cultivation of bacteria in liquid LB medium, a single colony was transferred to a proper volume of liquid LB medium supplemented with the corresponding antibiotics and incubated at 37°C o/n on a shaker at 200rpm. Two ml liquid culture were used for purification of plasmid DNA by MiniPrep (4.3.1.2), whereas larger cultures of 250ml were used for Maxi Preparation (4.3.1.3). For long-term storage of verified (sequenced) bacterial clones, 1ml of a liquid culture was transferred to a 2ml cryotube and 300µl glycerol were added. The glycerol stocks were stored at -80°C.

3.1.2. Preparation of Electrocompetent Bacteria

The electrocompetent bacteria used for transformation (4.1.3) derived from the bacterial strain MegaX DH10. Before preparing the starting culture, MegaX DH10 were plated from a glycerol stock on a LB agar plate without antibiotics and incubated at 37°C o/n. A single colony was transferred to 25ml LB medium and inoculated at 37°C o/n on a shaker with 200rpm. After overnight incubation, 5ml of the bacterial culture were transferred to 400ml of fresh LB medium and inoculated at 37°C and 200rpm until the culture reached an optical density (OD_{600}) of 0.5-0.6. The bacterial culture was then chilled on ice for 30min and harvested by centrifugation at 6.000rpm for 10min at 4°C. The pellet was resuspended in 30ml ice-cold H_2O and transferred to a dialysis tube and dialysed against H_2O o/n at 4°C. The bacterial cells were then harvested by centrifugation at 4000rpm for 10min at 4°C and resuspended in 600µl ice-cold 10% glycerol solution. Ten µl of the bacterial suspension were diluted 1:100 in 990µl 10% glycerol and the OD_{600} was measured. The obtained OD_{600} was multiplied with the volume of the stock suspension (600µl) and the calculated value in µl of glycerol was added to the bacterial solution. Aliquots of 40, 80 and 120µl were prepared and snap-frozen in liquid nitrogen and stored at -80°C.

3.1.3. Transformation of Bacteria by Electroporation

For transformation, electroporation cuvettes were pre-cooled and an aliquot of electrocompetent bacteria (4.1.2) was thawed on ice. After the cell were thawed, 1µl of the corresponding ligation mix (4.3.2.4) or purified plasmid DNA was transferred to a 1,5ml reaction tube and mixed by pipetting with 40µl electrocompetent cells. The mix was transferred to a pre-cooled electroporation cuvette and exposed to an electric pulse of 2.5kV and 200Ω for approximately 5ms. This electric pulse led to the formation of pores in the cell wall and the following uptake of DNA by the electrocompetent bacteria. Subsequently after electroporation, 300µl pre-warmed (37^{o}C) LB medium without antibiotics were added to the cells which were then incubated at 37^{o}C for at least 1h. After incubation between 20-150µl of the bacterial suspension were plated on a selective agar plate and further incubated overnight at 37^{o}C to allow the generation of single clone colonies.

3.2. *Cultivation and Manipulation of Eukaryotic Cell*

3.2.1. Cultivation of Mammalian Cells

All cell lines were cultivated in an incubator at 37^{o}C, 5% CO_2 and 90% humidity. Passaging of the cells was performed when cells reached around 80% confluency. For this, the medium was aspirated and the attached cells were washed once with 1x PBS. To detach the cells from the cell culture flask, 0.05% trypsin EDTA or 0.25% trypsin EDTA was added to the cells, respectively, depending on the cell line used. The cells were incubated for 2-3 minutes and detached by gentle tapping the flask. The trypsin was then neutralized by addition of supplemented medium and after proper resuspension, the cells were transferred to a 15ml Falcon tube for centrifugation (1900rpm/5min). The cell pellet was resuspended in an adequate volume of fresh, supplemented medium, counted in a haemocytometer and seeded for experiments and maintenance of the stem culture.

3.2.2. Cryopreservation and Thawing of Mammalian Cells

For cryopreservation, the cells were cultivated in 150cm^2 culture flask until they reached a confluency of about 80%. The cells were then harvested by trypsinization and centrifugation, as described in 4.2.1. After centrifugation, the cell pellet was resuspended in 2ml cryomedium and aliqouted into 2 cryotube. Freezing of the cells was performed in a slow freeze chamber with isopropanol at -80^{o}C for at least 24h before the cells were transferred to liquid nitrogen. To thaw cryopreserved cells, the vial was incubated in the water bath at 37^{o}C until the suspension was thawed completely. The cells were immediately transferred to a 15ml Falcon tube containing 10ml supplemented medium and centrifuged at 1900rpm for 5min. This step was repeated once before

the cells were resuspended in a proper volume of supplemented medium and transferred to a new cell culture flask for cultivation.

3.2.3. Transfection of Mammalian Cells with Turbofect

For transfection of a 10cm cell culture dish, around 3-4x10^6 cells were seeded in 10ml supplemented medium and incubated at 37°C, 5% CO_2 (see 4.2.1) for 24h. The transfection was performed by preparing the transfection mix, containing 10-15µg plasmid DNA in 1ml medium without supplements and 2µl Turbofect per µg DNA (20-30µl). To allow the formation of the transfection complex, the mix was incubated at RT for 15-20min. After incubation the transfection mix was added drop-wise to the cells. For proper protein expression the cells were incubated with the transfection mix for 48-72h at 37°C. The amount of DNA and Turbofect was adjusted corresponding to manufacturer´s instructions for different cell culture plates (table 1).

Table 1: Overview of the transfection procedure in different formats

Cell Culture Plate	No. of adherent cells	Amount of DNA (µg)	Volume of Turbofect (µl)
96-well plate	0,5-1,2x10^4	0.2µg	0.4µl
48-well plate	1,0-3,0x10^4	0.5µg	1µl
24-well plate	2,0-6,0x10^4	1µg	2µl
12-well plate	0,4-1,2x10^5	2µg	4µl
6-well plate	0,8-2,4x10^5	4µg	6µl
15cm dish	6-8x10^6	20µg	40µl

3.2.4. Transfection of Mammalian Cells with Polyethylenimine (PEI)

For transfection of a 10cm cell culture dish, around 3-4x10^6 cells were seeded in 10ml supplemented medium and incubated at 37°C, 5% CO_2 (see 4.2.1) for 24h. To prepare the transfection mix, 62µl H_2O were transferred into a 15ml Falcon tube as well as 10µg DNA, 1.5ml medium without supplements and 31µl PEI transfection reagent. The mix was then vortexed for 10sec and incubated at RT for 10min to allow the formation of the transfection complex. After incubation, 8.5ml supplemented medium were added to the transfection mix and vortexed again. To apply the transfection mix to the cells, the medium was aspirated, the transfection mix was added and incubated at 37°C, 5% CO_2. The transfection mix was removed from the cells, 4-14h after transfection and fresh supplemented medium was added. For proper protein expression the cells were incubated for another 48h at 37°C, 5% CO_2.

3.2.5. siRNA Knockdown

All siRNAs used for the knockdown experiments were obtained from Qiagen in Hilden, Germany. The knockdown was performed in 2.4x10^4 HeLa cells, seeded in 500µl supplemented medium in a 24-well plate and incubated for 30-120min at 37°C, 5% CO_2. Meanwhile, the transfection mix was prepared by dilution of 75ng siRNA in 100µl medium without supplements. To complete the transfection mix, 4.5µl HiPerFect transfection reagent were added to the diluted siRNA and incubated at RT for 5-10min. The transfection mix was then added drop-wise to the cells and the plate was swirled gently to distribute the mix. To allow proper knockdown, the cells were incubated under normal growth conditions for 48h at 37°C.

3.3. Molecular Biological Methods

3.3.1. Purification of plasmid DNA

3.3.1.1. QIAprep Spin MiniPrep Kit

Isolation of plasmid DNA with the QIAprep Spin Mini Prep Kit was performed from a single bacterial colony previously cultured in 2ml liquid LB medium containing the corresponding antibiotics. The preparation of plasmid DNA was performed according to manufacturer´s instructions.

3.3.1.2. MiniPrep by Birnboim-Doly Method

Isolation of plasmid DNA according to the Birnboim-Doly method was performed from a single bacterial colony previously cultured in 2ml liquid LB medium containing the corresponding antibiotics. The cells were harvested from 1.5ml bacterial culture by centrifugation at 13.000rpm for 2min. The cell pellet was resuspended in 100µl glucose mix and incubated on a shaker for 5-10min at RT. To lyse the bacterial cells for the extraction of the plasmid DNA, 200µl lysis buffer were added and the mixture was incubated for 5-10min on ice. By addition of 150µl 3M NaAc and incubation on ice for 5-10min the lysis reaction was stopped. Afterwards, 450µl phenol were added to the lysed cells and the sample was incubated for another 5-10min on a shaker at RT followed by centrifugation at 13,000rpm for 5min. The sample was removed from the centrifuge and 380µl of the supernatant were transferred to a fresh tube containing 450µl Isopropanol. For precipitation of the plasmid DNA, the sample was then incubated at -70°C for 10min. The precipitated DNA was collected by centrifugation at 13.000rpm for 20-30min at 0°C and washed once with 500µl 70% EtOH (13,000rpm/ 5min/0°C). The washing step was repeated once using 500µl EtOH abs. instead of 70% EtOH. After the pellet was dried under the cell culture hood, it was resuspended in 60µl H_2O. The isolated plasmid DNA was stored at 4°C.

3.3.1.3. Qiagen MaxiPrep Kit

Isolation of plasmid DNA with the Qiagen MaxiPrep Kit was performed using 250ml LB medium with corresponding antibiotics which were inoculated with either a few µl from a liquid bacterial culture or from a bacterial glycerol stock. The preparation of the plasmid DNA was performed according to manufacturer´s instructions.

3.3.1.4. QIAquick Gel Extraction Kit

For purification of specific DNA fragments from an analytical agarose gel, the QIAquick Gel Extraction Kit from Qiagen was used. The DNA fragments were either produced by PCR or enzymatic restriction to cut a specific region of the plasmid DNA. After the DNA fragments were separated by agarose gel electrophoresis (4.3.3.1), DNA was visualized with the help of a 254nm UV-light to excise the corresponding part of the gel for purification. The following purification procedure was carried out according to the manufacturer´s instructions. After purification of the DNA, 5µl of the sample were analyzed on a mini agarose gel.

3.3.2. Manipulation of DNA

3.3.2.1. Polymerase Chain Reaction (PCR)

The Polymerase Chain Reaction (PCR) was performed to amplify the DNA sequences of interest for cloning into selected destination vectors. The DNA sequences were amplified using corresponding template DNAs encoding for the sequence of interest. Primers needed for the amplification process were generated with the help of Clone Manager CMSuite9 (3.9) and ordered as well as produced at MWG Eurofins, Ebersberg, Germany. Each Primer was generated for a specific cloning process, containing different restriction sites and potentially necessary additional sequences (e.g. Kozak sequence). The sites to be included into the primer sequence were selected depending on the specific destination vector used for later cloning steps. All PCRs were performed using the KOD HiFi DNA Polymerase Kit from Novagen/Merck, according to the manufacturer´s instructions (table 2 and table 3). The annealing temperature, as well as the number of amplification cycles, strongly depends on the primers used for the PCR reaction and were determined by testing different conditions.

Table 2: Constituents of PCR reaction mix and volumes

Component	Volume per reaction (50µl)
10-50ng template DNA	xµl
10x KOD Buffer #2	5µl
dNTPs (2.5mM each)	2µl
$MgCl_2$ (25mM)	2µl
Fwd Primer (100µM)	1µl
Rev Primer (100µM)	1µl
KOD Polymerase	1µl
H_2O	Add up to 50µl

Table 3: Standard PCR program for KOD HiFi Polymerase Kit

Temperature	Time	
98°C	3min	
98°C	20sec	32 cycles
60°C	10sec	
72°C	25sec	
72°C	5min	
4°C	∞	

3.3.2.2. StrataClone Blunt PCR Cloning Kit (TOPO cloning)

The cloning of blunt end PCR products into the TOPO vector was carried out using the StrataClone Blunt PCR Cloning Kit from Stratagene. The cloning procedure was performed according to manufacturer´s instructions using the Quick-Reference Protocol, provided with the kit.

3.3.2.3. Enzymatic restriction

To test isolated plasmid DNA for the absence or presence of a specific insert, 5µl of the DNA sample were transferred to a new Eppendorf tube. For enzymatic restriction a master mix was prepared containing the 2µl of the 10x buffer, 0.5µl RNAse, as well as 11µl H2O and 0.5µl of the specific enzyme/s per reaction. The 10x buffer used for the master mix is selected according to the recommendation of the manufacturer. Afterwards 45µl of the master mix were added to the DNA. The reaction was incubated at 37°C for at least 2h. To analyze the restricted plasmid DNA, 5µl reaction were mixed with 1µl 6x loading dye and a horizontal agarose gelelectrophoresis (4.3.3.1) was performed. For a preparative digest of DNA, which was used for ligation, the reaction was scaled up to a final volume of 200µl. The digest was performed overnight at 37°C. After incubation the

reaction was mixed with 6x loading dye and loaded on an analytical Agarose gel (4.3.3.1) and further extracted by gel purification (4.3.1.4).

3.3.2.4. Annealing of shRNA Oligonucleotides for Cloning

The forward and reverse oligonucleotides for the production of the lentivirus shRNA vectors were ordered and produced at MWG Eurofins in Ebersberg, Germany. The sequences were selected, using The RNAi Consortium (TRC) portal (http://www.broadinstitute.org/rnai/public/) either by a high score and non-overlapping target sequences or by comparison with previously verified target sequences used by Sigma-Aldrich for shRNA knockdown. The oligonucleotides were designed to create a double-stranded DNA fragment containing restriction enzyme-like cleavage ends (5´-AgeI, 3´-EcoRI) after annealing. Therefore, a digestion for cloning was not necessary. Furthermore, the oligonucleotides were ordered as phosphorylated version to increase the cloning efficiency in the later cloning steps. To generate the shRNA encoding DNA fragments for cloning, the corresponding forward and reverse oligonucleotides had to be annealed. Therefore, 2.5µl of the forward oligo (top-strand 100pmol/µl) and 2.5µl of the reverse oligo (bottom-strand 100pmol/µl) were diluted in 40µl H_2O and 5µl 10x annealing buffer. The reaction was heated up to 95°C for 5min in the water bath. After 5min the water bath was turned off and the oligonucleotides were annealed by cooling down to room temperature o/n. The annealed oligonucleotides were stored at 4°C until direct ligation into the dephosphorylated destination vector.

3.3.2.5. Dephosphorylation of DNA ends

Dephosphorylation was performed to prevent vector self-ligation while cloning. Therefore the 5´-phosphate groups of the cleaved vector were removed by addition of 2 units calf-intestinal alkaline phosphatase (CIP) after enzymatic restriction of the vector. The reaction was incubated at 37°C for 15min, followed by a second incubation at 58°C for 15min. To remove the phosphatases after dephosphorylation, the vector was gel extracted as described in 4.3.1.4.

3.3.2.6. Ligation of DNA fragments

The ligation mix was prepared on ice, according to manufacturer´s instruction from NEB (table 4). Vector DNA and insert were used in a molar ratio of 1:3. The ligation mix was either incubated at RT for 20min or at 16°C o/n.

Table 4: Ligation mix

Component	Volume per reaction (20µl)
10x T4 DNA Ligase Buffer	2µl
Vector DNA	0.020pmol
Insert DNA	0.060pmol
T4 DNA Ligase	1µl
H_2O	Add up to 20µl

3.3.3. Analysis of DNA

3.3.3.1. Agarose Gel Electrophoresis

The horizontal agarose gel electrophoresis was performed to analyze DNA fragments after analytical enzyme restriction. Therefore, 1% agarose gels were prepared in 1x TAE buffer (3.3.6.2) and 0.006% ethidium bromide was added (final concentration 0.72µg/ml). For standard analyses, three mini gels were prepared from 100ml agarose solution, whereas for analytical agarose gels, used for gel extraction of DNA fragments, 120ml of a 1% agarose solution was used for a single gel. Before application of the DNA samples to the gel, the samples were mixed with 6x DNA loading dye in a ratio 1:6. To determine the size of the corresponding DNA fragments, λ/HindIII-marker as well as 100bp-marker (3.3.6.2) was loaded on the gel. The electrophoresis was performed at 95V and the DNA fragments were visualized by 366nm UV-light. In case of an analytical gel, the voltage was increased to 120V for electrophoresis and further preparations were executed using a 254nm UV-light to prevent UV dependent mutations.

3.3.4. Protein Analysis

3.3.4.1. SDS-polyacrylamid Gel Electrophoresis (SDS-PAGE)

SDS-polyacrylamide gels were prepared by combining two kinds of gels with different pore size and pH, the stacking gel (3% polyacrylamide, pH 6.8) and the separation gel (12.5% polyacrylamide, pH 8.8). The protein samples were prepared by adding 3x loading buffer (containing SDS and β-mercaptoethanol) and a denaturation step of the sample at 95°C for 10min. After the polymerized SDS polyacrylamide gel was placed into the destined running system, 1x TGS running buffer was added and the protein samples to be analyzed as well as 3µl protein marker were applied to the pockets of the gel. Until the proteins reached the interface of stacking gel to separation gel the power was set to 80V and increased afterwards to 120V for separation of the proteins according to their molecular weight.

3.3.4.2. Coomassie-blue Staining of Protein Gels

After the protein samples had been separated according to their size by SDS-polyacrylamide gel electrophoresis (4.3.4.1), the protein bands were visualized by staining the gel with Gel Code® Blue Stain Reagent according to manufacturer´s instructions.

3.3.4.3. Western Blot Analysis

For western blot analysis, the proteins had to be transferred from the SDS-polyacrylamide gel to the nitrocellulose membrane, where the proteins could be analyzed by specific antibody detection. According to the transfer direction determined by the western blot transfer chamber, the polyacrylamide gel, soaked in 1x EMBL was placed on top of the nitrocellulose membrane which was previously placed on top of three 1xEMBL (3.4.3) saturated Whatman papers. The stack was covered with another three Whatman papers that had also been immersed in 1xEMBL. The transfer was then performed at 150mA/per gel for 75min to ensure an adequate transfer of all proteins to the nitrocellulose membrane. To block remaining protein binding sites on the nitrocellulose membrane, the membrane was incubated in 5% skim milk dissolved in 1xPBS-T at RT for 1h. Meanwhile, the primary antibody, directed against the protein of interest, was diluted in 5% skim milk PBS-T, according to manufacturer´s instructions. The antibody solution was then applied to the membrane and incubated either at RT for 1h or at 4^{o}C o/n. After incubation with the primary antibody, excess antibody was removed by washing the membrane three times with 1xPBS-T for 10min. The corresponding secondary antibody conjugated with horse reddish peroxidase (HRP) was diluted 1:10.000 in 5% skim milk PBS-T and added to the membrane (RT for 1h). The previously described washing steps were repeated after incubation of the secondary antibody to remove unbound antibody from the membrane. For detection of the proteins solution A, containing luminol plus enhancer and solution B, a peroxide solution of the chemiluniscence kit (3.9) were mixed in a 1:1 ratio and the membrane was incubated in the substrate solution for 1min. The position of the bound secondary antibody and therefore indirectly the protein of interest were visualized using light sensitive ECL films exposed to the emitted light of the luminescence reaction.

3.3.4.4. Determination of Protein Concentration by Bradford Assay

To determine the concentration of protein of a specific sample, a BSA calibration curve was generated by titration in a 96-well plate. Therefore a 10µg/µl BSA stock solution was diluted in H_2O to get a final concentration of 2µg/µl BSA. From this BSA starting dilution a 1:2 dilution series was prepared, starting at 2µg/µl up to 0.016µg/µl. H_2O alone was used as blank within the Bradford assay. The protein samples to be tested were used in 3 different dilutions (in H_2O), ranging from a 1:1

dilution to a 1:4 dilution. All the samples, as well as the calibration curve and the blank were tested in duplicates and the final volume of each sample to be measured was 5µl per well. According to manufacturer´s instructions the Bradford reagent was diluted 1:5 in H_2O and 200µl were added to each well. The absorbance at 595nm was measured after incubation of the Bradford reagent at RT for 5min and the protein concentration of the test samples were calculated based on the BSA calibration curve.

3.3.5. Mass Spectrometric Analysis

To identify potential interaction candidates, co-purified by TAP (4.4.1) or IP (4.4.2), the samples were handed over to the Genomics and Proteomics Core Facility (GPCF) at DKFZ for MS analysis. The samples were trypsinized, excised from a SDS gel and the peptides were analyzed by MS.

3.4. Immunological Methods

3.4.1. Immunoprecipitation (IP) from PsV Infected Cells

To prepare CNBr beads for IP, 0.57g CNBr sepharose powder (3.5.3.2) was gently resuspended in 10ml 1M HCl and incubated at RT for 20min while shaking. The beads were then transferred to a PolyPrep Chromatography column and washed four times to dryness with 15ml 1M HCl, followed by two washing steps using 15ml coupling buffer (3.5.3.1). One bead volume coupling buffer was then used to transfer the beads to a new 15ml Falcon tube and the 50% slurry was split in 5x 1ml fractions, transferred to a 1.5ml tube and the supernatant was discarded after centrifugation at 1,200rpm for 2min at 4°C. For antibody coupling 1µg antibody per 1µl beads was diluted in coupling buffer to a final volume of 750µl. The antibody suspension was added to the CNBr beads and incubated at 4°C o/n with end over end rotation.

After the coupling process, the supernatant was removed (1,200rpm/2min/4°C) and the beads were washed 4-5 times with 1ml coupling buffer. To block remaining binding sites on the CNBr beads, 1ml blocking buffer (3.4.3.1) was added and incubated at RT for 2h. The beads were then washed with five cycles of 1ml coupling buffer, followed by 1ml acetate buffer. The washing was finished by a final wash with 750µl coupling buffer followed by a single wash with 20% ethanol. The beads were resuspended 1:1 in 20% ethanol and stored at 4°C until further use.

For IP from PsV infected cells, $1{,}9x10^6$ HeLa or HEK 293TT cells were seeded in 6cm dishes and incubated at 37°C, 5% CO_2 o/n. The cells were then synchronized at 4°C for 30min and incubated for another 30min at 4°C after addition of PsV diluted 1:200 to allow binding of the viral particles to the cell surface. Different PsV were used for infection of the cells, containing HPV16 L1/L2 PsV, HPV16 L1

only PsV as well as AAV2 luciferase vectors as control. The cells were transferred to 37°C and incubated for 8h (PsV infection) and 6h (AAV2 infection), respectively. Afterwards, the cells were trypsinized for 30min at 4°C, harvested and washed with ice-cold 1xPBS. Centrifugation was performed at 1,900rpm for 5min. For lysate preparation, the pellet was resuspended in 500µl ice-cold EBC lysis buffer (3.5.3.1) and centrifuged at 13,000rpm for 10min at 4°C. Meanwhile, 40µl of the antibody coupled CNBr slurry was transferred to a new 1.5ml tube and washed three times with NET-N buffer (3.5.2.2). The cell extract was then added to the beads and incubated at 4°C o/n with end over end rotation.

The supernatant and therefore the non-bound protein was removed from the beads by centrifugation at 1,200rpm for 2min at 4°C and the beads were washed five times with 1ml NET-N buffer. After the excess buffer was removed completely, the beads were resuspended in 20µl 1x loading buffer without β-mercaptoethanol (3.5.3.1) and boiled at 95°C for 10min. The supernatant was collected in a new 1.5ml reaction tube and 10µl 3x loading buffer (+β-mercaptoethanol) was added. After denaturation of the sample at 95°C for 10min, it was stored at -20°C for further analysis by western blot and MS.

3.4.2. Immunoprecipitation (IP) of Overexpressed Proteins

IP was performed from HEK 293TT cell extracts previously transfected (4.2.3) with the Myc-tagged potential interaction candidate together with either HPV16L2 or an empty vector. The cell extracts were prepared by resuspending the cell pellet, previously washed with ice-cold 1xPBS, in 500µl NDLB lysis buffer (3.5.4.1) and incubated on ice for 30min. The lysate was cleared by centrifugation at 13,000rpm for 10min at 4°C.

For IP, 40µl Protein G sepharose slurry were transferred into a 1.5ml tube and washed twice with 500µl ice-cold NET-N buffer (3.5.4.1). All the centrifugation steps were performed at 1,200rpm for 1min at 4°C. The corresponding antibodies, used for IP were coupled to the beads by the addition of 200µl NET-N buffer containing 1µg antibody and incubation at 4°C o/n on a rotating wheel.

The cleared lysate was added to the antibody-coupled beads and incubated at 4°C o/n with constant rotation. To remove unspecifically bound contaminants, the beads were washed five times with NET-N buffer. After the last washing step, excess liquid was removed from the beads and 40µl 1x loading buffer were added. The sample was then denatured at 95°C for 10min and a small proportion (5µl) was used for western blot analysis whereas the remaining sample analyzed by MS.

3.4.3. Immunofluorescence (IF)

For the analysis of proteins by IF, $2x10^4$ HeLa cells were seeded on a cover glass, placed in a 24-well plate. The cells were transfected with the corresponding DNA constructs encoding for the proteins of interest (4.2.3).

At the beginning of the staining procedure, the cells were washed once with 1xPBS and fixed on the cover glass with 2% PFA at RT for 15min. To reduce autofluorescence based on the aldehyde fixation, 50mM ammoniumchlorid were added twice to the cells and incubated at RT for 5min. Permeabilization of the cells was performed using 0.2% TritonX-100 in PBS at RT for 10min followed by three washing steps with 1xPBS. Potential unspecific binding sites were blocked with 1% BSA in PBS at RT for 20-30min before application of the primary antibody diluted in 1% BSA at 37°C for 1h. Excess antibody was removed by washing the sample 4-5 times with 1xPBS to reduce unspecific staining and background fluorescence. The secondary antibody was also diluted in blocking solution (1:800) and a dilution of 1:100 DAPI (final concentration 1µg/ml) was added. The solution was applied to the cells and incubated at 37°C for 1h. Afterwards the cells were washed 4-5 times with 1xPBS and the cover glass was removed from the 24-well plate. One drop of mounting medium was applied to the cell covered side of the cover glass which was mounted onto a slide. To avoid drying-out of the sample, the margin of the cover glass was sealed with transparent nail polish. The sample was stored at 4°C under dark conditions to avoid bleaching of the fluorophores, coupled to the secondary antibody.

3.4.4. Enzyme-linked Immunosorbant Assay (ELISA)

To start the ELISA, a microtiter plate was coated with the corresponding coating buffer (3.5.7.2). In case of the biotinylated peptide ELISA, 50µl of a coating buffer containing 2.5µg/ml streptavidin was added to each well of the microtiter plate. The plate was then incubated at 37°C o/n without a lid, to allow the evaporation of the liquid and the coupling of the streptavidin to the surface of the plate. After coating, the remaining binding sites on the surface of the plate were blocked with 2% casein in PBS (blocking buffer) at RT for 1h. The peptides to be coupled to the plate were diluted in the blocking buffer to a final dilution of 0.25µg/µl. Fifty µl of the peptide solution were then added per well and incubated for another hour at RT. Unbound peptide was removed from the plate by three washing steps with 1xPBS-T before the primary antibody (1:200 in blocking buffers) was applied to the wells. The antibody was incubated at RT for 1h and the plate was washed three times to eliminate excess primary antibody. The corresponding secondary antibody with conjugated horseradish peroxidase was diluted 1:5,000 in 1xPBS-T and 50µl per well were added to the plate. After 1h at RT, the plate was washed three times with 1xPBS-T and 100µl substrate solution (3.5.7.2)

were added to each well. The reaction was carried out for 10-20min and the absorbance was measured at 450nm

3.5. Tandem Affinity Purification (TAP)

For TAP, 10x15cm dishes of HEK 293TT cells were transfected (4.2.3) with the corresponding DNA constructs. After 72h the cells were harvested by centrifugation at 1,900rpm for 5min and the cell pellet was washed twice with 1-5ml ice-cold 1xPBS. The cells were lysed for protein extraction by resuspending the pellet in 5ml lysis buffer (3.5.2.1) and incubating on ice for 30min. To remove cell debris from the protein extract, the reaction was centrifuged at 13,000rpm for 10min at 4^{o}C and the supernatant was collected for purification. The first purification step was performed by binding of the protein A part of the TAP-tag to IgG sepharose beads. Therefore 75µl IgG sepharose beads were transferred to a 1.5ml tube and washed 5 times with 1ml lysis buffer. After centrifugation at 1,200rpm for 2min at 4^{o}C, the IgG sepharose beads were added to the protein extract and incubated on a rotating wheel at 4^{o}C o/n.

To harvest the bound protein after incubation, the sample was centrifuged at 1,200rpm for 2min at 4^{o}C, transferred to a 1,5ml tube and the beads were washed three times with 1ml lysis buffer to remove unspecifically bound proteins and contaminants. Another three washing steps were performed using 1ml of TEV buffer (3.5.2.1). To elute the protein from the IgG beads, the beads were resuspended in 225µl TEV buffer and 75µl TEV protease (0.7mg/ml) were added to the sample. The cleavage reaction was performed at 4^{o}C o/n.

The eluted protein was collected by centrifugation at 1,200rpm for 2min at 4^{o}C and the supernatant was transferred to a 2ml tube. To avoid a loss of eluted protein with the IgG beads, the beads were resuspended twice in 300µl TEV buffer and centrifuged at 1,200rpm for 2min at 4^{o}C and the supernatant was harvested in the 2ml tube together with the supernatant from the initial centrifugation step. The TEV protease in the 900µl collected supernatant was inhibited by the addition of 5µl 1M iodoacetamid (5mM) and 7µl 1M $CaCl_2$. Meanwhile, the calmodulin beads were prepared for the second purification step by washing 75µl calmodulin beads 5 times with calmodulin binding buffer (3.5.2.1). The beads were then transferred to the collected TEV cleaved supernatant and incubated on a rotating wheel at 4^{o}C o/n.

The reaction was centrifuged at 1,200rpm for 2min at 4^{o}C and the beads were washed twice with 1ml calmodulin binding buffer and twice with 1ml calmodulin wash buffer (3.5.2.1). The bound protein was finally eluted by denaturation of the sample in 1x loading buffer (SDS and β-mercaptoethanol) at 95^{o}C for 10min.

Samples for analysis of the purification procedure were collected at each step of the purification process and denatured in 3x loading buffer for analysis by western blot.

3.6. Peptide Pull Down (PPD)

The PPD was performed with cell extract from HEK 293TT and HaCaT cells which had either been non-transfected or transfected with DNA encoding for a Myc-tagged version of the potential interaction candidate.

Biotinylated HPV16L2 peptides, aa 20-38, aa 28-42 and aa 64-81 were immobilized on avidin beads. Therefore, 100µg lyophilized peptide were resuspended in 400µl 1xPBS to get a final peptide concentration of 0.25µg/µl. Avidin beads were washed 3-4 times with 400µl 1xPBS/0.1% TritonX-100. After the last washing step, excess buffer was removed completely and the beads were resuspended 1:1 with the previously prepared peptide suspension. Thus, the final concentration of peptide to beads was 0.25µg peptide to 1µl avidin beads. To allow proper coupling of the peptides to the beads, the peptide-beads mix was incubated at RT for 3h on a rotating wheel. Remaining unbound peptide was removed afterwards by washing the beads 3 times with 1xPBS/0.1% TritonX-100. To generate a 50% bead slurry, the bead-bound peptides were diluted 1:1 in 1xPBS containing 0.1% sodium azide. The bead slurry was stored up to one month at 4°C.

The cells used for PPD were resuspended in a proper volume of EBC lysis buffer (3.5.4.1), incubated on ice for 30min and centrifuged at 13,000rpm for 10min at 4°C. The supernatant containing the protein extract was analyzed by Bradford assay and the total protein concentration was determined. 2mg total protein was pre-cleared using 80µl of the immobilized avidin bead slurry without peptide, which had previously been washed twice with EBC lysis buffer. The protein extract avidin mixture was incubated at 4°C for 1h with rotation and the supernatant was collected afterwards by centrifugation. To prepare the peptide-bound beads for PPD, 40µl of the corresponding slurry was washed once with EBC lysis buffer and excess buffer was removed carefully. The pre-cleared protein extract was then added to the peptide-bound beads and incubated at 4°C o/n on a rotating wheel.

The supernatant was removed from the beads and unspecifically bound contaminants were removed by washing the beads 5 times with 400µl EBC lysis buffer. Peptide-bound proteins were either eluted with two rounds of incubation in 2 bed volumes of 100mM glycin pH 2.8 with following pH neutralization using 1M Tris pH 8.0 or prepared for western blot analysis by denaturation of the proteins in 1x loading buffer at 95°C for 10min.

3.7. Pseudovirions (PsV)

3.7.1. Production

For each pseudovirus (PsV) production, 10x10cm tissue culture dishes with 3-4x10^6 HEK 293TT cells in 10ml supplemented medium were prepared and incubated at 37°C, 5% CO_2 for around 24h to allow attachment of the cells to the dish. The transfection using the corresponding plasmid DNAs, encoding the HPV late proteins and the Gaussia luciferase reporter was performed as described in 4.2.3. After incubation, the cells were harvested by resuspension and centrifugation at 1,900rpm for 5min. The pellet was washed with 1ml DPBS, transferred to a 1.5ml tube and centrifuged at 1,900rpm for 5min at 4°C. The pellet was resuspended in an adequate volume of lysis buffer (3.6.2), corresponding to the volume of the pellet and incubated at 37°C on a rotating wheel for 24h. The next day, the cell suspension was incubated on ice for 5min before adding 0.17 volumes 5M NaCl and another, 5min incubation on ice. Cell debris were removed by centrifugation at 10.000rpm for 5min at 4°C and the supernatant was transferred to a new 1.5ml tube. The pellet was resuspended in 300µl DPBS/0.8M NaCl and centrifuged for a second time at 10.000rpm for 10min at 4°C. The supernatant was combined with the supernatant from the previous centrifugation step, 1µl benzonase (100 units) was added and incubated at 37°C for 1h. The crude extract was harvested by centrifugation (10.000rpm/10min/4°C) and collected in a new 1.5ml reaction tube. A small aliquot of the crude extract was taken and analyzed in eight serial dilutions, starting at 1:1000 in a PsV-based infection assay (4.5.3). The remaining crude extract was used for PsV purification (4.5.2).

3.7.2. Purification of pseudovirions

PsV were purified on an iodixanol (OptiPrep™) density gradient. Therefore, a 27%, 33% and 39% Iodixanol solution in DPBS/0.8M NaCl was prepared from the 60% (w/v) iodixanol stock solution. Additionally, 100µl phenol red (0.005%) were added to 10ml of the 39% iodixanol solution and a SW41Ti centrifuge tube was prepared to produce the density gradient. The iodixanol solutions were then carefully stacked on top of each other, starting with 3.3ml 39% iodixanol solution, followed by 3.3ml 33% and 3.3ml 27% solutions. To allow softening of the interphases, the gradient was incubated at 4°C o/n. For purification of PsV from the crude extract, the collected extract (4.5.1) was carefully loaded onto the 27% iodixanol solution of the density gradient and centrifuged at 37,000rpm for 5h at 16°C. After centrifugation, eight fraction of 500µl were collected, starting from 1cm below the 39%-33% interface of the gradient. A needle was inserted into the wall of the centrifuge tube at the desired position and used as a drip to collect eight 500µl fractions drop-wise in 1.5ml LowBind reaction tubes. The collected fractions were put on ice immediately and the infectivity

was analyzed by an infection assay using a constant dilution of 1:1000 of each fraction (4.5.3). The fractions were stored at -80°C.

3.7.3. Pseudovirus-based Infection Assay

To test the crude extract (4.5.2) and the purified PsV fractions (4.5.3) for PsV infection activity, the crude extract was tested in a serial dilution of eight 1:2 dilution steps starting at 1:1,000. Whereas, purified fractions were tested in constant 1:1,000 dilutions. In each assay a neutralizing antibody control, using K18L2 in a final dilution of 1:1,000 and a neutralization control, using a final concentration of 1µg/ml carrageenan was used. The dilution of the crude extract, used for the neutralization control was 1:1,000 and the purified fractions used in the control were fraction 2 and fraction 3 of the gradient with a final dilution of 1:1,000. The neutralization controls served for distinguishing the luciferase activity of free Gaussia luciferase expressed during the PsV production process and the activity due to PsV infection during the PsV-based infection assay. First of all, the corresponding dilutions of either the crude extract or the fractions were prepared in supplemented medium and 50µl were added to each well of a 96-well cell culture plate. For the neutralization controls 50µl of a 1:500 dilution of K18L2 and 1:625 of a 1.25mg/ml stock solution carrageenan in supplemented medium were added to the corresponding PsV containing wells, respectively. The controls were incubated at RT for 20min. 50µl supplemented medium were added to the wells containing the crude extract or the purified fractions. Finally, 50µl of a $2{,}5x10^5$ per ml HeLaT cell suspension were added to each well. The plate was wrapped in polythene foil and incubated in a melamine chamber containing moist paper towels for 48h at 37°C and 5% CO_2. For read out of the luciferase activity, the corresponding cell culture plates were incubated at RT for 10min and 10µl supernatant were transferred to a white 96-well LIA plate. The Gaussia luciferase substrate was prepared by adding 100µl Coelenterazine (50X) to 10ml Glow Juice (3.9). 100µl substrate were added to 10µl supernatant and the activity was measured in a microplate luminometer after 5 and 15min.

To determine the specific dilution of a PsV preparation for use in further experiments, active fractions were pooled and tested in serial dilutions as described for the crude extract. In further experiments the corresponding PsV preparation was used with the dilution giving a RLU of 1,000,000 after 15min of substrate incubation. For storage 50µl aliquots of the pooled PsV preparation were prepared and stored at –80°C.

3.8. Lentiviruses

3.8.1. Production using Four Plasmid Transfection System

For the production of lentiviruses, using the four plasmid transfection system $3x10^6$ HEK 293TT cells were seeded in 10cm dishes and incubated at 37°C and 5% CO_2 o/n. HEK 293TT cells are well transfectable and usually show high transfection efficiency. However, unlike the Phoenix cells, this cell line does not express any lentiviral packaging proteins. Therefore the cells need to be transfected (4.2.4) with the packaging plasmids, encoding gag/pol, rev and VSV G, as well as the corresponding plasmid DNA to be packaged. After addition of the transfection mix, the cells were incubated at 37°C and 5% CO_2 for 24h. The medium was changed and the cells were incubated at 37°C and 5% CO_2 for another 24h. Forty-eight h after transfection, the supernatant was collected in a 15ml Falcon tube and the cells were discarded. To concentrate the produced lentiviruses, the collected supernatant were centrifuged at 13,500rpm for 5h at 4°C and the viral pellet was resuspended in 100µl 1xPBS. Aliquots of 20µl of each sample were prepared and stored at -80°C until further use.

3.8.2. shRNA Knockdown

The shRNA nucleotides were obtained from MWG Eurofins in Ebersberg, Germany and cloned into the pLKO.1 TRC control vector for production of lentiviruses (4.6.2). For transduction of the cells with the corresponding lentiviruses, $0{,}25x^4$ HeLa cells were seeded in a 96-well plate with a final volume of 200µl and incubated at 37°C, 5% CO_2 o/n. When the cells were around 30-50% confluent, the medium was removed and 100µl fresh medium containing polybrene with a final concentration of 4µg/ml were added. After gently swirling the plate, 0.8µl of the lentiviruses in 100ml fresh medium were added. The plate was incubated at 37°C, 5% CO_2 o/n before the medium was changed. After incubation for another 48h at 37°C, 5% CO_2 fresh medium was added to the cells containing 1µg/ml Puromycin for selection of transduced cells. Afterwards the cells were passaged as described in 4.2.1 and continuously expanded to bigger cell culture plates. After expansion to the $150cm^2$ flask, the lentivirus transduced knockdown cells were used for the PsV-based infection assay (4.5.3).

3.9. Computer-Based Analysis of Protein Sequences (in silico)

3.9.1. Eukaryotic Linear Motif Resource (ELM)

The ELM is an online tool for the prediction of potential functional sites in protein sequences. The program can only analyze functional sites which are described as linear motifs, which are then predicted based on regular expression patterns. Additionally, the results are filtered by cell compartment, phylogeny, globular domain clash and structure to provide core functionality. Though the ELM contains a large collection of potential functional sites, the analysis by ELM covers not the complete set of potential functional sites.

In addition to the HPV16 L2 full length sequence, also the identified short MEME motifs (4.7.1) were analyzed by ELM to identify potential functional sites in the sequence patterns recurring in different HPV types.

4. Results

4.1. Purification and Identification of Host Cell Proteins Interacting with HPV16 L2

The HPV L2 protein plays an important role in the early and late of a viral infection, though it is dispensable for the L1 capsid formation. It is known that L2 has several structural and non-structural functions during viral infection for example during viral entry. However, many functions of L2 during the different stages of the viral life cycle are still not known. Although some functional domains, mainly in the N-terminal part of the L2 sequence, have been described, potential functions in the remaining protein are still unrevealed. Therefore, three experimental approaches were conducted to identify novel HPV L2 interaction partners and to determine their function during viral infection.

First, the tandem affinity purification (TAP, 5.1.1) was applied in which HPV16 L2, fused to the TAP tag, was overexpressed in mammalian cells and purified by a two-step procedure. Second, cells were infected with HPV16 pseudovirions (PsV) and the L2 was precipitated using specific monoclonal antibodies directed against L2. The infection with PsV mimics the pathway of a natural infection and therefore allowed the co-purification of candidates interacting during viral entry. Third, a pull down was performed using three epitopes of HPV16 L2 (aa 20-38, aa 28-42 and aa 64-81). These epitopes have been demonstrated to be targets for (cross-) neutralizing antibodies, preventing HPV infection *in vitro* and *in vivo.* Based on this observation, the three epitopes analyzed in this experiment are supposed to have a specific function during viral infection, which might be disrupted by the antibody binding. All experiments were conducted under non-denaturing conditions, allowing the co-purification of L2 bound proteins for further analysis.

4.1.1. Tandem affinity purification of HPV16 L2 and potential interaction candidates

For a first identification of potential HPV16 L2 interaction partners, the tandem affinity purification (TAP) method was used. This two-step purification method is based on the expression of a HPV16 L2 TAP-tag fusion protein, which contains a calmodulin binding protein (CBP), a Tobacco Etch Virus Protease cleavage site (TEV) and Protein A (ProtA) fused to the target protein HPV16 L2. Four different versions of the TAP-tagged protein were produced for purification. First of all, a HPV16 L2 full length protein, containing the whole amino acid sequence of the uncleaved HPV16 L2. Besides, three overlapping HPV16 L2 fragments were fused to the TAP-tag: HPV16 L2_Fr.1 comprised amino acids 1-193, HPV16 L2_Fr.2 amino acids 130-334 and HPV16 L2_Fr.3 amino acids 262-473 (Figure 8A). HEK 293TT cells were transfected with the corresponding construct and the lysates were used for purification 72h post transfection.

In the first purification step of the TAP, the corresponding HPV16 L2 TAP tag fusion protein was purified by IgG Sepharose, allowing the binding of the ProtA part of the TAP tag to the beads (Figure 9B). Cellular proteins interacting with HPV16 L2 were co-purified because of the non-denaturing conditions of the cell lysis and the TAP procedure. After binding of the fusion protein to the beads, unspecifically bound contaminants were removed by several washing steps. To prepare the protein for the second round of purification it was eluted from the IgG beads by cleavage with the TEV protease, cutting off the ProtA part of the TAP-tag. The eluted protein was then used for the second purification step, where it was coupled to calmodulin beads assured by the CBP still fused to the HPV16 L2 construct. After binding to the calmodulin beads and the following washing steps, the beads were boiled in 1x SDS sample buffer to elute the protein and the co-purified potential interaction candidates. At each step of the purification procedure, an aliquot of the supernatant (snt) and the beads was taken and analyzed by western blot analysis (Figure 9A HPV16 L2 full length, B HPV16 L2_Fr.1, C HPV16 L2_Fr.2 and D HPV16 L2_Fr.3). TEV cleavage to remove the bound HPV16 L2 TAP-tag construct from the IgG beads, was performed twice (HPV16 L2_Fr.1, HPV16 L2_Fr.2 and HPV16 L2_Fr.3) or in case of the HPV16 L2 full length construct, three times. The obtained supernatants were used separately for binding to the calmodulin beads and the following purification steps. The western blots were stained with a HPV16 L2-specific antibody (K18L2 aa20-38, serum #7 and α-C-terminal-L2 8c-1) and therefore representing the efficiency of the purification process of the different HPV16 L2 TAP-tag constructs. Figure 9A presents the purification of the HPV16 L2 full length TAP-tag protein. The first two lanes show samples of the aliquots from the snt and the beads, taken after binding of the target protein to the IgG beads. The detected signal showed comparable amount of L2 protein in both samples, indicated by the red arrow: HPV6 L2 CBP-ProtA. This indicated that only 50% HPV16 L2 TAP-tag was bound and 50% of the protein stayed in the snt even after binding to the IgG beads. In the samples taken during the TEV cleavage, a similar result can be observed comparing the snt #1 sample with the sample from the beads, also indicating that about 50% of the target protein cannot be eluted properly from the IgG beads. Furthermore, the second and third round of protease cleavage could not elute additional target protein from the beads, since HPV16 L2 is hardly detectable in snt #2 and snt #3. The shift in the molecular weight of the target protein is based on the cleavage of the ProtA part (~15kDa) from the TAP-tag. The second purification step is represented by the lanes marked with “Purification by Calmodulin beads” also containing aliquots of the supernatants (snt #1, snt #2 and snt #3) and the beads (beads #1, beads #2 and beads #3), boiled in sample buffer after binding.

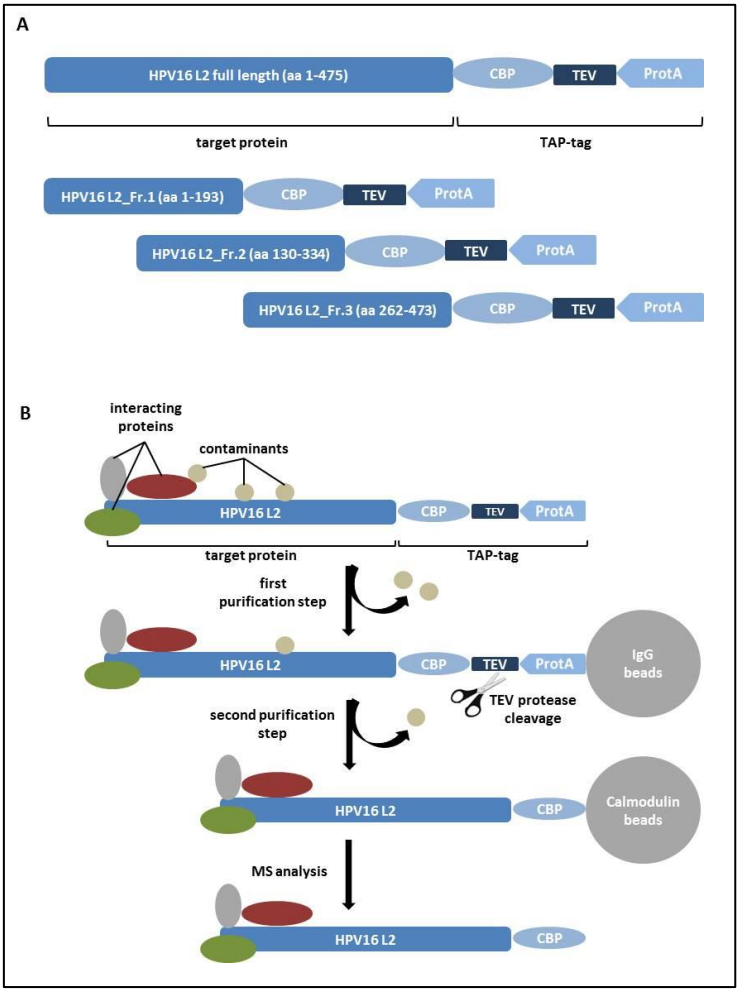

Figure 8 HPV16 L2 TAP-tag purification and constructs. A Overview of the HPV16 L2 constructs used for TAP. HPV16 L2 full length contains the amino acids 1-473, therefore the complete HPV16 L2 sequence. As controls for the MS analysis in the later steps, three overlapping HPV16 L2 fragments were generated. HPV16 L2_Fr.1, containing aa 1-193, HPV16 L2_Fr.2, containing aa 130-334 and HPV16 L2_Fr.3, containing aa 262-473. All HPV16 L2 constructs are fused to the TAP-tag consisting of a calmodulin binding protein (CBP), a TEV (Tobacco Etch virus) protease cleavage site (TEV) and a Protein A (ProtA). **B** Overview of the Purification Process. The target protein putatively interacts with cellular proteins (green, red and grey) upon expression in the cell. After lysis of the cells, the complex is purified in a first purification step by binding to IgG beads via the ProtA part of the TAP-tag and contaminants (beige) are removed by washing. The complex is eluted by TEV protease cleavage and purified by a second purification step mediated by binding of the CBP to Calmodulin beads and further washing steps. The beads are then boiled in 1x SDS buffer and the supernatant is analyzed by western blot analysis and mass spectrometry.

The detection of HPV16 L2 in these fractions demonstrated, that almost all of the target protein could bind to the beads, since there was no detectable signal in the snt samples. However, comparable amounts of HPV16 L2 protein can be detected in the TEV protease cleavage snt #1, representing the input of protein into the calmodulin purification and the bead fraction #1 of the purification by calmodulin, representing the bound target protein. In addition, the aliquots of bead sample #2 and bead sample #3 after calmodulin binding also show less HPV16 L2 compared to the bead sample #1, corresponding to the reduced HPV16 L2 input from snt #2 and snt #3 after the second and third TEV protease cleavage.

The western blots representing the TAP of HPV16 L2_Fr.1 (Figure 9B) and HPV16 L2_Fr.3 (Figure 9D) show similar results as the TAP of HPV16 L2 full length in A. Even though the ratios of purified protein were slightly different in some of the purification steps compared to the full length TAP, the amount of bound protein after the binding to the calmodulin beads was sufficient for MS analysis. A different observation could be made for the TAP process of HPV16 L2_Fr.2, shown in figure 9C.

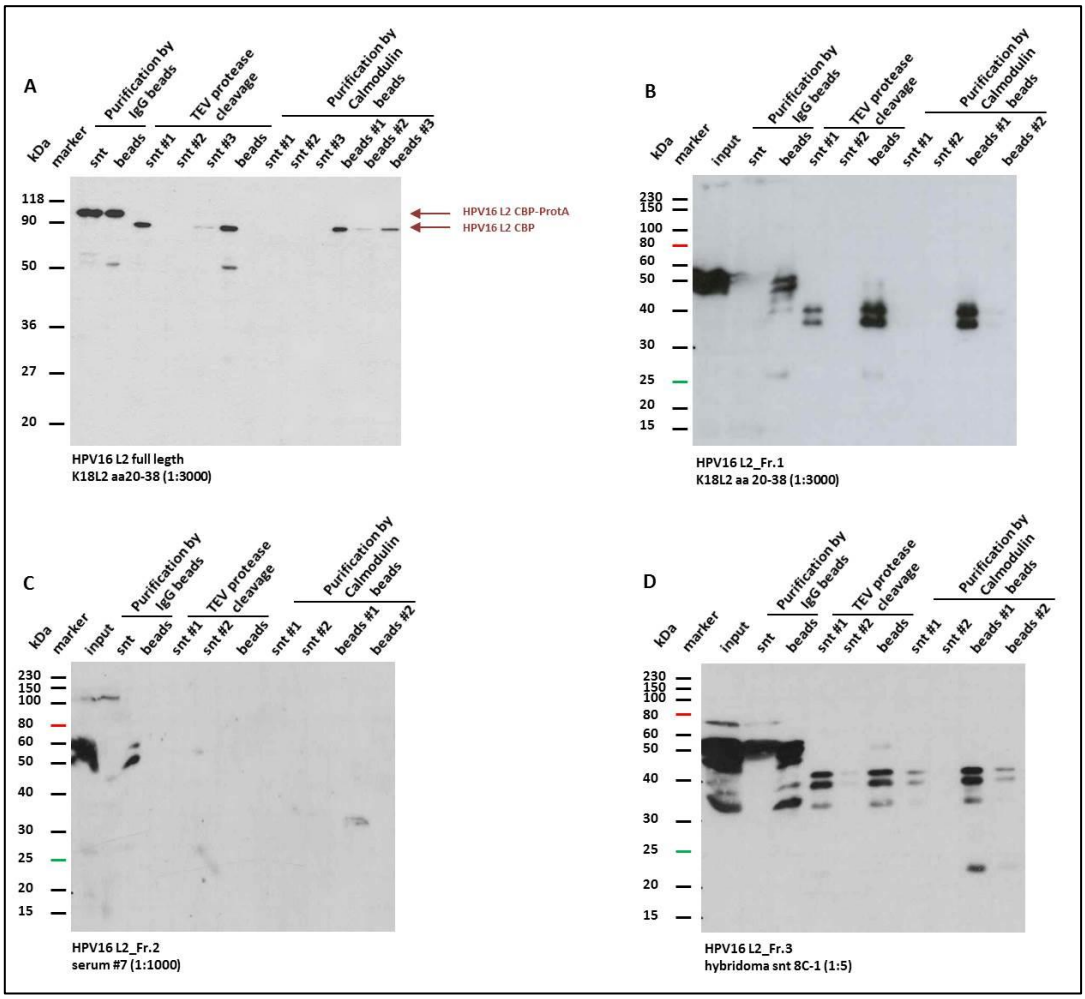

Figure 9 Tandem Affinity Purification. A western blot analysis of the purification using HPV16 L2 full length TAP-tag construct. During the purification process, aliquots of the supernatant (snt) and bead fractions were taken at each purification step. Volumes loaded to the gel for analysis were adjusted to the corresponding volumes used during the purification process. Red arrows indicate the HPV16 L2 full length protein containing the TAP-tag before and after TEV cleavage. **B** Purification using HPV16 L2_Fr.1 TAP-tag construct, containing HPV16 L2 aa 1-193. No antiserum was available, detecting this part of L2. **C** Purification using HPV16 L2_Fr.2 TAP-tag construct, containing HPV16 L2 aa 130-334. **D** Purification using HPV16 L2_Fr.3 TAP-tag construct, containing HPV16 L2 aa 262-473.

At the beginning of the purification, there was still some protein detectable in the input as well as in the beads after the IgG binding. However, after binding to the IgG beads, there is no protein detectable in any of the following samples. Since the protein can be detected neither in the snt fraction nor in the beads after TEV cleavage, the absence of a signal rather indicates that the polyclonal HPV16 L2 antibody (serum #7) was not suitable to detect HPV16 L2_Fr.2. Because of a lack of suitable antibodies detecting the amino acid region 130-334, the elution of HPV16 L2_Fr.2 was

analyzed by MS even without having a confirmation by western blot analysis. The corresponding snt from the calmodulin beads, boiled in 1x SDS sample buffer, were pooled and assigned to the Genomics and Proteomics Core Facility (GPCF) at the DKFZ for MS analysis.

4.1.2. Mass Spectrometric Analysis and Selection of Candidates from TAP

The samples derived from the tandem affinity purification were analyzed by MS at the GPCF at the DKFZ. Two peptide databases were screened to identify potentially interacting candidates. The first database used for the identification comprised peptides and the corresponding proteins derived from different species. Therefore it was used to confirm the presence of the HPV16 L2 protein and thus served as an additional control for a successful purification. The second database was restricted to peptides and the corresponding proteins derived from mammalian species and served as basis for the actual selection of potential candidates. However, for each of the purifications, the number of identified proteins in the different samples required the application of additional selection criteria to reduce the number of potential candidates. Therefore, several selection steps were executed to filter for the most promising potential HPV16 L2 interaction candidates (Figure 3).

First of all, the commonly contaminations, appearing regularly in MS analyses were discarded from the provided lists of identified proteins. Amongst others, these proteins were for example keratins and IgG proteins, which were introduced to the samples because of the handling or the material used during the purification process. Furthermore, identified proteins which were indicated to be derived from non-human species were analyzed for the existence of human equivalents. Therefore, the peptide sequences identified by the MS, representing the corresponding protein were compared to the set of peptides expected for a corresponding human protein. Only proteins that had the same peptide set for the human equivalent were selected for further analysis, whereas proteins without human equivalent were discarded. The remaining proteins were then compared between the different samples analyzed. For this, each protein hit was checked for its appearance in each protein list derived from the other TAP purifications. Proteins showing up either in a single screen or in more than one but in screens using overlapping target proteins were considered as potential partners of HPV16 L2. Proteins appearing in the protein lists of non-overlapping target proteins, not sharing any amino acid sequences (HPV16 L2_Fr.1 and HPV16 L2_Fr.3), were eliminated from the lists of potential interaction candidates. In order to further reduce the number of potential candidates and increase the chance of selecting the most promising candidates, also protein hits from a single screen were finally discarded, even though this might lead to elimination of true interaction partners. After the selection steps, a final set of 29 potentially specific interaction candidates remained and were checked in detail by literature research. For further experiments, the focus was set on proteins that

had already been published to have a potential function in context of viral infection of any virus, except HPV. This selection procedure reduced the number of potential HPV16 L2 interaction candidates to a set of 12 potential candidates (Table 5).

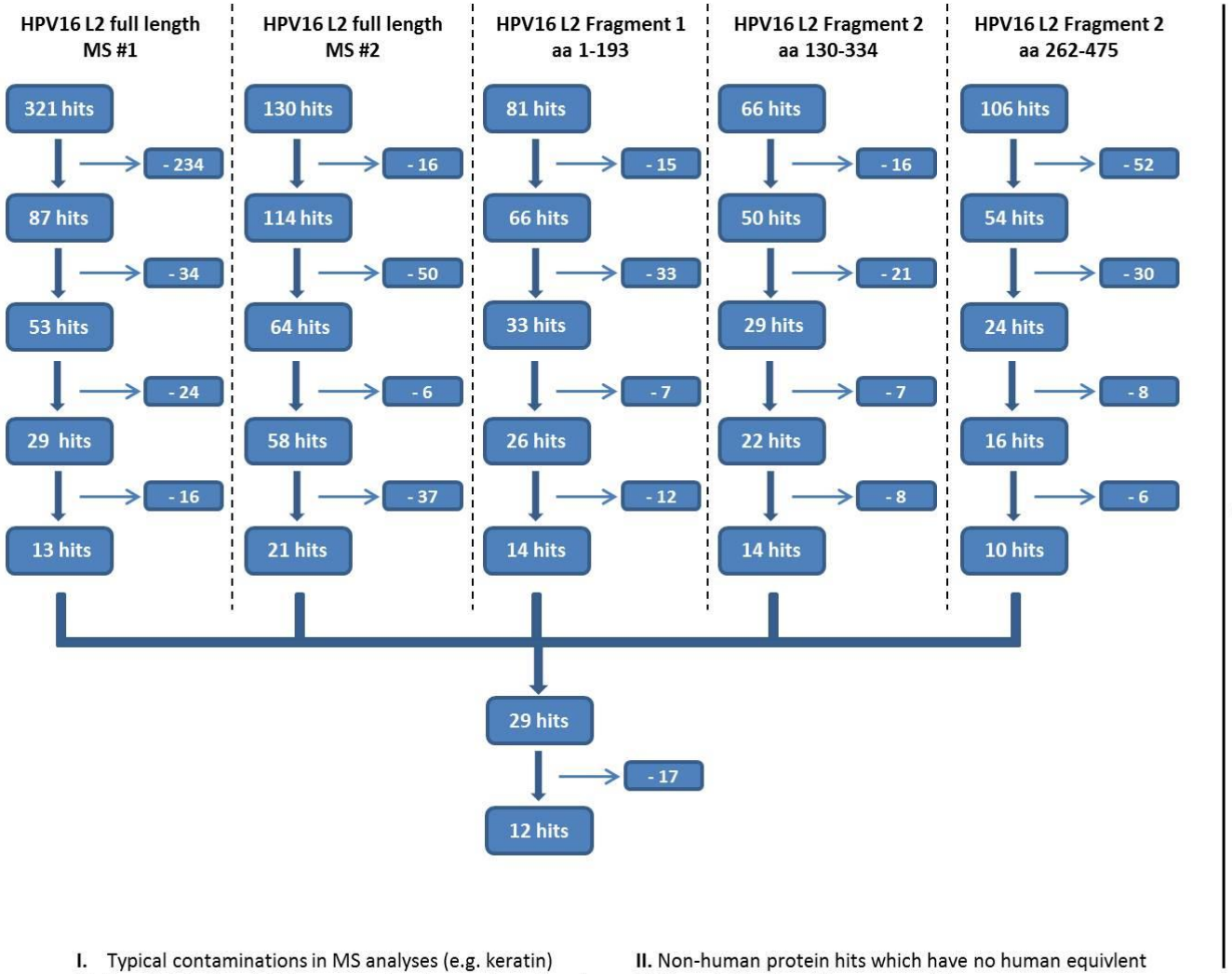

Figure 10 Overview of candidate selection. The TAP was performed twice, using the HPV16 L2 full length TAP construct and once with each of the L2 fragments (HPV16 L2_Fr.1, HPV16 L2_Fr.2 and HPV16 L2_Fr.3). Each MS analysis revealed a different number of protein hits from which the generally known contaminants, like keratins were exclude in the first step of the selection procedure (step I.). Since peptides identified in the MS analysis were compared with a database of mammalian proteins, not all of the listed proteins were of human origin. Therefore the non-human proteins listed had to be analyzed in detail if the detected peptide set is equivalent to corresponding human proteins (step II.). Proteins missing a human equivalent were discarded from the candidate list. In the third step the five protein hit lists were compared among each other, to identify proteins from non-overlapping fragments, e.g. HPV16 L2_Fr.1 and HPV16 L2_Fr.3 (step III.). To further reduce the number of potential candidates, proteins that have not been validated by a second screen were also discarded from the list of potential candidates (step IV.). From the remaining 29 candidates, 12 were selected based on literature research and their potential function in context of viral infection (step V.).

Table 5: Potential HPV16 L2 interaction candidates identified by tandem affinity purification

Protein/Description	HPV16 L2 fl.	HPV16 L2_Fr.1	HPV16 L2_Fr.2	HPV16 L2_Fr.3
HPV16 L2*	6 peptides	2 peptides	3 peptides	-
Sorting nexin 17 (SNX17) (aa 160-164, aa 254-258)**	-	6 peptides	2 peptides	-
eEF1A1 (elongation factor 1 alpha)	11 peptides	-	2 peptides	-
CAPN2 (Calpain large subunit 2)	4 peptides	3 peptides	-	-
PSMD12 (26S proteasome non-ATPase regulatory subunit isoform 12)	2 peptides	2 peptides	-	-
YWHAZ (14-3-3 protein/cytosolic phospholipase A2)	1 peptide	2 peptides	-	-
PSMD11 (26S proteasome subunit 11)	1 peptides	2 peptides	-	-
FLG-2 (Filaggrin 2)	1 peptide	-	-	1 peptide
CSE1L (Exportin-2)	2 peptides	2 peptides	-	-
Skp1 (S-phase kinase-associated protein 1)	1 peptide	-	-	1 peptides
TGM3 (Transglutaminase E3)	-	-	1 peptide	1 peptides
hnRNPK (transformation upregulated nuclear protein)	3 peptides	-	1 peptides	1 peptides
IRS4 (insulin receptor substrate 4)	2 peptides 4 peptides	-	-	4 peptides
CAND1 (cullin-associated NEDD8-dissociated protein 1)	3 peptides	2 peptides	-	-

* representing the target protein
** previously published HPV16 L2 interaction partner
The number of peptides indicated, describes the number of independent peptides identified for the corresponding protein.

4.1.3. Immunoprecipitation of L1 and L2 from PSV infected cells (PsV-IP)

Another approach to identify potential HPV16 L2 interaction candidates was the identification of proteins co-purified by IP from cells infected with HPV16 PsV. In contrast to the tandem affinity purification, where the HPV16 L2 constructs were overexpressed in the cells, the infection with PsV was performed with a non-tagged version of the L2 protein in context of the HPV16 capsid. This was supposed to mimic the natural infection pathway *in vitro*. The infection with HPV16 PsV allowed the L2 protein to meet potential interaction partners on its way into the cells in respect of its packaging state within the capsid. However, a disadvantage of the IP from infected cells was based on L1/L2 stoichiometry of the HPV capsid, containing 72 pentamers of the L1 protein but only estimated 12 molecules of the HPV16 L2 protein.

4.1.3.1. Selection of antibodies suitable for PsV-IP from infected cells

To select suitable antibodies for the IP of HPV16 L2 from cell extracts, HEK 293TT cells were infected with HPV16 PsV for 5h, 6h, 7h, 8h and 9h after synchronization of the PsV binding to the cell surface. After the indicated time of infection, cells were lysed and the cell extract was used for purification of HPV16 proteins, using different L1- and L2-specific antibodies, respectively, coupled to Protein G Sepharose. Moreover, purified HPV16 PsV, in a non-cellular context, were tested in the IP, to verify the general precipitation capability of the specific antibodies. For this initial test, two HPV16 L1-specific antibodies were used, the 1.3.5.15_L1 which is a mouse derived L1-specific monoclonal antibody and the 4543 rabbit L1-specific polyclonal antiserum. These antibodies served as a positive control, since both of them are able to precipitate the highly abundant L1 from the infected cells. Furthermore, three HPV16 L2-specific monoclonal mouse antibodies were tested for their ability to precipitate HPV16 L2 from infected cells. K1L2 aa64-81, targeting the amino acid region aa 64-82 whereas the antibodies K4L2 aa20-38 and K18L2 aa20-38 are raised against the L2 region aa 20-38. In addition to the L1- and L2-specific antibodies, a HPV16 E7-specific antibody was used as a negative control. After precipitation, the beads were boiled in 1x SDS sample buffer to elute the precipitated proteins for the western blot analysis (Figure 11).

Analysis of HPV16 L1-specific antibodies for PsV-IP from infected cells

Figure 11A shows the results of the HPV16 L1 precipitation using the 1.3.5.15_L1 and the 4543 antiserum. The detection was performed with a mouse-monoclonal HPV16 L1-specific antibody (MD2H11_L1). Detection of the HPV16 L2 protein was neglected, due to the low abundance of HPV16 L2 and hypothesis that even after 9h the L1 and the L2 protein are still assembled in the capsid and not yet dissociated. Consistingly, L1 co-precipitated with L2, using L2-specific antibodies. In both IPs

(Figure 11A), the HPV16 L1 is clearly detectable at about 55kDa (red arrow HPV16 L1) with a detection peak at 8h post infection. Additional, the positive control (PsV only) confirms the precipitation ability of the used antibodies, whereas the negative control from w/o PsV does not show any detectable HPV16 L1. Since the 1.3.5.15_L1 as well as the antibody used for the detection in the western blot derived from the same species (mouse), the heavy chain of the 1.3.5.15_L1 (~50kDa) appears as an additional signal in all of the samples derived from the IP with 1.3.5.15_L1 (red arrow Ab heavy chain). The 1.3.5.15_L1 seemed to be more efficient, demonstrated by stronger HPV16 L1 signals detected in the samples of the 1.3.5.15_L1 IP.

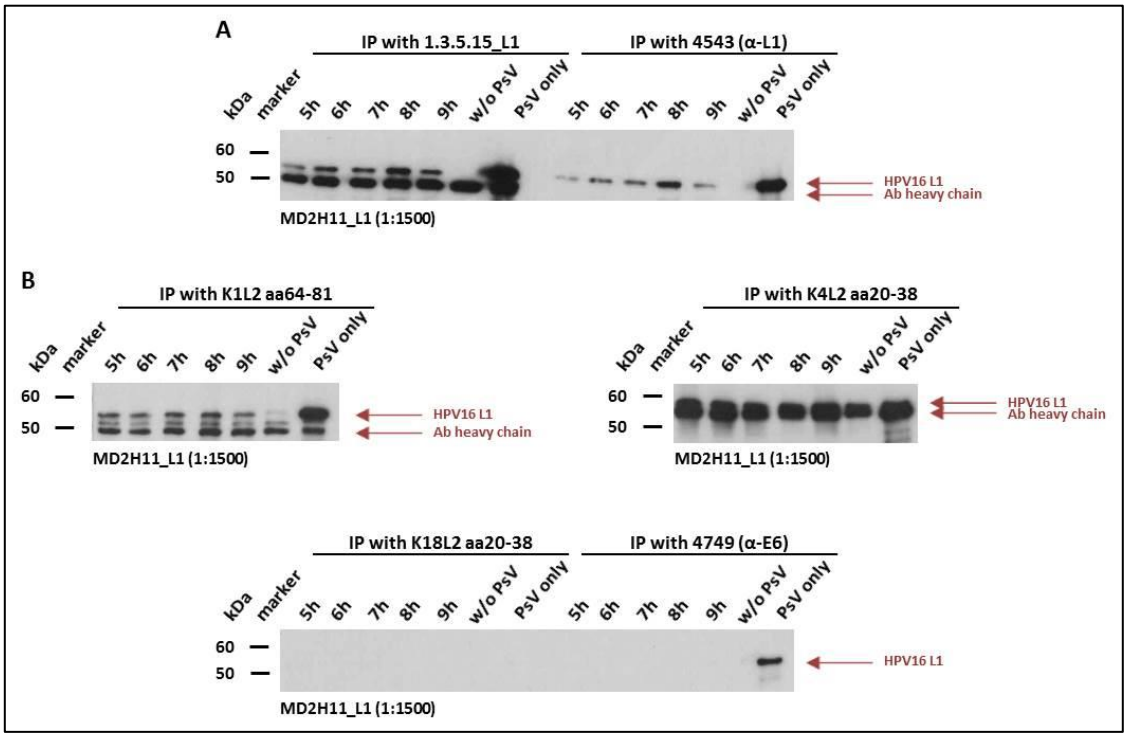

Figure 11 Western blot analysis of IP from PsV infected cell extracts. A IP was performed using the HPV16 L1-specific antibodies 1.3.5.15_L1 (mouse monoclonal) and 4543 (rabbit polyclonal). The analyzed samples were collected 5h, 6h, 7h, 8h and 9h after PsV infection. In addition cell extract from non-infected cells as well as PsV only were analyzed after IP with the indicated antibodies. Red arrows indicate bands corresponding to either HPV16 L1 or IgG heavy chain. **B** The IP was performed with HPV16 L2-specific antibodies to select for a suitable antibody for the PsV-IP experiment. In addition the 4749 (HPV16 E6-specific) antibody was used as negative control. Samples were collected as describe in A. The IP using the K1L2 aa64-81 antibody showed a faint signal in the control w/o PsV which was probably because of a spillover while loading of the gel. Besides, HPV16 L1 was detected in the PsV only sample of the 4749 IP probably due to unspecific precipitation.

Analysis of HPV16 L2-specific antibodies for PsV-IP from infected cells

In the experiment shown in figure 4B the IPs were performed with the HPV16 L2-specific antibodies K1L2 aa64-81, K4L2 aa20-38 and K18L2 aa20-38 and the precipitation negative E7 antibody 4749. The detection of the western blot was performed with the HPV16 L1-specific antibody MD2H11_L1. Successful precipitation of the PsV could be demonstrated with K1L2 aa64-81 and K4L2 aa20-38. The HPV16 L1 protein was detected in all of the samples infected with HPV16 PsV (5h, 6h, 7h, 8h and 9h) as well as in the positive control (PsV only). As described previously, a detection peak could be

observed after 8h, using the K1L2 aa64-81 for precipitation. Additional bands detected in these samples derive from the heavy chain of the antibody, since the precipitation as well as the detection was performed with mouse derived antibodies. For the K4L2 aa20-38 IP samples, the observation of a detection peak was not clear, since the L1 and the heavy chain formed a strong double band in the infected samples and the positive control (PsV only). Because of the signal intensity and the proximity of the two signals, it is not clearly visible if there are differences in the IP efficiency at the different time points after infection. The lower panel in Figure 4B shows the results of the IPs using K18L2 aa20-38 (L2-specific) and 4749 (E7-specific). Even after infection, none of the two antibodies showed precipitation of PsV, demonstrated by the absence of a detectable L1 signal. However, the western blot shows a signal after IP of PsV only with the E7-specific 4749 antibody at the expected molecular weight of HPV16 L1, indicating that there might be some unspecific binding of L1 to the beads coupled with 4749. Based on the results in Figure 4, the antibodies 1.3.5.15_L1, K1L2 aa64-81 and K4L2 aa20-38 were selected for further experiments to identify potential HPV16 L2 interaction candidates.

4.1.3.2. Covalent binding of suitable antibodies to CNBr-beads

Since the previous experiment demonstrated a high abundance of IgG in the samples after IP when using Protein G coupled antibodies, an optimization of the IP protocol was necessary to reduce IgG contamination for MS analysis. For this, the Protein G Sepharose was replaced by CNBr beads which allow a covalent coupling of antibody and where supposed to reduce the amount of IgG in the samples. First of all the coupling efficiency of the selected antibodies (5.1.3.1) to the CNBr beads was determined by testing different aliquots, taken during the coupling procedure by SDS-PAGE. Aliquots to be tested were taken before coupling to the CNBr beads (Figure 12, input), from the supernatant (snt) after coupling and the beads (beads). In addition to the selected antibodies from 5.1.3.1, the A20_AAV2 antibody was used in the experiment. The A20_AAV2 antibody served as negative control in the following IP experiment.

Coupling efficiency of different antibodies to CNBr beads

Figure 12 demonstrates that the coupling was successful for all of the antibodies used in the experiment. In each sample, the input showed a high amount of heavy and light chain. The signal disappeared after the coupling step (snt), indicating that the IgGs are almost completely bound to the beads. Even after denaturation, there was only a faint signal detectable (beads), representing the corresponding heavy and light chain. The SDS-PAGE showed clear differences in the amount of antibody used in the different input samples. Nevertheless, the results showed that the coupling to

the CNBr beads is highly efficient and might be advantageous compared to the use of Protein G Sepharose because of reduced abundance of IgG contaminations in the samples.

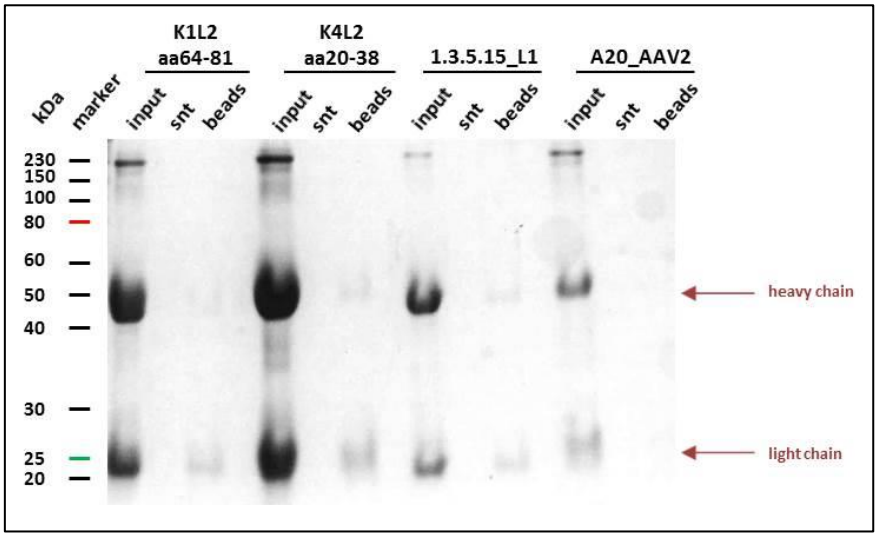

Figure 12 Coomassie staining of antibody coupling to CNBr beads. The coupling efficiency of different antibodies (K1L2 aa64-81, K4L2 aa20-38, 1.3.5.15_L1 and A20_AAV2) to CNBr beads was tested using the standard protocol provided by the manufacturer. On the Coomassie-blue stained SDS gel, aliquots of the input (amount of antibody used for the coupling procedure), the supernatant (snt) after coupling and the beads were analyzed. The arrows indicate the heavy and light chain of the antibodies.

Immunoprecipitation of PsV from infected cells using CNBr-coupled K1L2 aa64-81

An initial IP experiment to test CNBr-coupled antibody for PsV precipitation was performed using the K1L2 aa64-81 in two different concentrations (1µg/µl and 2µg/µl) (Figure 13). For this, CNBr-coupled K1L2 aa64-81 was used in the experimental setup describe in 5.1.3.1. The western blot in Figure 13 shows the detection of HPV16 L2 by K4L2 aa20-38 (upper panel) as well as the detection of HPV16 L1 by MD2H11_L1 (lower panel). As described previously, the IP was performed 5h, 6h, 7h, 8h and 9h after infection with HPV16 PsV as well as from cell extract of non-infected cells (w/o PsV).

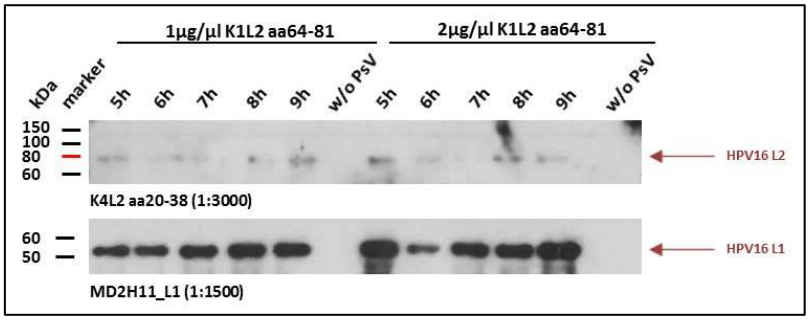

Figure 13 Western blot analysis of IP using CNBr coupled K1L2 aa64-81 antibody. 1µg/µl K1L2 aa64-81 and 2µg/µl K1L2 aa64-81 were coupled to CNBr beads. The following IPs were performed at different time points after PsV infection (5h, 6h, 7h, 8h and 9h) and as a negative control cell extract of non-infected cells was used for IP (w/o PsV). The upper panel shows a western blot using HPV16 L2-specific antibody (K4L2 aa20-38) whereas the lower western blot shows the detection with a HPV16 L1-specific antibody (MD2H11_L1), suitable for the detection of denatured protein. The arrows indicate either HPV16 L2 or HPV16 L1 in the corresponding blots.

All time points post infection showed a clear HPV16 L1 signal, for the IP with either 1µg/µl K1L2 aa64-81 or the 2µg/µl K1L2 aa64-81. In addition, the absence of an L1 signal in the non-infected control samples could be observed. However, for the lower concentration of K1L2 aa64-81, the previously described peak of HPV16 L1 detection at 8h could be observed, though, the differences in the signal intensity comparing the different time points are not as pronounced as in Figure 4. However, the IPs with the higher amount of K1L2 aa64-81 showed the strongest L1 signal at 5h post infection and a constant increase from 6h to 9h post infection. The detection of HPV16 L2 revealed only faint bands, due to the small abundance of HPV16 L2 within the HPV capsid. Nevertheless, the L2 protein could be detected in each sample except the w/o PsV control. The results of the precipitation experiment demonstrated that the IP using antibodies coupled to CNBr beads lead to efficient precipitation of the HPV16 capsids from infected cells and further reduced the amount of IgG contaminations within.

4.1.3.3. PsV-IP from infected cells using CNBr-coupled antibodies

The IP of PsV to be analyzed by MS was performed by infecting either HEK 293TT or HaCaT cells with HPV16 PsV, containing the L1 and the L2 protein (HPV16 L1/L2) or HPV16 PsV, containing only the L1 protein (HPV16 L1 only) for 8h. The L1 only PsV infection served as a control to distinguish potential HPV16 L1- from HPV16 L2-interaction candidates, since candidates of both proteins were co-purified by precipitation of the assembled HPV16 capsids. As an additional control for the MS analysis, another batch of cells was either infected with AAV2 for 6h or mock infected (w/o virus). The IP was performed from each infection, using four different antibodies, two HPV16 L2-specific antibodies, targeting different regions of the protein (K1L2 aa 64-81 and K4L2 aa 20-38), one HPV16 L1-specific antibody (1.3.5.15_L1) and the A20_AAV2 antibody. The antibodies were previously coupled to CNBr beads in a ratio of 1µg antibody to 1µl beads. Aliquots of the input from the infection, the supernatants (snt) and the beads were taken during the precipitation procedure and analyzed by western blot before samples were analyzed by MS.

Figure 14 shows the result of the IP of HPV16 L1/L2 and HPV16 L1 only PsV, whereas the upper panel was detected with an L2-specific antibody (K4L2 aa20-38) and the lower panel with the MD2H11_L1. The detection of HPV16 L2 did not lead to any dependable result, since the method was not sensitive enough to detect the small amount of HPV16 L2 in the IP samples. However, detection with the HPV16 L1-specific antibody demonstrated that the L1 protein could be found in the aliquots of the IP, the α-L1 antibody 1.3.5.15_L1 but also the L2-specific antibodies K1L2 aa64-81 and K4L2 aa20-38 (Figure 14A). HPV16 L1, present in the aliquots of the snt indicated the unbound L1 proportion. This might be due to saturation of the binding capacity of the beads coupled antibody sites. The detection of HPV16 L1 in the aliquots taken from the bead fractions after purification demonstrated the

precipitated L1 by K1L2 aa64-81, K4L2 aa20-38 and 1.3.5.15_L1. Compared to K1L2 aa64-81 and 1.3.5.15_L1, the IP using K4L2 aa20-38 showed a reduced level of precipitated L1, indicating lower precipitation efficiency. The IP of HPV16 L1/L2 PsV with the A20_AAV2 antibody therefore showed only a HPV16 L1 signal in the input and snt samples. There is no detectable L1 signal in the bead fraction of the IP.

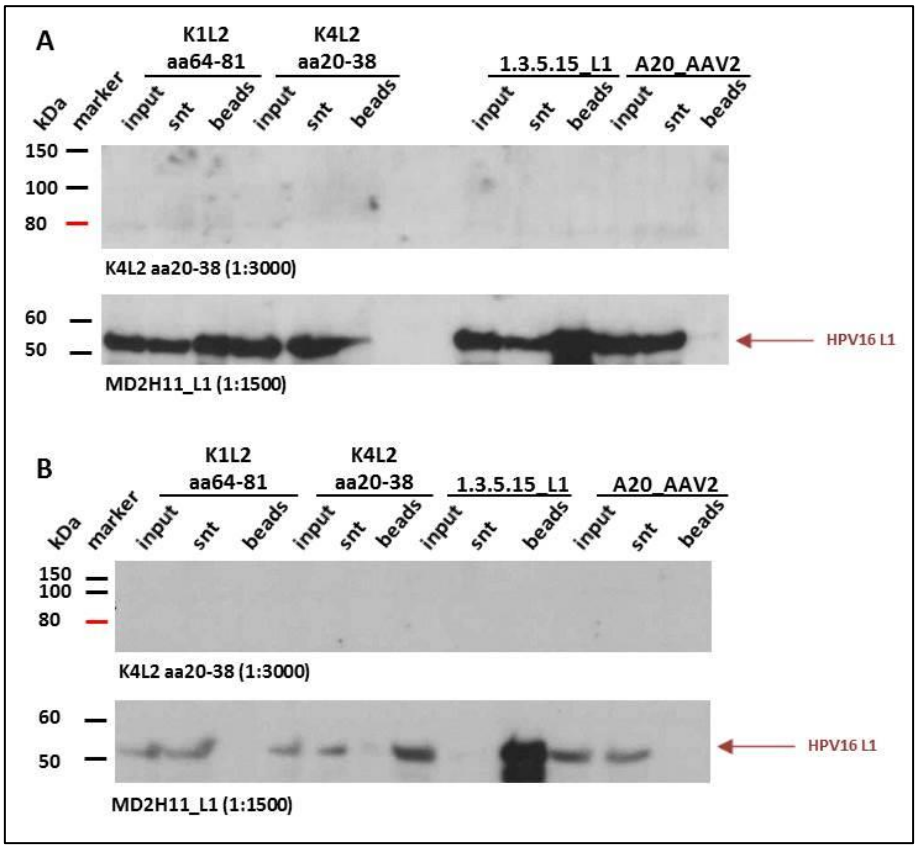

Figure 14 IP of HPV16 PsV from infected cell extracts. A PsV-IP from cell extracts infected with HPV16 L1/L2 PsV using different antibodies (K1L2 aa64-81, K4L2 aa20-38, 1.3.5.15_L1 and A20_AAV2) coupled to CNBr beads. The samples analyzed were taken before IP (input), and after IP (snt, beads). **B** PsV-IP from cell extracts infected with HPV16 L1 only PsV. Antibodies used for the IP and fractions analyzed were the same as described in A. The upper western blot was detected with a HPV16 L2 antibody (K4L2 aa20-38) whereas the lower western blot was detected with a HPV16 L1-specific antibody (MD2H11_L1) in A and B.

The result of the IP of HPV16 L1 only PsV is shown in Figure 7B. Using K1L2 aa64-81, K4L2 aa20-38 and the A20_AAV2 for precipitation lead to the detection of L1 in the input and the snt exclusively. Thus, confirming that the HPV16 L1-only PsV cannot be precipitated by any of the three antibodies. In contrast to the antibodies targeting HPV16 L2 and AAV2, the 1.3.5.15_L1 was able to precipitate the HPV16 L1 only PsV, represented by detection of HPV16 L1 in the input and in the bead sample. There was no detectable signal for HPV16 L1 in the snt fraction after binding to the beads, indicating that all PsV could be precipitated from the cell extract. IP samples from 293TT cells infected with HPV16 L1/L2, HPV16 L1 only and AAV2 (data not shown) as well as from non-infected cells (data not shown), using the four different antibodies were analyzed by MS by the GPCF at the DKFZ.

4.1.4. Mass spectrometric analysis and selection of candidates from PsV-IP

As described previously in paragraph 5.1.2, two protein databases were screened for protein identification. One comprised species from different classes, also including viral proteins, thus this database served to identify purified HPV16 L1 and HPV16 L2. However, only the IP of HPV16 L1/L2 and HPV16 L1-only using the 1.3.5.15_L1 antibody could identify HPV16 L1, none of the screens identified HPV16 L2. The database comprising species of the mammalian class was used for the identification of co-purified interaction candidates. The number of identified proteins was very high and required additional selection criteria to reduce the number of candidates (Figure 15). Like in 5.1.2, generally known contaminants were eliminated in the first selection round (step I.). The second selection criterion was based on the comparison of MS results of the different antibodies within the same PsV-infected extracts. Co-purified proteins of the A20_AAV2 negative control IP were discarded as potential candidates (step II.). Since A20_AAV2 is not able to precipitate either HPV16 L1 or HPV16 L2, as confirmed by the MS data, co-purified proteins were suggested to be unspecific. For the set of IPs from HPV16 L1 only PsV infected cells, also proteins co-purified with K1L2 aa64-81 and K4L2 aa20-38 were used as negative control. Remaining proteins from the HPV16 L1-only IP were assigned as potential L1 interaction candidates and served as control to distinguish between potential L1 and L2 candidates in a later selection step (V.). Additionally, unspecifically co-purified proteins, identified in the screens from AAV2 (step III.) and non-infected (step IV.) cells were discarded from the candidate list. From the remaining 73 candidates of the HPV16 L1/L2 infections, 15 candidates overlapped with the HPV16 L1-only candidate list. Therefore these 15 proteins were suggested to be potential L1 interaction candidates (step V.). Finally, proteins with no human equivalent (step VI.) as well as proteins with less than two independently identified peptides (step VII.) were eliminated.

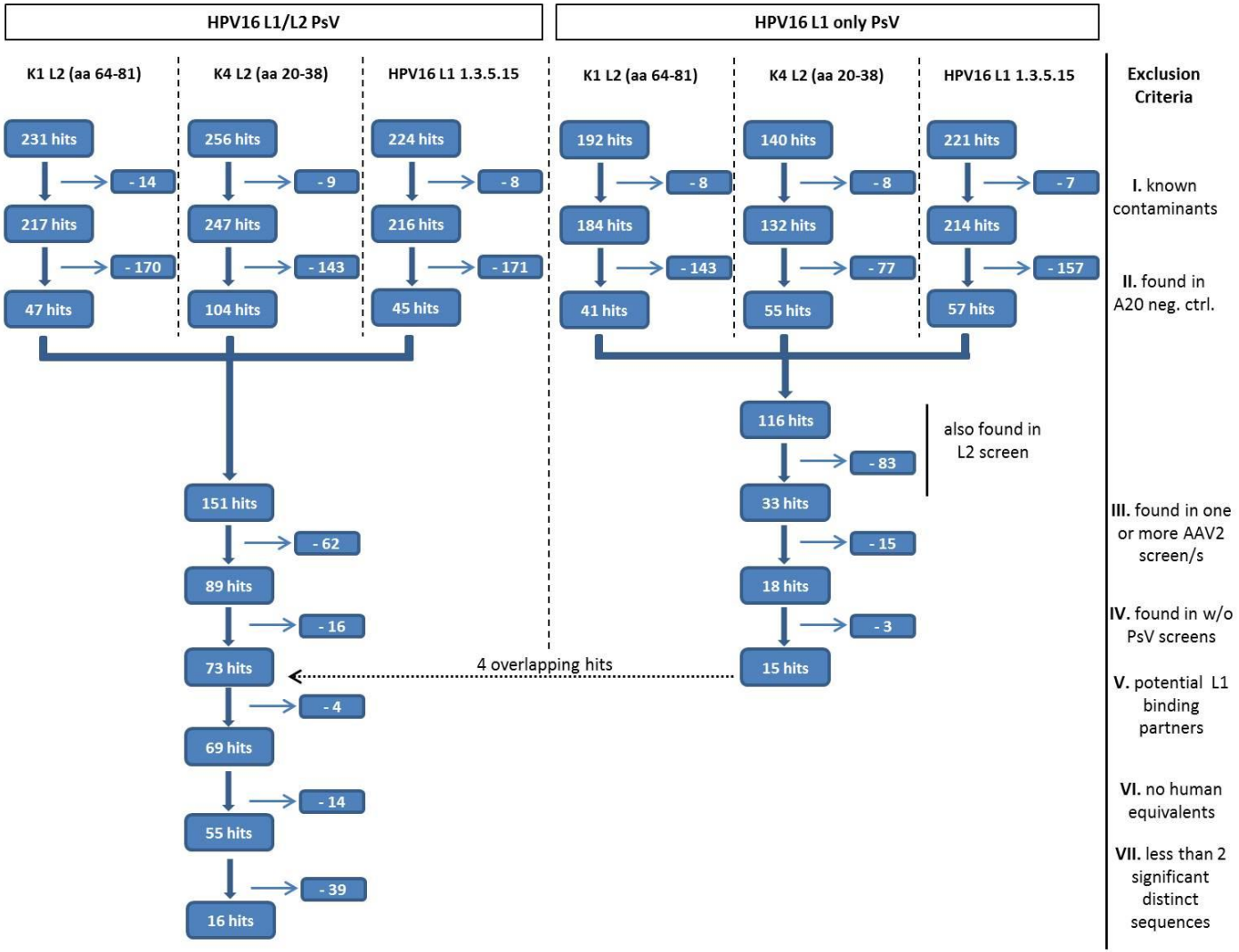

I. Typical contaminations in MS analyses (e.g. keratin)
II. Protein hits found in the corresponding control using a unspecific antibody A20 for IP
III. Protein hits found in screens infected with AAV2
IV. Protein hits found in screens using not infected cell extract
V. Protein hits identified as L1 interaction partnes
VI. Non-human protein hits which have no human equivlent
VII. Less than 2 independent peptides were identified by MS

Figure 15 Overview of the interaction candidate selection. The PsV-IP was performed using cells infected either with HPV16 L1/L2, HPV16 L1 only, and AAV2 or w/o virus. For each infection four antibodies were used for IP (K1L2 aa64-81, K4L2 aa20-38, 1.3.5.15_L1 and A20_AAV2). Each MS analysis revealed a different number of protein hits from which the generally known contaminants, like e.g. keratins were excluded in the first selection step (step I.). In step II, the K1L2 aa64-81, K4L2 aa20-38 and 1.3.5.15_L1 protein hit were compared to the corresponding A20_AAV2 protein hits of the same virus infection to exclude HPV16 unspecific protein hits. The remaining proteins were then compared to the four AAV2 infected and w/o virus IPs and overlapping hits were discarded (step III & step IV). Furthermore, protein hits appearing in the K1L2 aa64-81 and K4L2 aa20-38 IP from cells infected with HPV16 L1 only PsV were excluded from the corresponding 1.3.5.15_L1 IP to identify potential HPV16 L1 interaction candidates. These protein hits were compared to the K1L2 aa64-81, K4L2 aa20-38 and 1.3.5.15_L1 proteins hits and previously identified L1 interaction candidates were removed (step V). The last selection step (step VI) was based on the identification of protein hits with human equivalents as potential HPV16 L2 interaction candidates. Finally, protein hits with less than two independent peptides identified by MS were discarded from the list of potential interaction candidates (step VII).

Table 6: Potential HPV16 L2 interaction candidates identified by PsV-IP

Protein/ Description	PsV-IP
RPS2 40S ribosomal protein S2	3 independent peptides
HIST1H2BB Histone H2B type 1-B	5 independent peptides
HIST1H1C Histone H1.2	4 independent peptides
HIST1H2BC Histone H2B type 1-C/E/F/G/I	5 independent peptides
H3F3A Histone H3.3	4 independent peptides
CCT5 T-complex protein 1 subunit epsilon	4 independent peptides
CCT3 T-complex protein 1 subunit gamma	2 independent peptides
CCT4 T-complex protein 1 subunit delta	2 independent peptides
PKM Pyruvate kinase PKM	5 independent peptides
SDHA Succinate dehydrogenase [ubiquinone] flavoprotein subunit, mitochondrial	2 independent peptides
TPM2 Tropomyosin beta chain	4 independent peptides
VIM Vimentin	3 independent peptides
MYH9 Myosin-9	3 independent peptides
SNRPG Small nuclear ribonucleoprotein	2 independent peptides
SRI Sorcin	4 independent peptides
CAD CAD protein	3 independent peptides
CSE1L * Exportin-2	1 independent peptides

* was considered as potential candidate because of the identification as potential candidate in paragraph 5.1.2. Though, this protein would have been sorted out in the selection process in figure 8 step VII.
The number of peptides indicated, describes the number of independent peptides identified for the corresponding protein.

4.1.5. Peptide pull down (PPD) of potential, epitope interacting candidates from cell extracts

The peptide pull down (PPD) experiment was performed using three different, biotinylated HPV16 L2 epitopes (aa 20-38, aa 28-42 and aa 64-81) which had previously been demonstrated to be targets for neutralizing antibodies. Binding of these regions by antibodies during viral infection has been demonstrated to prevent an efficient viral infection *in vitro*. This observation leads to the hypothesis, that the binding of the antibody might inhibit essential steps of the viral infection pathway possibly preventing the interaction with a specific cellular protein. To analyze these L2 regions in more detail, the corresponding biotinylated peptide was immobilized on avidin beads. The pull down was performed using cell extracts from HEK 293TT and HaCaT cells and co-purified proteins were analyzed by MS analysis.

4.1.5.1. Coupling efficiency of biotinylated peptides to avidin beads

The coupling efficiency of the biotinylated peptides to the avidin beads was confirmed by ELISA. For this, the ELISA plate was coated with streptavidin and the input of biotinylated peptide used for binding to the avidin beads was analyzed. In addition, the supernatant after binding (snt) and the supernatant after low pH glycine treatment (elution) were titrated on the plate (Figure 16). The low pH treatment was performed to test the peptide-bead-affinity under elution conditions. A high amount of eluted peptide from the beads could probably tamper with the following MS analysis. Thus, it was important to optimize the elution conditions to keep the coupled peptides bound to the beads while eluting potentially co-purified proteins.

In Figure 16A,B and C, the titrations of the input, snt and elution sample derived from the three coupling processes are presented. The initial amount of peptide, used for the coupling (input), clearly demonstrated the presence of the corresponding peptide in the input samples. Comparing the input with the snt, representing unbound peptide, the snt showed reduced amount of peptide, indicating the successful coupling of the peptide to the avidin beads. This is represented by a lower absorbance and a faster decline of the titration curve. The low pH treated (elution) samples of the three HPV16 L2 peptides show a similar detection level as the corresponding snt samples. Therefore, the result indicates, that low pH treatment did not lead to a notable release of the HPV16 L2 peptides from the avidin beads. Compared to the L2 peptides aa 20-38 and aa 28-42, the peptide aa 64-81 showed a slightly reduced binding efficiency to the avidin beads. In contrast to the other peptides, the snt with the unbound peptide of aa 64-81 showed a higher absorbance relative to the input. Nevertheless, most of the peptide was bound to the avidin beads, represented by the instant decline of the titration curve (Figure 16C).

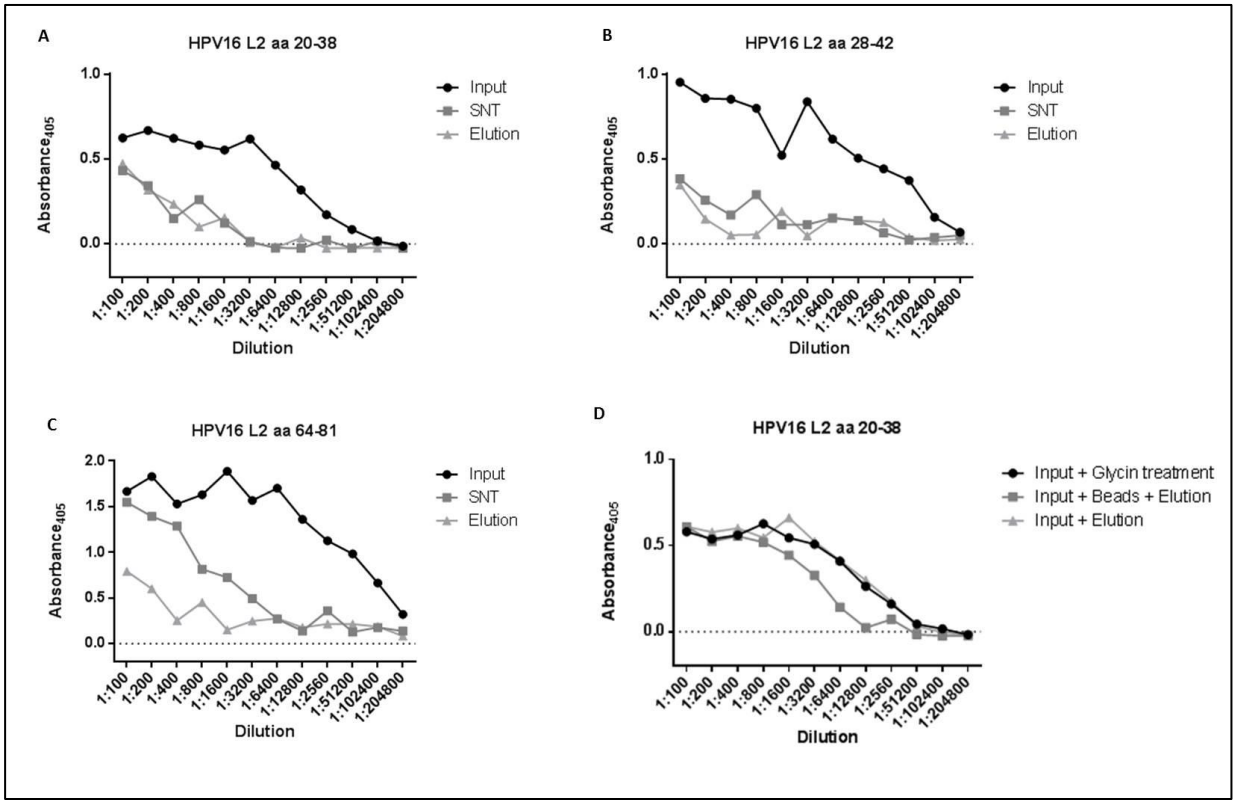

Figure 16 Coupling efficiency of biotinylated peptide to avidin beads and influence of low pH treatment on peptide recognition in ELISA. The peptides used for the immobilization on the avidin beads were corresponding to the N-terminal epitopes targeted by neutralizing antibodies (HPV16 L2 aa 20-38, HPV16 L2 aa 28-42 and HPV16 L2 aa 64-81). The coupling of the biotinylated peptides was performed as described in 4.4.5. Aliquots of the input, used for coupling to the beads as well as the supernatant (snt) after binding and the supernatant after low pH elution (elution) were analyzed by ELISA. **A** Coupling efficiency of HPV16 L2 aa 20-38 to avidin beads. The detection was performed using the mouse monoclonal K18L2 aa20-38 antibody and the corresponding secondary antibody. **B** Coupling efficiency of HPV16 L2 aa 28-42 to avidin beads. The detection was performed using the mouse monoclonal K8L2 aa28-42 antibody and the corresponding secondary antibody. **C** Coupling efficiency of HPV16 L2 aa 64-81 to avidin beads. The detection was performed using the mouse monoclonal K1L2 aa64-81 antibody and the corresponding secondary antibody. **D** Test of the influence of the low pH glycine treatment on the ability of the specific antibody to recognize the corresponding peptides in ELISA. A sample of the input was treated with the elution buffer for 10min before neutralizing the pH with Tris pH 8 (Input+Glycine treatment, black). The second input sample was added to peptide coupled beads before treatment with the low pH buffer (Input+Beads+Elution, dark grey). The third sample represents the input finally added after Tris pH 8 neutralization (Input+Elution, light grey). Exemplarily D shows the result of the treatments, using HPV16 L2 aa 20-38. The detection was performed with the monoclonal mouse antibody K18L2 aa20-38 and the corresponding secondary antibody (HPV16 L2 aa 28-42 and HPV16 L2 aa64-81, data not shown).

In order to rule out any effect of the low pH treatment on the detection efficiency of the peptides in the ELISA, the input samples were tested in different setups for the detection ability. In the first approach, the low pH glycine buffer was added directly to the aa 20-38 input (Figure 9C, Input + Glycine treatment, black). Additionally, the input was either added to bead-coupled aa 20-38 peptide before the low pH treatment (Input + Beads + Elution, dark grey) or to the elution aliquot after low pH treatment of bead-coupled peptide (Input + Elution, light grey). The data shown in Figure 9D demonstrates the representative result of the experiment using the HPV16 L2 aa 20-38 (aa 28-42 and aa 64-81, data not shown). The detection levels of the three different samples show a similar titration profile development according to the titration of the samples. Thus, low pH treatment does not influence the detection of the corresponding peptide in the ELISA assay performed.

4.1.5.2. PPD of epitope-specific interaction candidates from cell extracts

After establishing the immobilization of the peptides representing the L2 neutralizing epitopes, the pull down was performed as described in 4.4.5 to identify putative L2 cellular interaction partners. As input, either 2mg total protein derived from crude cell extract of either HEK 293TT or HaCaT were loaded onto the peptide coupled beads. As controls for the functionality of the assay, two additional samples of each peptide were prepared, containing either 25µg of the corresponding, epitope-specific antibody or a control antibody for the respective peptide. Aliquots of each sample were tested by ELISA (Figure 17). In contrast to the previously described ELISA, the plate was coated with the biotinylated peptides and the eluted samples were tested for the presence of the co-purified positive control antibody.

For the peptide aa 20-38, the K18L2 aa20-38 antibody (Figure 17B) was used as a positive control for the co-purification potential of the pull down protocol. K8L2 aa28-42 antibody served as positive control for the aa 28-42 peptide (Figure 17E) and K1L2 aa64-81 (Figure 17H) as positive control for the pull down with the aa 64-81 peptide. For each peptide, the input of antibody (input, black), the unbound antibody after pull down (snt, dark grey) and the antibody eluted from the beads (elution, light grey) was analyzed. The input sample demonstrates the presence of the corresponding antibody in the sample by a high absorbance in the ELISA. Furthermore, the results showed a successful binding of the antibody to the specific epitopes, since the absorbance in the snt samples is clearly reduced. After elution with the low pH glycine buffer, the antibody could be found in the corresponding fraction. The increased amount of antibody in the elution compared to the snt, indicates that treatment with a low pH buffer interferes with the binding of the antibody and the specific epitope and allows elution from the bead-coupled peptide. Comparing the three peptides, aa 20-38, aa 28-42 and aa 64-81 slight differences could be observed. Whereas, elution of the K8L2 aa28-42 and K1L2 aa64-81 showed almost the same absorbance as the corresponding input, the elution of the K18L2 aa20-38 showed a clear reduction in the amount of antibody compared to the input. However, around half of the antibody bound to the HPV16 L2 aa 20-38 peptide could be eluted from the beads by the low pH treatment. Thus, the previously described pull down protocol allows the binding and co-purification of proteins interacting with the corresponding epitope and the elution of the proteins for MS analysis.

Moreover, the specificity of the pull down protocol was determined by testing negative control antibody in the previously described experimental set up. For this, the HPV16 L2 aa 20-38 (Figure 17C) and HPV16 L2 aa 28-42 (Figure 17F) peptides were tested for pull down of the K1L2 aa64-81 and the HPV16 L2 aa64-81 peptide for the pull down of K18L2 aa20-38 (Figure 17I). The results demonstrated that the negative control antibody did not cross-react with any of the peptides since

there was no antibody detectable. Beside the controls, using either a specific or an unspecific antibody, a pull down with cell extract w/o antibody was performed for each peptide (Figure 17A, D and G). Since no antibody was added to the corresponding cell extract, the results of the ELISA are negative for all of the samples. The elutions derived from the pull down of Figure A, D and G, analyzed by MS. In addition to the samples of the PPD from the HEK 293TT extract, the corresponding PPDs, using HaCaT cell extract were performed and sent to the GPCF for MS analysis.

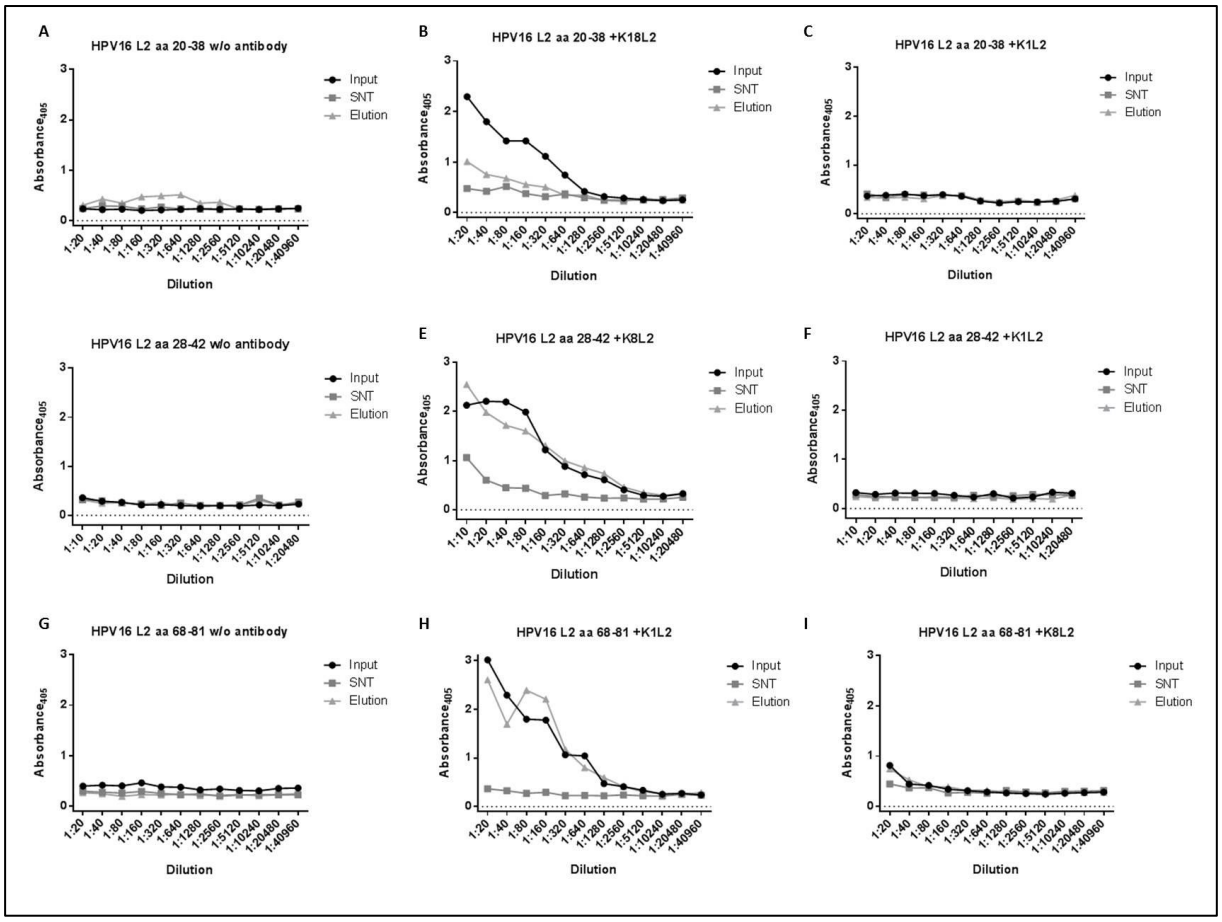

Figure 17 Validation of the PPD protocol and the suitability to pull-down and elute potentially interacting candidates. Samples of the indicated fractions before (input) and after (snt) the pull down as well as after the low pH treatment (elution), were tested for the presence of epitope-specific antibodies by ELISA. **A, D and G** Samples sent for MS analysis, no antibody added. **B, E and H** Positive controls, antibody specific for the corresponding peptides was added to the pull down. **C, F and I** Negative control, peptide unspecific antibody was added to the pull down.

4.1.6. *Mass spectrometric analysis and selection of candidates from PPD*

The selection of candidates from the PPD, provided by the GPCF, was similar to the selection steps I.-III., described in 5.1.2, starting with the elimination of generally known contaminants (Figure 18, step I.). Since the database screened for potential interaction candidates of the PPD comprised only human proteins, there were no non-human proteins to remove from the list of potential candidates. In step II., protein hits of the aa 20-38 and aa 28-42, respectively, were compared to the PPD of aa 64-81 to eliminate hits appearing in non-overlapping peptides. Finally, proteins with less than two independent peptides identified were discarded (step III.). The selection process narrowed down the number of potential candidates to 124 identified for HEK 293TT and 11 in HaCaT cells. Out of these, four candidates were overlapping between the HEK 293TT MS screens and the MS HaCaT screens. The control database comprising different classes confirmed the results from the experiment in 5.1.5.1, demonstrating that the bead-coupled peptide remains bound to the beads after elution of co-purified proteins. HPV16 L2 was identified only in the sample derived from the HPV16 L2 aa 20-38 PPD prepared with the HEK 293TT cell extract but not in any of the other samples.

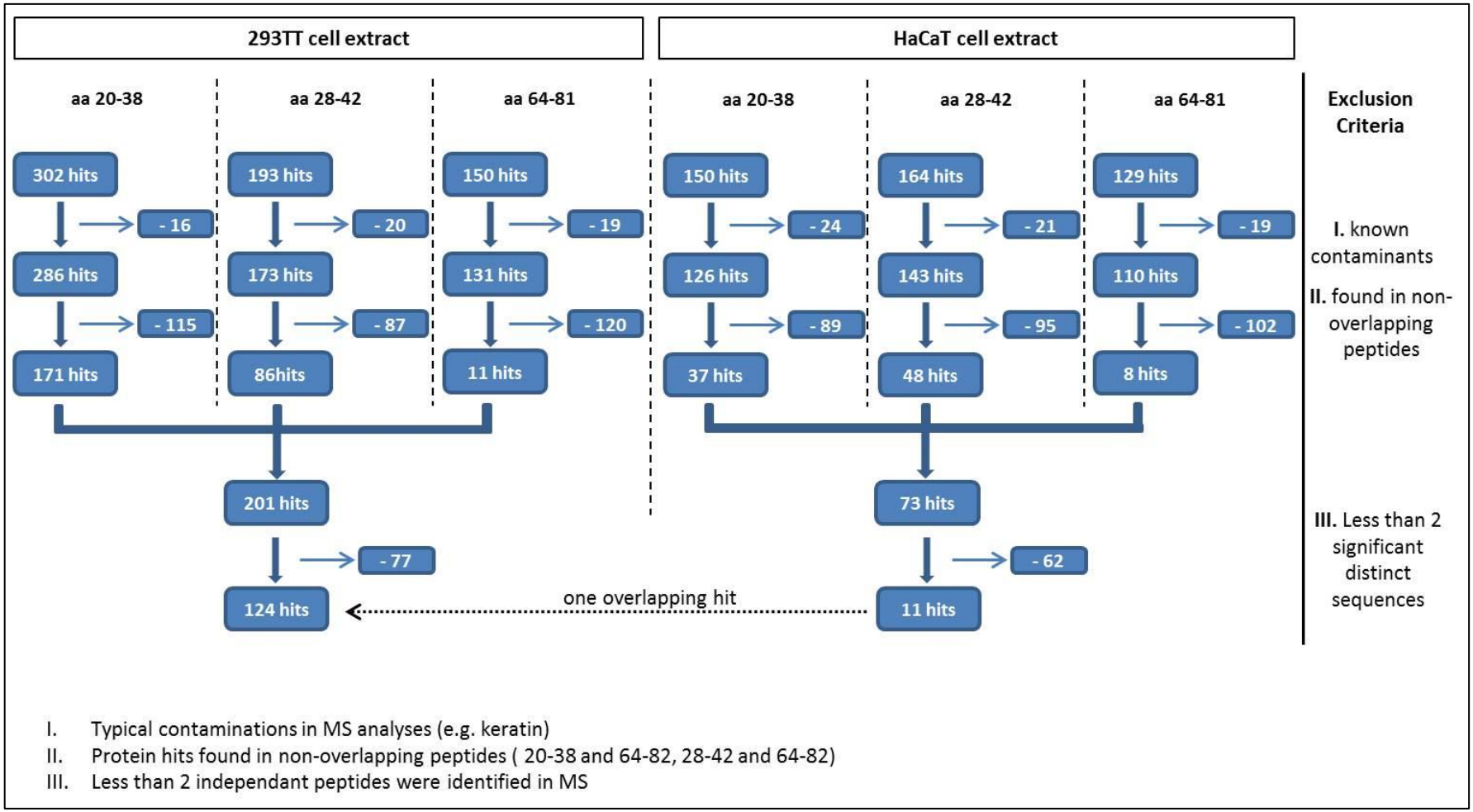

Figure 18 Overview of the interaction candidate selection. The PPD was performed with three different biotinylated HPV16 L2 peptides (aa 20-38, aa 28-42 and aa 64-81), using crude extract of either HEK 293TT or HaCaT cells. Each MS analysis revealed a different number of protein hits from which the generally known contaminants, like keratins were exclude in the first step of the selection procedure (step I.). In a second step the five protein hit lists derived from the same cell extract were compared to each other, to identify proteins from non-overlapping peptides, e.g. HPV16 L2 aa 20-38 and HPV16 L2 aa 64-81 and proteins appearing in the lists of non-overlapping peptides were suggested to be unspecific (step II.). In step III., proteins with less than 2 independent peptides, identified for the corresponding protein, were also eliminated as potential interaction candidates.

Potential, epitope-specific HPV16 L2 interaction candidates identified by PPD

Table 7: aa 20-38 from 293TT cell extract

Protein	Description
TUBA1A	Tubulin alpha-1A chain
HNRNPK	Heterogeneous nuclear ribonucleoprotein K
CCT4	T-complex protein 1 subunit δ
YBX3	Y-box-binding protein 3
ANXA5	Annexin A5
ILF3	Interleukin enhancer-binding factor 3
EIF5A	Eukaryotic translation initiation factor 5A-1
PUR6	Multifunctional protein ADE2
PARK7	Protein DJ-1
HNRH1	Heterogeneous nuclear ribonucleoprotein H
ADT2	ADP/ATP translocase 2
HNRPD	Heterogeneous nuclear ribonucleoprotein D0
PABP1	Polyadenylate-binding protein 1
SYIC	Isoleucine--tRNA ligase, cytopl.
CCT3	T-complex protein 1 subunit γ
RS16	40S ribosomal protein S16
NACAM	Nascent polypeptide-associated complex subunit alpha, muscle-specific form
DYHC1	Cytoplasmic dynein 1 heavy chain 1
ADT3	ADP/ATP translocase 3
YWHAB	14-3-3 protein beta/alpha
CAD	CAD protein
EF1D	Elongation factor 1-delta
IF2B1	Insulin-like growth factor 2 mRNA-binding protein 1
EFTU	Elongation factor Tu,mitochondrial
RL13A	60S ribosomal protein L13a
PCBP2	Poly(rC)-binding protein 2
ODP2	Dihydrolipoyllysine-residue acetyltransferase component of pyruvate dehydrogenase complex, mitochondrial
RL10A	60S ribosomal protein L10a
CN166	UPF0568 protein C14orf166
SAHH	Adenosylhomocysteinase
CCT5	T-complex protein 1 subunit ε
XRCC5	X-ray repair cross-complementing protein 5
HNRPC	Heterogeneous nuclear ribonucleoproteins C1/C2
PSA7	Proteasome subunit alpha type-7
F10A1	Hsc70-interacting protein
RL5	60S ribosomal protein L5
RL35	60S ribosomal protein L35
RM12	39S ribosomal protein L12, mitochondrial
LRC59	Leucine-rich repeat-containing protein 59

Table 8: aa 28-42 from 293TT cell extract

Protein	Description
TBB4B	Tubulin beta-4B chain
PERM	Myeloperoxidase
SPB4	Serpin B4
LEG7	Galectin-7
STIP1	Stress-induced-phosphoprotein1
HBA	Hemoglobin subunit alpha
H2B1B	Histone H2B type 1-B
CATD	Cathepsin D

Table 9: aa 20-38 and aa 28-42 from 293TT cell extract

Protein	Description
CH60	60 kDa heat shock protein, mitochondrial
PYC	Pyruvate carboxylase, mitochondrial
ENOA	Alpha-enolase
KPYM	Pyruvate kinase PKM
VIME	Vimentin
TPIS	Triosephosphate isomerase
RLA0	60S acidic ribosomal protein P0
RSSA	40S ribosomal protein SA
ATPA	ATP synthase subunit alpha, mitochondrial
TCPQ	T-complex protein 1 subunit theta
ATPB	ATP synthase subunit beta, mitochondrial
RL12	60S ribosomal protein L12
YWHAZ	14-3-3 protein zeta/delta
SYDC	Aspartate--tRNA ligase, cytopl.
KCRB	Creatine kinase B-type
XRCC6	X-ray repair cross-complementing protein 6
YWHAE	14-3-3 protein epsilon
LDHB	L-lactate dehydrogenase B chain

ECH1	Delta(3,5)-Delta(2,4)-dienoyl-CoA isomerase, mitochondrial
YWHAQ	14-3-3 protein theta
TCPA	T-complex protein 1 subunit alpha
COF1	Cofilin-1
PPIA	Peptidyl-prolyl cis-trans isomerase A
PDIA4	Protein disulfide-isomerase A4
LDHA	L-lactate dehydrogenase A chain
C1QBP	Complement component 1 Q subcomponent-binding protein, mitochondrial
PRDX6	Peroxiredoxin-6
ENPL	Endoplasmin
TCPZ	T-complex protein 1 subunit zeta
MDHM	Malate dehydrogenase, mitochondrial
SERA	D-3-phosphoglycerate dehydrogenase
CH10	10 kDa heat shock protein, mitochondrial
ALDOA	Fructose-bisphosphate aldolase A
EF1G	Elongation factor 1-gamma
SYRC	Arginine--tRNA ligase, cytoplasmic
RS19	40S ribosomal protein S19
EF1B	Elongation factor 1-beta
IF4A1	Eukaryotic initiation factor 4A-I
PCNA	Proliferating cell nuclear antigen
NDKA	Nucleoside diphosphate kinaseA
TPM3	Tropomyosin alpha-3 chain
MCA3	Eukaryotic translation elongation factor 1 epsilon-1
ROA2	Heterogeneous nuclear ribonucleoproteins A2/B1
RS26	40S ribosomal protein S26
BLMH	Bleomycin hydrolase
PCBP1	Poly(rC)-binding protein 1
PROF1*	Profilin-1
PRDX3	Thioredoxin-dependent peroxide reductase, mitochondrial
GLU2B	Glucosidase 2 subunit beta

Table 10: aa 64-81 from 293TT cell extract

Protein	Description
LCN1	Lipocalin-1
GSDMA	Gasdermin-A

*Protein was identified in PPD aa 20-38 and aa 28-42 from 293TT cell extract as well as in PPD aa 28-42 from HaCaT cell extract

Table 11: Potential candidates, aa 20-38 from HaCaT cell extract

Protein	Description
TRFL	Lactotransferrin
ZG16B	Zymogen granule protein 16 homolog B
HS71L	Heat shock 70 kDa protein 1-like
APOD	Apolipoprotein D
CLUS	Clusterin
BPIB1	BPI fold-containing family B member 1

Table 12: Potential candidates, aa 28-42 from HaCaT cell extract

Protein	Description
PROF1*	Profilin-1

*Protein was identified in PPD aa 20-38 and aa 28-42 from 293TT cell extract as well as in PPD aa 28-42 from HaCaT cell extract

Table 13: Potential candidates, overlapping aa 20-38 and aa 28-42 from HaCaT cell extract

Protein	Description
SPB12	Serpin B12
SPB3	Serpin B3
S10A7	Protein S100-A7

No proteins, matching the exclusion criteria in Figure 18 were identified for the peptide aa 64-81 from HaCaT cell extract.

4.1.7. Shortlisting of candidates from the different MS analyses for further analysis

In order to select for the most promising HPV16 L2 interaction candidates, the results of the MS analyses from paragraphs 5.1.2, 5.1.4 and 5.1.6 were compared. Comparing the selected candidates, two proteins were observed to appear in the MS results of two independent experiments. The CSE1L was detected in the MS analysis of the TAP (full length HPV16 L2 and HPV16 L2_Fr.1, Table 5) as well as in the MS analysis of the PsV-IP (HPV16 L1/L2 K1L2 aa64-81 and MD2H11_L1) (Table 6). Whereas, CSE1L was identified in the TAP analysis with at least 2 independent peptides, the result from the PsV-IP revealed only one independent peptide in the corresponding screens. Additionally, YWHAZ was identified in two MS analyses of basically different experiments (TAP and PPD). The TAP analysis showed YWHAZ to be co-purified with the full length HPV16 L2 protein as well as the HPV16 L2_Fr.1 (aa 1-193). Furthermore, YWHAZ was identified in the PPD from HEK 293TT extracts, using the overlapping epitopes aa 20-38 (2 peptides) and aa 28-42 (5 peptides). The PPD from HaCaT cell extract identified YWHAZ only in the screen using the epitope aa 28-42 (1 peptide). No further overlaps could be observed between the MS analyses from the different experimental set ups. Nevertheless, IRS4, CAPN2 and CAND1 were selected as promising interaction candidates of HPV16 L2. Each of these proteins was detected in the TAP MS in more than one screen of different HPV16 L2 constructs. Moreover, the number of identified, independent peptides, corresponding to the specific protein, was observed to be between 2 and 5. Each protein had at least one peptide set of 3-5 peptides. From the potential interaction candidates shown in Table 1, three proteins were discarded subsequently since they were identified only with a single peptide (FLG2, Skp1, and TGM3). Furthermore, the elongation factor 1 alpha was also rejected as potential candidate, since this protein appeared unspecifically in each screen of the PsV-IP as well as the PPD samples.

The PsV-IP MS analysis revealed another set of 16 potential candidates. However, some of these candidates were excluded subsequently, since they might have been co-purified because of HPV16 L2 independent interactions. Amongst others, these proteins were histone proteins, HIST1H1C, HIST1H2BC and H3F3A, which might rather be connected to the reporter DNA, still encapsidated by L1 and L2. The identification of histones could be considered as positive control for successful IP of the PsV from the cells extracts. Several proteins were identified, interacting with actin, a common contaminant of MS analyses and therefore might be co-purified with actin instead of HPV16 L2 specifically (TPM2, VIM, MYH9). Another group of co-purified proteins belong to the T complex proteins (CCT5, CCT3 and CCT4), a family of chaperons, involved in protein folding and ciliogenesis. Moreover, the ribosomal protein (RPS2), two enzymatic proteins (PKM and CAD), a protein involved in mitochondrial electron transport (SDHA) as well as SNRPG (RNA binding component of the spliceosome) an SRI (activator of the RYR2 calcium channel) were rejected as potential candidates

because of the lack of sufficient evidence for a potential function as HPV16 L2 interaction candidate. Furthermore, there were no additional candidates selected from the MS of the PPD, since the number of candidates was still too large, even after the selection process (Figure 18) to select for any promising candidate from the list of protein hits.

Table 14: Summary of L2 interaction candidates shortlisted for further analysis

Protein	5.1.2 TAP	5.1.4 PsV-IP	5.1.6 PPD
IRS4	full length L2_1: 2 peptides full length L2_2: 4 peptides HPV16 L2_Fr.3: 4 peptides	not identified	not identified
YWHAZ	full length L2_2: 1 peptide HPV16 L2_Fr.1: 2 peptides	not identified	aa 20-38: 5 peptides (293TT) aa 28-42: 2 peptides (293TT) aa 28-42: 1 peptide (HaCaT)
CSE1L	full length L2_2: 2 peptides HPV16 L2_Fr.1: 2 peptides	K1L2 aa64-81: 1 peptide MD2H11_L1: 1 peptide	not identified
CAPN2	full length L2_1: 4 peptides HPV16 L2_Fr.1: 3 peptides	not identified	not identified
CAND1	full length L2_2: 3 peptides HPV16 L2_Fr.1: 2 peptides	not identified	not identified

The number of peptides indicated, describes the number of independent peptides identified for the corresponding protein.

4.2. *Validation of the Selected Potential Interaction Candidates*

The previously selected interaction candidates (5.17) were further analyzed to verify their potential to physically interact with HPV16 L2. Therefore, specific candidates were selected and expressed as a fusion protein containing a myc- and flag-tag, respectively. The following experiments were performed using the tagged versions of the interaction candidates, as well as an untagged version of HPV16 L2 to validate the predicted interaction capacity of the proteins.

4.2.1. *Co-immunoprecipitation (Co-IP) of candidates and L2 after overexpression*

The Co-IP to validate the selected candidates was either performed using an α-myc monoclonal antibody for precipitation of the candidate or a polyclonal HPV16 L2-specific rabbit serum (serum #7) for precipitation of HPV16 L2. The cell extracts, containing the overexpressed proteins, for both IPs derived from the same transfection of cells. The amount of protein used for the IP was analyzed by western blot, using either the α-myc or the K4L2 aa20-38 antibody (Figure 19A, B). The candidates tested in the presented experiment were IRS4, CAND1, CAPN2, CSE1L, YWHAZ as well as eEF1A1 and hnRNPK (both serve as control for unspecific co-purification) which were overexpressed in HEK 293TT cells either in absence or presence of HPV16 L2. The red stars in figure 19 highlight unspecifically co-purified candidates, whereas green stars highlight specifically co-purified candidates. Though detection with the α-myc antibody demonstrated that each candidate was expressed, there are differences in the expression levels comparing the candidates among each other (Figure 19A). Also expression levels of the same candidate varied slightly in absence (w/o) and presence (w/) of HPV16 L2. It seemed that co-transfection of L2 led to a decreased expression level of the corresponding candidates, except for eEF1A1 which showed an increased expression level when co-expressed with HPV16 L2. Beside the specific bands, highlighted with stars, unspecific protein bands were detected in some samples (e.g. eEF1A1 and IRS4). Figure 19B shows the expression of HPV16 L2 in the corresponding cell lysates. The result demonstrated that HPV16 L2 was expressed at similar levels in each sample, except for the sample co-transfected with CAPN2.

Co-IP of HPV16 L2 by precipitation of myc-tagged candidates using an α-myc antibody

The result of the precipitation with the α-myc antibody is presented in figure 19C and D. The co-precipitation of HPV16 L2 in the corresponding samples is presented in figure 19D. IP of all myc-tagged candidates led to co-purification of HPV16 L2, while no L2 was detected when lysates without myc-tagged protein were used. The signal intensity of HPV16 L2 was highly different among the different precipitations. YWHAZ showed only a very faint band for co-purified HPV16 L2, whereas the samples showed higher amounts of L2. As positive control for precipitation, the samples were tested

by western blot after IP for the presence of the myc-tagged candidates (C). The result showed that the precipitation of the target proteins was successful as each myc-tagged candidate could be detected. Precipitation efficiency varies for the different candidates, but also comparing the same candidate in the IP w/o and w/ HPV16L2. Since the IP and the detection of the western blot were performed both, using the α-mouse secondary antibody, the heavy (~50kDa) and the light chain (~25kDa) were detected additionally.

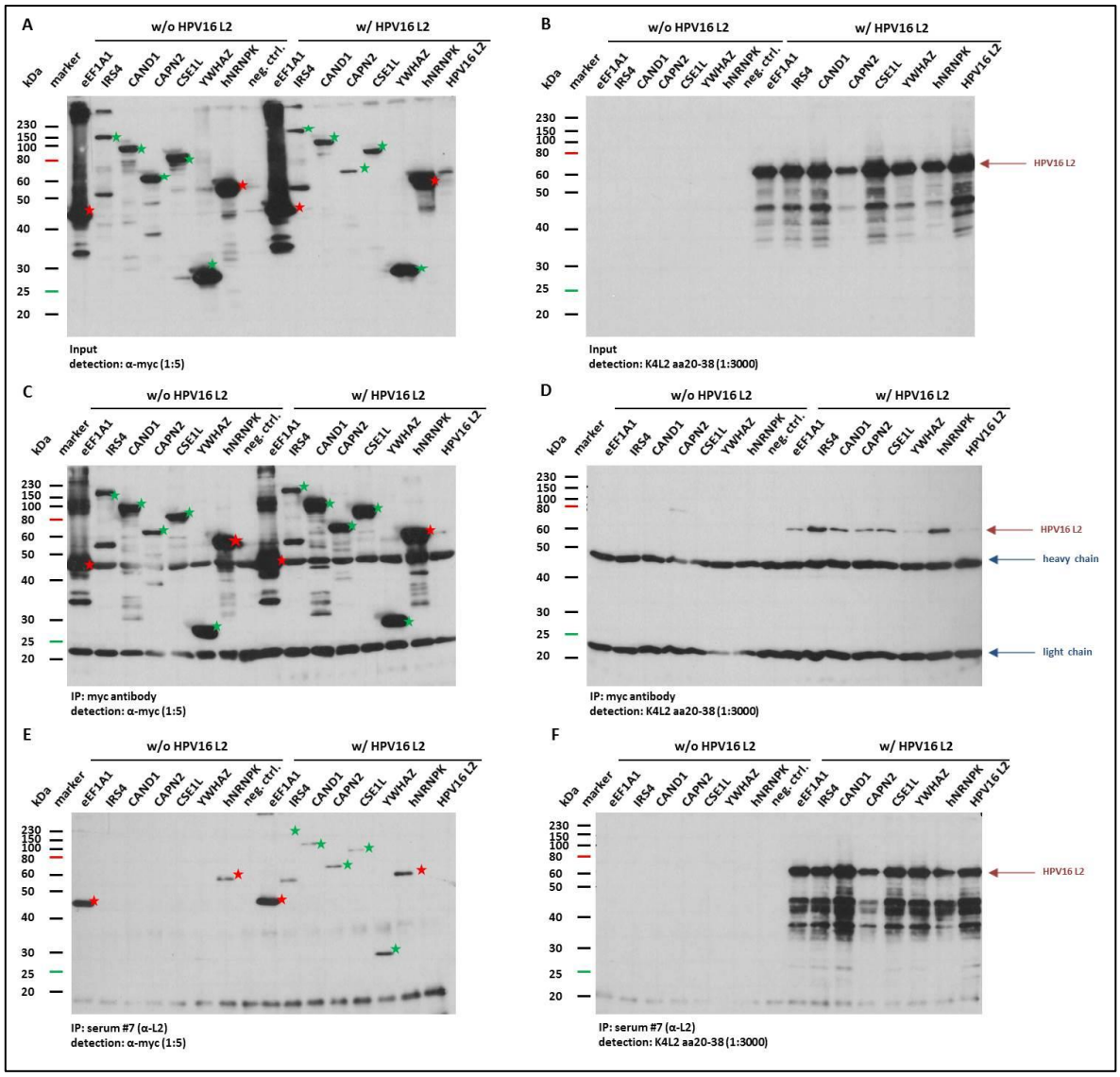

Figure 19 Co-IP of interaction candidates after overexpression with and without HPV16 L2. The Co-IP was performed using either a polyclonal HPV16 L2 rabbit serum (serum #7, diluted 1:100) or a monoclonal α-myc antibody (undiluted). The Input of the myc-tagged candidate as well as the HPV16 L2 protein was analyzed by western blot detected either with an α-myc (**A**) or an α-HPV16 L2 antibody (**B**). The corresponding extract was splitted into two parts, whereas one part was used for an IP of the myc-tagged candidates (**C** and **D**) and the other part for an IP against HPV16 L2 (**E** and **F**). Red stars highlight unspecifically co-purified interaction candidates, green stars highlight the verified candidates and red arrows highlight HPV16 L2. Heavy and light chain, derived from the antibodies used for IP, are highlighted with blue arrows.

Co-IP of myc-tagged candidates by precipitation of HPV16 L2

IP of HPV16 L2 was performed using a polyclonal rabbit serum (serum #7). Figure 19F confirms the successful precipitation of L2 from the lysates transfected with HPV16 L2 (w/ HPV16 L2). According to the lower expression level of L2 when co-expressed with CAPN2 (Figure 19B) the corresponding IP revealed less HPV16 L2. Co-precipitation of the myc-tagged candidates was analyzed, using the α-myc antibody for western blot detection (Figure 19E). All of the candidates were co-purified with HPV16 L2 (w/ HPV16 L2), however, showing different precipitation efficiency. IRS4, CAND1, CAPN2, CSE1L and YWHAZ were demonstrated to be specifically co-precipitated, since the corresponding signals were only detected in the IP w/ HPV16 L2. In contrast, eEF1A1 and hNRNPK could also be detected in the samples w/o HPV16 L2. These two proteins seemed to be unspecifically co-purified during the IP. The result confirms the ability of a physical interaction of HPV16 L2 with IRS4, CAND1, CAPN2, CSE1L and YWHAZ.

4.2.2. *PPD of potential candidates after overexpression*

To further validate the candidates and maybe verify potential interaction sites, the myc-tagged candidates were analyzed by PPD after overexpression. For this, 293TT cells were transfected with the specific candidate (SNX17, IRS4, YWHAZ, CSE1L, CAPN2 and SPOP) and cell extracts were used for pull-down with the three different, biotinylated HPV16 L2 peptides (aa 20-38, aa 28-42 and aa 64-81). SPOP as a cellular factor for transduction was not identified in any of the previous experiments but derived from an independent study (Burkart et al. unpublished) screening for potential AAV VP1 interaction candidates. Therefore it was included as negative control for further experiments. As controls for the specific interaction with the epitopes, blocking of the corresponding binding sites were included using either an epitope-specific (K18L2 aa20-38, K8L2 aa28-42 or K1L2 aa64-81) or unspecific antibody (mouse serum from a non-immunized mouse or K18L2 aa20-38). The results of the experiment are presented in figure 20. The first epitope to be tested was a biotinylated HPV16 L2 aa 20-38 peptide, which was previously immobilized on avidin beads (Figure 20A and B). The western blot analysis in figure 20A shows the PPD using the immobilized peptide without blocking of the corresponding peptide as well as blocked with the epitope-specific antibody K18L2 aa20-38. When the epitope was available for protein binding (w/o antibody) the purification of YWHAZ and CAPN2 could be observed. Furthermore, faint bands for IRS4 (~160kDa) and CSE1L (~80kDa), were detected in the corresponding PPDs. After blocking of the epitope with K18L2 aa20-38, none of the candidates was pulled down by PPD. The control western blot in figure 20B shows the samples of a second PPD w/o antibody and the negative mouse serum.

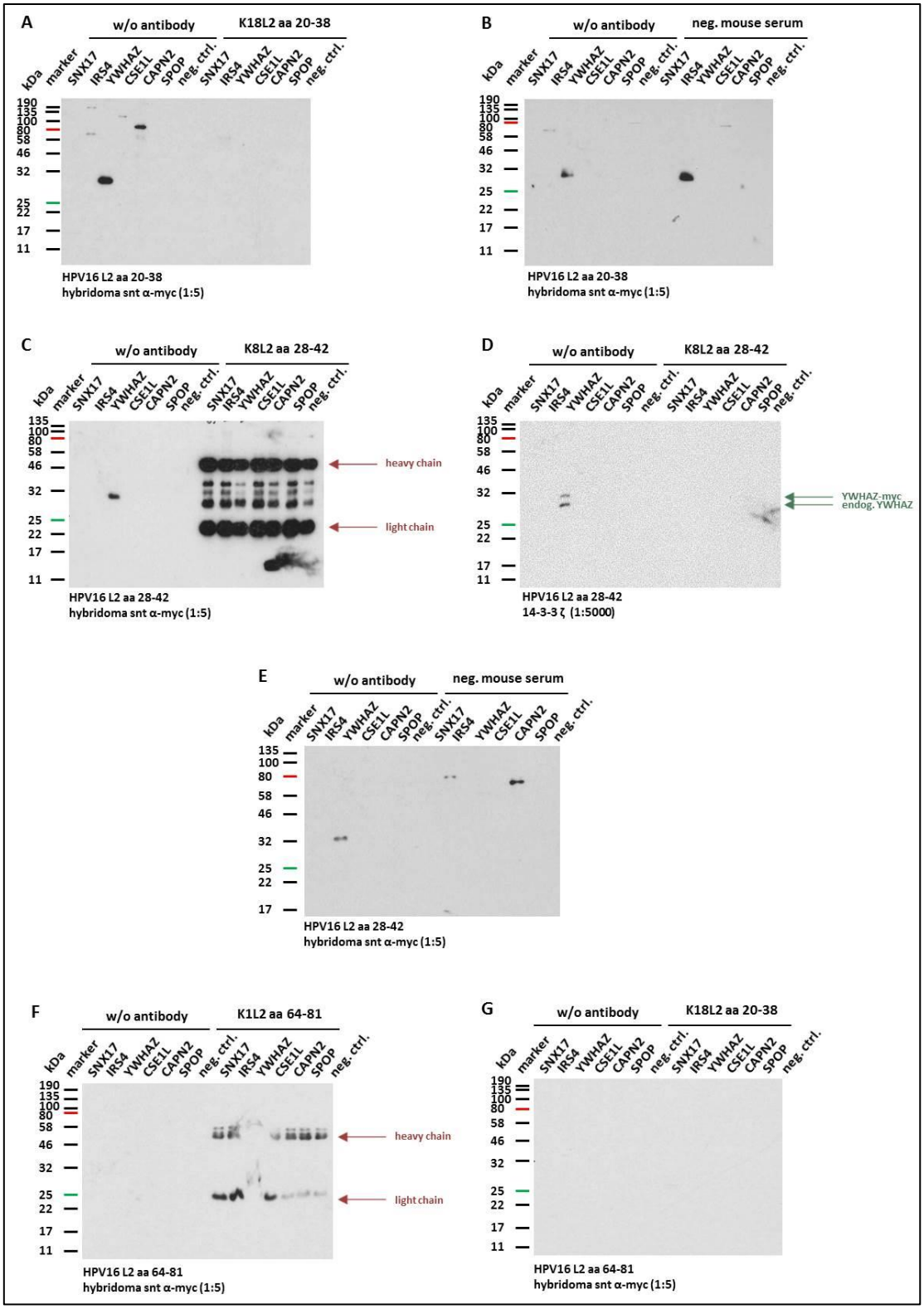

Figure 20 Binding of selected candidates to the HPV16 L2 epitopes aa 20-38, aa 28-42 and aa 64-81. The PPD was performed using cell extracts from transfected 293TT cells, overexpressing the indicated candidate either as myc-tagged protein (SNX17, IRS4, YWHAZ, CSE1L, CAPN2 and SPOP). For detection the indicated primary antibodies (α-myc antibody or 14-3-3ζ) were used. The immobilized peptides were either not treated at all (w/o antibody), with an epitope unspecific antibody (neg. mouse serum or K18L2 aa20-38) or with an epitope-specific antibody (K18L2 aa20-38, K8L2 aa28-42 or K1L2 aa64-81) to block potential interaction with the candidates. Heavy and light chains derived from the antibody, used to block potential binding sites, are highlighted with red arrows whereas the myc-tagged YWHAZ as well as the endogenous YWHAZ are highlighted with green arrows. **A and B** PPD using the immobilized HPV16 L2 aa 20-38 epitope. **C, D and E** PPD using the

immobilized HPV16 L2 aa 28-42 epitope. **F and G** PPD using the immobilized HPV16 L2 aa 64-81 epitope. Note: SPOP was identified as AAV interaction candidate (Burkart et al. unpublished).

The detection via the α-myc antibody after PPD correlates with the result from A at least in case of the YWHAZ. Comparing the two PPD w/o antibody in A and B, the signal representing CAPN2 and CSE1L could not be reproduced. A similar result can be observed for the IRS4, since in this sample, only the not specifically detected lower band could be detected after PPD w/o antibody. However, after treatment of the beads with the neg. mouse serum and the following PPD, YWHAZ could still be co-purified with the aa 20-38 biotinylated peptide. Additionally, a faint signal for CAPN2 in the neg. mouse serum treated sample was detectable.

The same experimental set up was performed using the HPV16 L2 aa 28-42 peptide. The samples were analyzed by western blot using either the α-myc antibody (C and E) or a α-YWHAZ antibody (D, 14-3-3ζ). In Figure 20C, the PPD was performed w/o antibody as well as with K8L2 aa28-42, supposed to specifically block binding of proteins to the aa 28-42 epitope. When the epitope was available for protein binding, YWHAZ could be purified, whereas none of the other samples showed a detectable amount of myc-tagged protein. After addition of the epitope specific K8L2 aa28-42, each of the antibody treated samples showed a strong detection of unspecific bands, derived from the antibody (heavy and light chain, highlighted with red arrows) since K8L2 aa28-42 and the α-myc antibody derived from the same host species. Binding of YWHAZ seemed to be inhibited by the epitope-specific antibody, though the intensity of unspecific signals was too high to conclude certainly. Therefore, the corresponding samples were tested, using an YWHAZ-specific antibody derived from rabbit for better detection of the protein (D). The result confirmed purification of YWHAZ when the epitope was available for binding. The upper band corresponds to the molecular weight of the myc-tagged YWHAZ, whereas the lower signal corresponds to the endogenous YWHAZ (green arrows). After blocking of the epitope with the K8L2 aa28-42, neither the myc-tagged YWHAZ nor the endogenous YWHAZ could be detected anymore. Figure 20E presents the result of the second experiment, performed without antibody or with the neg. mouse serum as a control. Repetition of the PPD w/o antibody showed a similar result as the previous experiment, detecting only YWHAZ-myc after PPD. Though, YWHAZ could not be purified after incubation of the coupled peptide with the neg. mouse serum. In addition, the detection shows pull down of CAPN2 and the unspecific band in the IRS4 sample, mentioned previously in Figure 20B. The PPD performed with the peptide aa 64-81 did not show any purified protein, independent of the availability of the epitope for binding (Figure 20F and G). As indicated by the red arrows, the only detectable signal found in F derived from the heavy and light chain of the K1L2 aa 64-81, used to block the aa 64-81 for protein interaction.

4.2.3. *Analysis of co-localization of the candidates and L2 after overexpression*

The IF was performed as previously described using myc- or flag-tagged candidates together with an untagged version of HPV16 L2. Both proteins were co-expressed in HeLa cells and stained afterwards with a rabbit derived myc-/flag-specific antibody and the K4L2 aa20-38 targeting HPV16 L2. The staining was analyzed using the Zeiss Cell Observer and the Zeiss Zen Black Software. As a positive control for interaction, a SNX17-GFP construct was used which was kindly provided by the group of Dr. Laurence Banks. The staining of the cells was conducted as described in 4.4.4. For quantification of subcellular localization of the candidates and HPV16 L2, 50 cells expressing the corresponding set of transfected proteins were counted on two independent slides and the localization of each protein was analyzed (Figure 21A and B).

Subcellular localization of potential candidates in absence and presence of HPV16 L2

Figure 21A presents the quantification of the potential candidates as well as the positive control SNX17-GFP in absence (w/o) and presence of HPV16 L2 (w/). SNX17-GFP, previously published to interact with L2 [109, 110] was localizes exclusively in the cytoplasm (black) when expressed w/o HPV16 L2. Figure 22A, demonstrates the cytoplasmic localization and shows the accumulation of SNX17-GFP in speckles throughout the cytoplasm (upper panel). However, co-expression with L2 shifted SNX17 localization to 70% cytoplasmic, 20% nuclear (dark grey) and 10% cytoplasmic/nuclear. Independent of the localization of SNX17-GFP, the protein was found in speckle-like structures. The merge of SNX-GFP and the L2 staining demonstrated the co-localization in the speckles, either in the cytoplasm or the nucleus (Figure 22A, lower panel). Beside the positive control, YWHAZ and CSE1L showed a change in subcellular localization when co-expressed with L2. In absence of L2, 50% of cells showed a cytoplasmic localization of YWHAZ, demonstrated in figure 22C (upper panel). In the remaining cells, YWHAZ was found in the nucleus (20%) or distributed in nucleus and cytoplasm (30%). When co-expressed with HPV16 L2 (YWHAZ w/) the proportion of cells with cytoplasmic localization of YWHAZ increased to 75%. Figure 22C (lower panel) shows an example of the YWHAZ localization in presence of L2. YWHAZ was mainly found in the cytoplasm and less in the nucleus. Co-localization could be observed when either L2 was found cytoplasmic together with YWHAZ or in some cells when YWHAZ was localized in the nucleus. CSE1L in absence of HPV16 L2 was observed to be localized in the nucleus in 98% of the cells. Co-expression of HPV16 L2 (CSE1L w/), however, led to an increased distribution of CSE1L in the nucleus and the cytoplasm (light grey). The change of the CSE1L localization pattern is demonstrated additionally in Figure 23A, comparing the upper panel (w/o L2) and the lower panel (w/ L2). Furthermore, figure 23A shows co-localization of CSE1L and HPV16 L2 at the perinuclear region (merge, lower panel). The influence of HPV16 L2 on the subcellular localization was observed to be less pronounced for CAPN2 and CAND1. For CAPN2 a

slight increase in the cytoplasmic localization (black) could be observed in presence of L2, whereas a decrease of cytoplasmic localization (black) was observed when CAND1 was co-expressed with L2.

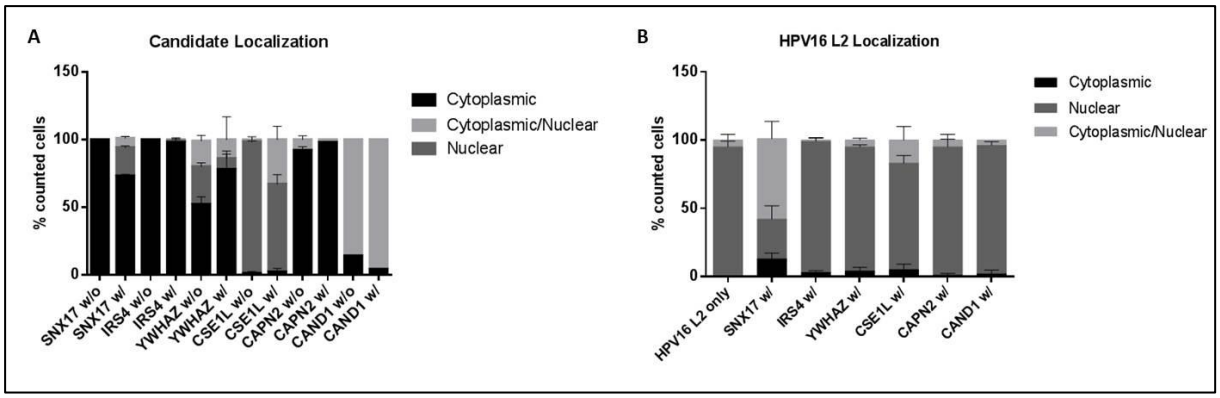

Figure 21 Subcellular localization of potential candidates in presence or absence of HPV16 L2. The quantification of the IF samples was performed by staining two slides with cells overexpressing either the indicated candidate in absence (w/o) or presence (w/) of HPV16 L2 or HPV16 L2 only in HeLa cells. The antibodies used for staining of the cells were rabbit derived α-myc and α-flag, respectively and the HPV16 L2-specific, mouse monoclonal K4L2 aa20-38. The secondary antibodies were coupled to Alexa595 (α-rabbit) and Alexa488 (α-mouse). On each slide, 50 cells expressing the transfected protein set were analyzed for the localization of the potential candidate and the localization of HPV16 L2. The quantification data was then summarized in the presented bar graphs. Cytoplasmic localization is shown in black, nuclear localization in dark grey and the light grey part does represent a localization distributed in the cytoplasm as well as in the nucleus. **A** Quantification of the candidate localization in absence (w/o) or presence (w/) of HPV16 L2. **B** Quantification of the distribution pattern of HPV16 L2 either expressed alone or in presence of the indicated candidate.

A co-localization of HPV16 L2 and CAPN2 could be observed at the perinuclear region or in some cases, when L2 was localized in the cytoplasm of the cell (Figure 23B, lower panel). A similar result was observed for the co-localization of CAND1 and HPV16 L2 (Figure 23C). The analysis of IRS4 did not show any changes in the localization pattern in presence of HPV16 L2. However, a small number of cells showed nuclear localization of IRS4 in a speckle-like pattern (Figure 22B). Co-localization of IRS4 and L2 was observed in the described nuclear speckles as well as in rare cases where L2 was found to be localized in the cytoplasm.

Subcellular localization of HPV16 L2 in absence or presence of the potential candidates

In addition to the localization of potential interaction candidates, the cellular distribution of HPV16 L2 was analyzed when expressed alone or together with the corresponding candidates (Figure 21B). When L2 was expressed in absence of potential interaction candidates, the protein was found to be localized mainly in the nucleus (dark grey, 95%). Co-expression with the known interaction candidate SNX17-GFP showed a strong effect on L2 localization. L2 was found to be distributed in the nucleus and the cytoplasm (light grey) in 50% of the cells, whereas the nuclear (black) proportion of L2 decreased to 30%. This result was confirmed by the co-localization experiment shown in figure 22A (lower panel). The remaining 20% of the cells showed an exclusively cytoplasmic localization of L2 when co-expressed with SNX17-GFP. The co-expression of L2 with CSE1L showed a shift towards a

more nuclear/cytoplasmic (Figure 21B,light grey and Figure 23A, lower panel) localization of L2, though to lower extend than the positive control. An effect on L2 localization could not be observed for any of the other candidates.

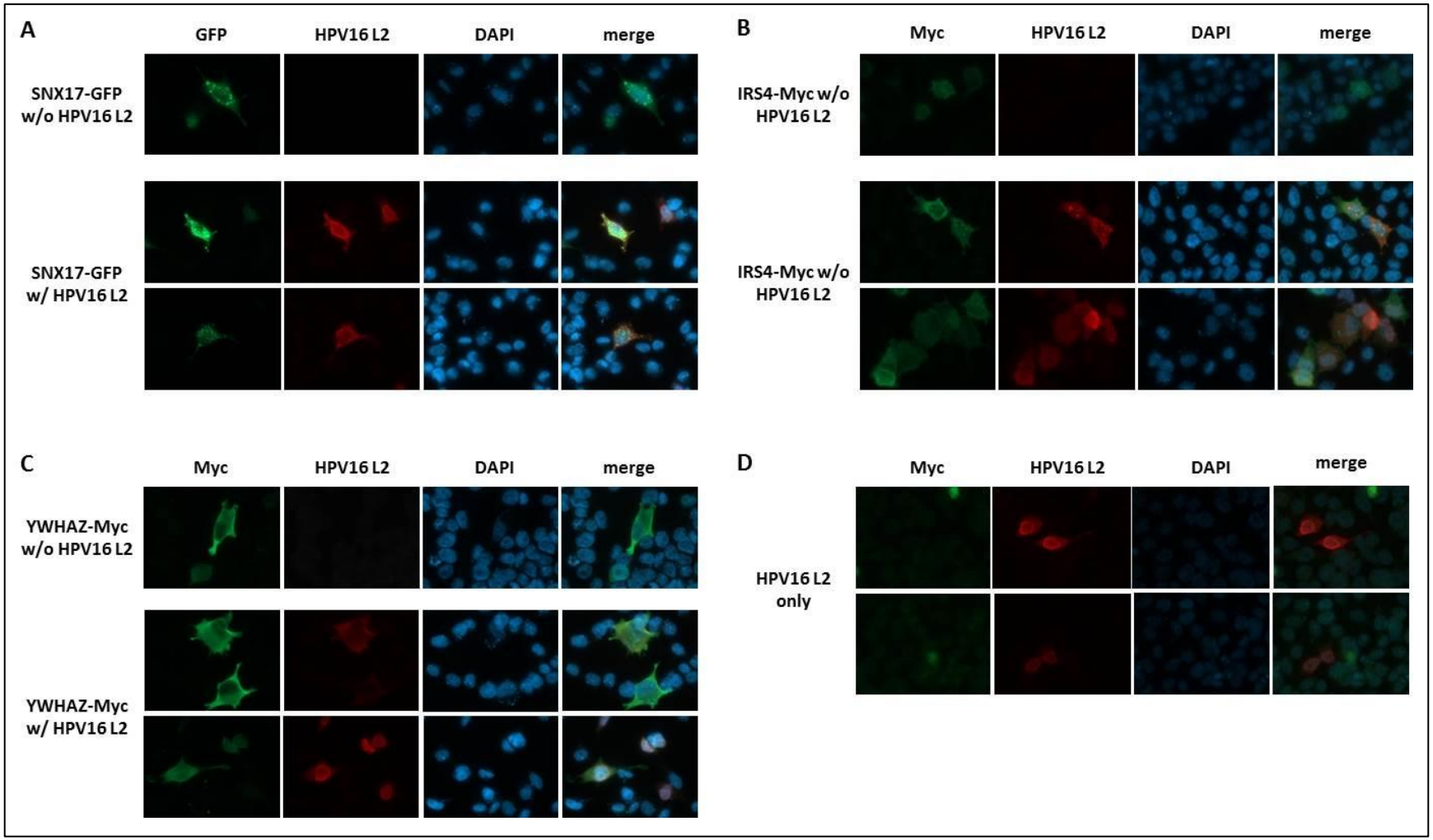

Figure 22 Subcellular localization of potential interaction candidates in absence and presence of HPV16 L2. The staining of the samples was performed using either a rabbit derived α-myc or a rabbit derived α-flag antibody in combination with the corresponding α-rabbit-A488 secondary antibody (green). HPV16 L2 was stained with K4L2 aa20-38 and a α-mouse-A594 antibody (red) as well as DAPI (blue) to stain the DNA in the nucleus. **A** SNX17-GFP expressed without (upper panel) or together with HPV16 L2 (lower panel). **B, C** Staining of the indicated myc-tagged candidates expressed without (upper panel) and with (lower panel) HPV16 L2. **D** Localization of HPV16 L2 localization when expressed in absence of overexpressed candidate interaction partner.

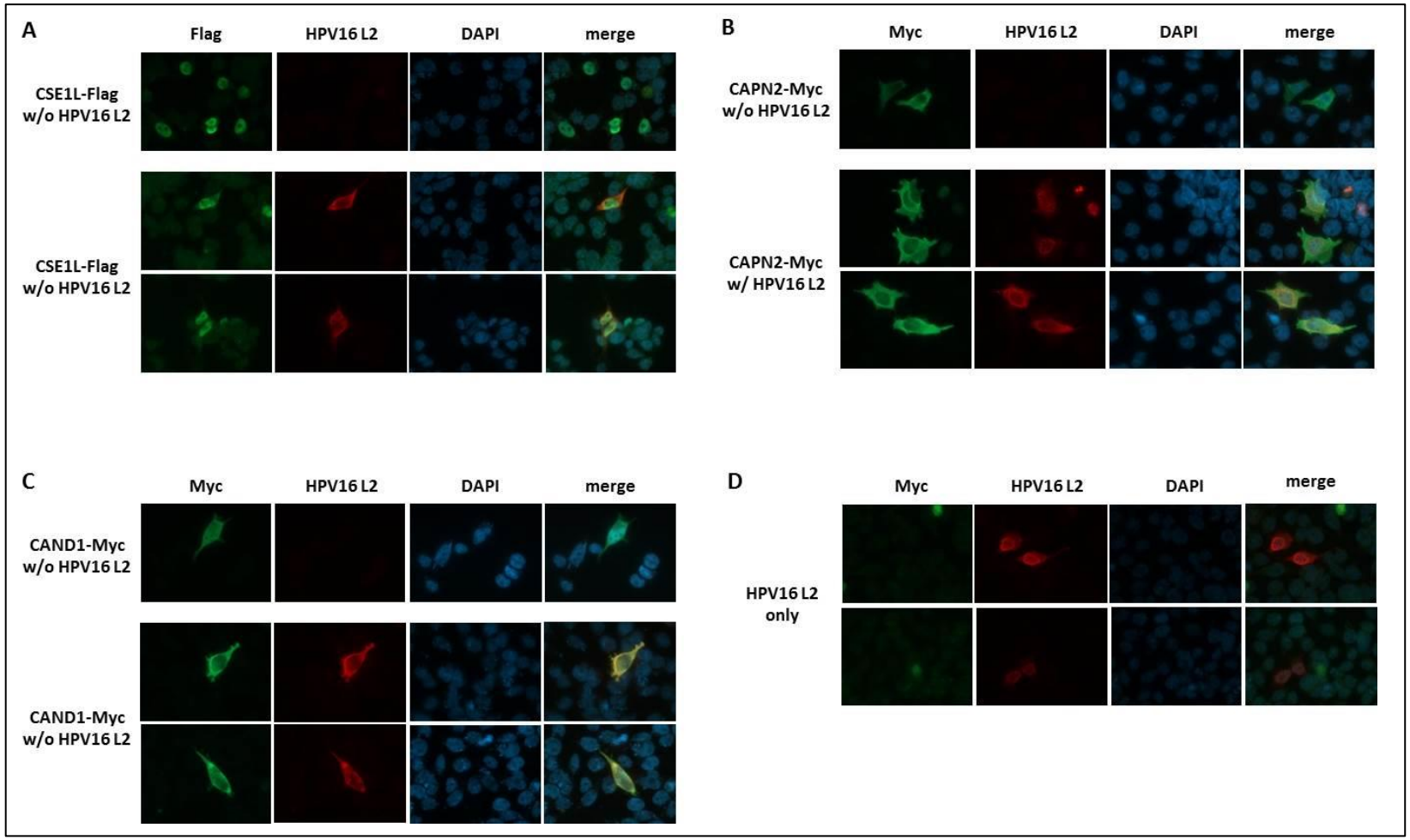

Figure 23 Subcellular localization of potential interaction candidates in absence and presence of HPV16 L2. The staining of the samples was performed using either a rabbit derived α-myc or a rabbit derived α-flag antibody in combination with the corresponding α-rabbit-A488 secondary antibody (green). HPV16 L2 was stained with K4L2 aa20-38 and a α-mouse-A594 antibody (red) as well as DAPI (blue) to stain the DNA in the nucleus. **A** Staining of flag-tagged CSE1L2 expressed without (upper panel) or together with HPV16 L2 (lower panel). **B, C** Staining of the indicated myc-tagged candidates expressed without (upper panel) and with (lower panel) HPV16 L2. **D** Localization of HPV16 L2 localization when expressed in absence of overexpressed candidate interaction partner.

Co-localization analysis of IRS4, YWHAZ and CSE1L with HPV16 L2

The co-localization of three selected candidates (IRS4, YWHAZ and CSE1L) as well as the positive control (SNX17) with HPV16 L2 was further analyzed by confocal microscopy (Figure 24). Since confocal microscopy is specifically designed to detect signals exclusively in the focal plane, this method is suitable to further analyze co-localization of the candidates with HPV16L2.

As described previously, SNX17-GFP was localized mainly in the cytoplasm with an overall staining pattern when expressed in absence of HPV16 L2 (Figure 24A, upper panel). After co-expression of SNX17-GFP (green) with HPV16 L2 (red) (Figure 24A, lower panels), both proteins were detected in dot-like structures mainly in the nucleus but also in the cytoplasm. For both localization patterns observed, co-localization in the described speckles could be observed, independent of nuclear or cytoplasmic localization. Overexpression of IRS4 alone showed an exclusive localization in the cytoplasm of transfected cells (Figure 24B, upper panel). However co-expression of IRS4 together with HPV16 L2 led to a more homogenous staining of the cells including staining in the cytoplasm as well as in the nucleus. HPV16 L2 seems to recruit some IRS4 to the nucleus, even though only in a few cells a partial co-localization at the periphery of the nucleus could be observed (Figure 24B, lower panels). In most of the cells co-expressing IRS4 and HPV16 L2 did not show co-localization of IRS4 and HPV16 L2 in the nuclear proportion of the proteins. A similar result was obtained analyzing YWHAZ. While YWHAZ is mainly localized in the cytoplasm when expressed in absence of HPV16 L2 (Figure 24C, upper panel), an increased proportion of the protein is located in the nucleus after co-expression of L2 (Figure 24C, lower panels). Co-localization of YWHAZ and HPV16 L2 in the nucleus could be observed in some of the transfected cells. However, transition of YWHAZ to the nucleus did not obligatory lead to co-localization of the two proteins. Staining of CSE1L, a member of the exportin family, showed a nuclear localization of the protein when expressed alone in the cells (Figure 24D, upper panel). In rare cases, an additional staining could be observed in the cytoplasm of CSE1L expressing cells in absence of L2 (not shown). When CSE1L was overexpressed together with HPV16 L2, the L2 staining was detected exclusively in the nucleus of the transfected cells. Also the CSE1L was located predominantly in the nucleus however the transfected cells additionally showed increased cytoplasmic CSE1L staining (Figure 24D, lower panels). Even though the intensity of the cytoplasmic staining varied, it was observed in most of the cells co-expressing CSE1L and HPV16 L2. Furthermore, co-localization of CSE1L and HPV16 L2 could be detected for the proteins localized in the nucleus with an accumulation of both proteins towards the periphery of the nucleus.

The results of the confocal microscopy analysis demonstrated a partial co-localization of IRS4 and YWHAZ, respectively, with HPV16 L2 after overexpression of the proteins. Even though the co-

localization was not observed continuously in all of the cells, an increased nuclear localization of IRS4 and YWHAZ was found in cells co-expressing HPV16L2. For both proteins, HPV16 L2 seemed to have an influence on the subcellular localization, though the interaction might by transient. Additionally co-localization of CSE1L with HPV16 L2 could be demonstrated towards the periphery of the nucleus and was observed in the majority of transfected cells.

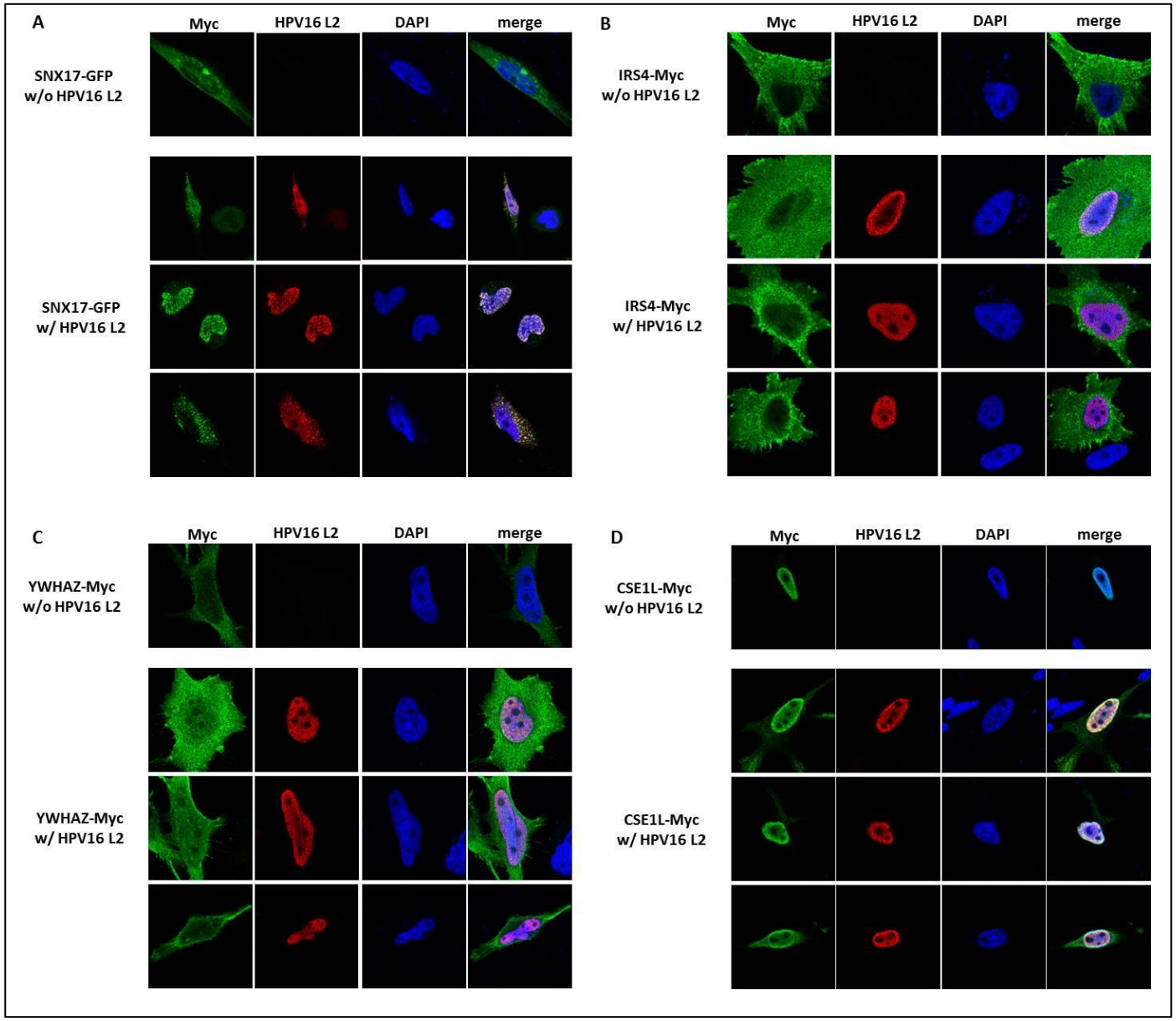

Figure 24 Subcellular localization of potential interaction candidates in absence and presence of HPV16 L2. Potential interaction candidates were expressed either in absence or presence of HPV16 L2. For visualization purposes, the candidates were used as a myc-tagged version, except SNX17, which was used as a fusion protein with GFP. The staining of the potential interaction candidates was performed using a rabbit derived α-myc antibody in combination with the corresponding α-rabbit-A488 secondary antibody (green). HPV16 L2 was stained with K4L2 aa20-38 and a α-mouse-A594 antibody (red). DAPI (blue) was used to stain the DNA in the nuclei. The analysis was performed by confocal microscopy. **A** Staining of SNX17-GFP expressed without (upper panel) or together with HPV16 L2 (lower panels). **B, C and D** Staining of the indicated myc-tagged candidates expressed without (upper panel) and with (lower panels) HPV16 L2.

4.2.4. *Influence of siRNA Knockdown of potential Candidates on HPV16 PsV transduction*

To gain further insight in the interaction of the selected candidates with HPV16 L2, siRNA knockdown of the corresponding candidates followed by HPV16 PsV transduction was performed. Therefore the expression of a specific candidate was down-regulated by treatment with siRNAs, targeting the mRNA of interest for degradation. 48h after siRNA treatment, the cells were infected with HPV16 PsV and the transduction efficiency was measured by Gaussia luciferase activity 48h post-infection. The experiment was performed to analyze the effect of the knockdown of distinct candidates on the infectivity of HPV16 PsV. For each candidate, a set of four different siRNAs was tested, targeting different regions of the corresponding mRNA. SNX17 was used as a positive control, since knockdown of SNX17 has previously been published to reduce HPV16 as well as HPV18 PsV transduction efficiency [109, 110]. For each assay performed in this study, the samples were tested in duplicates which were individually analyzed by western blot to determine the corresponding protein levels.

HPV16 transduction efficiency after siRNA knockdown of potential L2 interaction candidates

Figure 25A represents the summary of three independent siRNA knockdown experiments, using four different siRNAs for each candidate (IRS4, YWHAZ, CSE1L, CAPN2, CAND1 and SPOP) as well as the positive control SNX17. SPOP was included into the study, since it was previously identified as a AAV VP1 interaction candidate in a colleagues study (Burkart et al. unpublished). As negative control, cells were treated with a scrambled siRNA control which served as reference for PsV infectivity and represents 100% transduction (siRNA ctrl.). Additionally, one sample was not treated with any kind of siRNA (w/o siRNA). As published previously, knockdown of SNX17 expression led to reduced HPV16 PsV transduction at least in three out of the four tested siRNAs. The western blot analysis of the protein levels in the corresponding samples could validate successful knockdown for all of the siRNAs tested (Figure 25B). Also for the samples treated with the IRS4 siRNA, an inhibited transduction efficiency of HPV16 PsV could be observed in three of the tested samples. Even though the effect was slightly less pronounced compared to the positive control, the transduction was reduced to ~60% compared to the reference, treated with the siRNA ctrl.. However, the cells treated with the siRNA IRS4_3 showed an increased transduction with PsV of about 20% (Figure 25A). Knockdown of IRS4 could not be validated by western blot, due to a lack of a proper primary antibody targeting endogenous IRS4.

Additionally, HPV16 PsV transduction was observed to be decreased in three of the tested YWHAZ knockdown samples. Compared to the positive control, the inhibition of PsV infectivity was less

efficient with a transduction of about 80% remaining activity compared to the siRNA ctrl. reference. Cells treated with the siRNA YWHAZ_7 even showed a slightly increased infection level which was similar to the w/o RNA ctrl. (Figure 25A). This might indicate an insufficient knockdown, resulting in a higher amount of surviving cells after siRNA treatment.

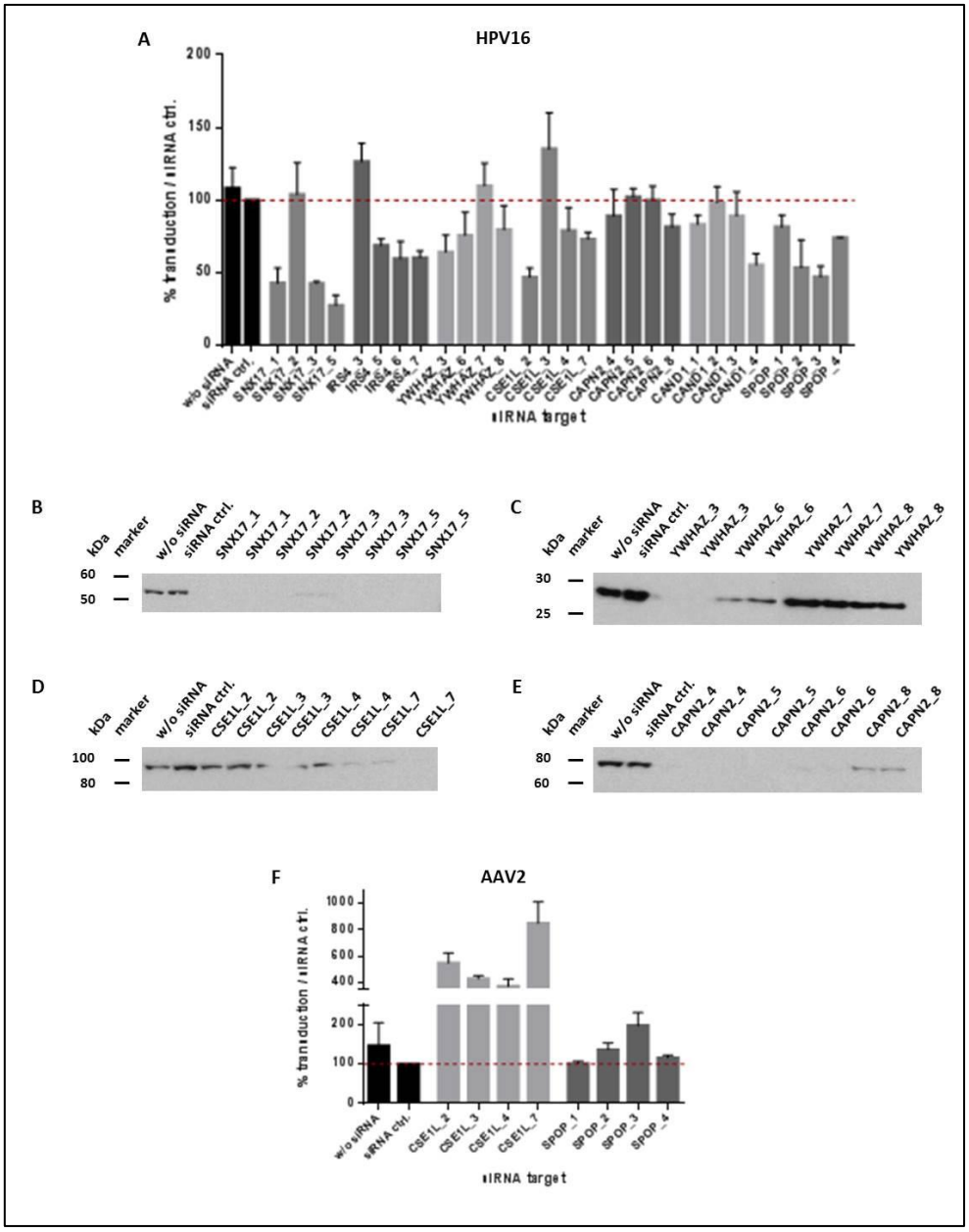

Figure 25 Influence of siRNA Knockdown of potential Candidates on HPV16 PsV transduction. A Cells were treated either with siRNAs targeting the potential interaction candidates (IRS4, YWHAZ, CSE1L, CAPN2, CAND1 and SPOP) or a scrambled siRNA control. For each candidate a set of four different siRNA, targeting different regions of the target mRNA, were used. As a positive control for reduced transduction with HPV16, siRNAs against SNX17 were included in the assay. The cells were infected with HPV16 PsV containing a Gaussia luciferase reporter plasmid and transduction was analyzed 48h after infection. **B, C, D and E** western blot analysis of proteins levels after knockdown of the indicated siRNAs and infection with HPV16 PsV. **D** reduced protein levels of CSE1L_3 might be due to incomplete transfer of proteins to the nitrocellulose membrane during western blot analysis. F Transduction of AAV2 was tested after knockdown with four different siRNAs targeting either CSE1L or SPOP compared to the cells treated with the scrambled siRNA control. The cells were infected with MOI 1000 of AAV2, containing a Gaussia reporter plasmid for 48h. Note: SPOP was previously identified as AAV interaction candidate (Burkart et al. unpublished).

The analysis of protein levels in the corresponding samples by western blot confirms an insufficient knockdown in the samples treated with siRNA YWHAZ_7. In the samples with reduced transduction of HPV16 PsV correlating knockdown efficiency on YWHAZ protein levels were observed (Figure 25C).

The treatment of cells with siRNAs targeting CSE1L led to inhibition of PsV infectivity in all the samples except the siRNA CSE1L_3 treated cells. The decrease of HPV16 PsV transduction efficiency was observed to be between 50% (CSE1L_2) and 20% (CSE1L_4 and CSE1L_7). However, the cells treated with CSE1L_3 showed an opposite effect on transduction with an increase of around 40% compared to the siRNA ctrl. (Figure 25A). According to the western blot analyzing of the protein levels of CSE1L, the knockdown was most efficient for the sample CSE1L_4 and CSE1L_7 (Figure 25D), both showing medium reduction levels in the transduction assay (Figure 25A). The strongest effect in the transduction assay was measured in the sample CSE1L_2, though the protein levels in the duplicates were only slightly reduced. Intermediate knockdown efficiency was detected for CSE1L_3 treated cells (Figure 25D) which showed increased transduction with HPV16 PsV (Figure 25A). However, the observed reduction in CSE1L protein level in this sample might also be due to incomplete transfer of the corresponding proteins during western blot analysis.

For the analysis of CAPN2 knockdown on the transduction with HPV16, no effect on infectivity could be observed (Figure 25A) even though knockdown efficiency was validated for all samples by western blot (Figure 25E). A similar result was obtained for CAND1, only a single siRNA (CAND1_4) showed a slight inhibiting effect on PsV infection. Since no suitable antibody against CAND1 was available, knockdown efficiency was not analyzed for the samples treated with siRNA against CAND1. Knockdown of SPOP led to decreased infection levels for all of the tested samples of about 50%-20% compared to the siRNA ctrl.. However, protein levels of the samples could not be analyzed since the endogenous SPOP protein level in untreated cells was below the detection limit in the western blot analysis. The results of the knockdown experiment indicated an inhibiting impact of IRS4, YWHAZ, CSE1L and SPOP knockdown on HPV16 PsV transduction. Whereas, knockdown of CAPN2 and CAND1 did not seem to have any influence on PsV infection.

Influence of siRNA knockdown of potential HPV16 L2 interaction candidates on AAV2 transduction efficiency

In addition to HPV16 infectivity, the transduction of AAV2 after knockdown of CSE1L and SPOP was analyzed. The two candidates were selected, since knockdown of CSE1L repeatedly showed a strong influence on AAV2 transduction while using AAV2 as a control for cell toxicity of the siRNA treatment. SPOP as a cellular factor for transduction originally derived colleague study (Burkart et al. unpublished) in which SPOP was found to be a potential AAV VP1 interaction candidate.

Knockdown of CSE1L followed by infection with AAV2 led to a strong increase of transduction efficiency for all of the siRNAs used (Figure 25F). According to the knockdown efficiency expected from the previously described experiment, the sample treated with CSE1L_7 had the strongest effect on AAV2 transduction. The infectivity with AAV2 was increased around 8 fold compared to the corresponding siRNA ctrl.. Additionally, SPOP knockdown was analyzed and showed no effect on AAV2 transduction for samples treated with SPOP_1 and SPOP_4, but a slight increase of transduction efficiency after knockdown with siRNA SPOP_2 and SPOP_3. However, the transduction with AAV2 in both cases was observed to be similar to the transduction of cells not treated with siRNA (w/o siRNA). These data indicate that the observed negative effects of knockdown of CSE and SPOP on HPV16 PSV transduction are not due to unspecific cellular toxicity. The same conclusion could be made for IRS4 and YWHAZ, both showing similar transduction rates as the siRNA ctrl. reference (data not shown).

4.2.5. *Lentivirus-mediated shRNA knockdown of potential candidates*

To further confirm the influence of the knockdown of candidates on HPV16 PsV transduction lentivirus mediated shRNA knockdown experiments were performed additionally. For this four out of the six candidates were selected, including IRS4, YWHAZ, CSE1L and SPOP for further analysis. In addition, lentiviruses containing either a shRNA against a non-mammalian target (shRNA ctrl.) or a GFP expression plasmid were used as controls for different steps of the experiment.

HPV16 transduction in selected Lentivirus shRNA knockdown cells

HeLa cells were infected with shRNA encoding lentiviruses and further selected for puromycin resistance. In this approach, only cells transduced with the lentivirus and expressing the corresponding plasmid with the puromycin resistance gene were used for further analysis. For each lentiviral construct two independent cell cultures were prepared and further tested individually. After several passages under puromycin treatment, the selected cells were used for a transduction assay with HPV16 PsV and AAV2.

Figure 26A and 26B represent summaries of two independent experiments. Luciferase activity in IRS4 and CSE1L knockdown cells, respectively, showed a reduction of infectivity by 50% (IRS4) and 20% (CSE1L) compared to the shRNA ctrl.. This observation was in concordance with the results from the siRNA knockdown in paragraph 5.2 as well as the results of an experiment with transiently lentivirus transduced HeLa cells (data not shown). However, the CSE1L knockdown showed an opposite effect in the transient lentivirus transduction experiment, described previously. For knockdown cells using shRNA targeting YWHAZ, one out of the two lentiviral transduced cell cultures did not show any

effect on HPV16 transduction, whereas the other culture had a 20% reduced transduction rate compared to the reference (shRNA ctrl.). This might be due to insufficient knockdown of YWHAZ in the cells showing no effect on HPV16 transduction. Compared to the control, the SPOP shRNA treated cells showed a slightly increased transduction rate with HPV16 PsV (~10%). As also the leintivirus-GFP transduced cells showed slightly elevated HPV16 transduction rates, the effect observed in the shRNA SPOP treated cells might be unspecific for the SPOP knockdown.

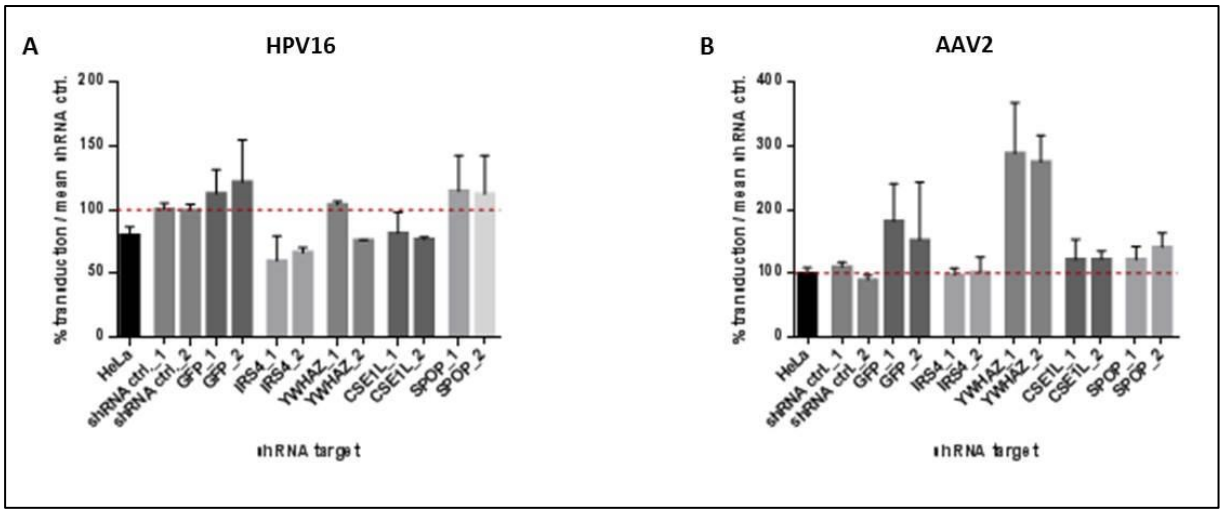

Figure 26 Transduction with HPV16 and AAV2 after lentivirus infection and selection for lentiviral transduced cells by puromycin. HeLa cells were transduced with lentiviruses encoding shRNAs for knockdown of selected candidates (IRS4, YWHAZ, CSE1L and SPOP) as well as a non-mammalian control (shRNA ctrl.) and a GFP control. 48h postinfection the cells were further cultured in a selection medium containing puromycin to select for lentiviral transduced cells. After several passages under puromycin selection, the cells were infected either with HPV16 PsV (A) or AAV2 (B) containing a Gaussia luciferase reporter plasmid. 48h post infection transduction was analyzed for luciferase activity.

The infection of untreated HeLa cells with PsV showed a reduced infection efficiency compared to PsV transduction of HeLa cells treated with the shRNA ctrl., indicating a slight effect of either lentivirus infection or puromycin selection on HPV16 PsV infection.

The same experiment was performed using AAV2 for transduction of the selected HeLa cells. After several passages of the cells under puromycin treatment strongly increased transduction could be observed for YWHAZ knockdown cells. Transduction efficiency of AAV2 was observed to be 3-fold over the shRNA ctrl. cultures in both of the YWHAZ knockdown cultures. Additionally, knockdown of CSE1L and SPOP showed increased AAV2 infectivity. However, the increase in AAV2 transduction was lower than the increase observed for the GFP expressing selected cells, maybe indicating an unspecific effect of lentiviral infection with CSE1L and SPOP encoding shRNA or puromycin selection.

4.3. *In silico analysis of different HPV L2 protein*

In parallel to the identification of interaction candidates, an *in vitro* analysis of L2 protein sequences from different HPV types was performed. For this, a set of 20 L2 sequences, comprising two low risk HPV sequences (HPV 6 and 11), 13 high risk HPV sequences (HPV 16, 18, 31, 33, 35, 39, 45, 51, 52, 56, 58, 59 and 66) and five sequences from potential high risk HPV types (HPV 25, 53, 68, 73 and 82) were analyzed. These sequences were screened by an online program (ELM) which predicts potential functional sites in protein sequences. A restriction of the program is the ability to analyze only functional sites which are described as linear motifs, thus missing conformational dependent sites. The overall analysis of the L2 sequences (between 450 and 473 aa), revealed around 150-200 potential functional sites. The results included protease cleavage sites, ligand binding sites and sites for protein modifications. Since HPV L2 is highly conserved, especially at the N-terminal part of the protein, a high number of overlapping hits could be observed in the analysis.

Because further evidence for the probability of specific functional sites was missing further analysis focused on the motifs with low probability values (0.00004-0.0005). A low probability value in the ELM analysis describes a high stringency of the corresponding motif sequence to be complied. The cut-off at a probability value of 0.0005 was selected since a known functional site, the furin cleavage site, which was detected for all of the HPV types shows a probability value of 0.0005. Therefore this value was suggested to be stringent enough for a reliable prediction based on the ELM data. Though, a lower probability value is not directly linked to an undependable prediction but rather describes functional sites with less stringent rules to be complied.

By analyzing the ELM results based on the stringency of the motifs, some motifs did stand out of the high number of potential functional sites. The ELM revealed a phosphotyrosin binding (PTB) domain (probability value 0.0001) which is known to act as an adapter or scaffold in several physiological process. These domains are known to be ligand binding sites for ligand activated growth factors, amongst other proteins and have been strongly associated with endocytic signaling pathways. Between two and four corresponding motifs were described in the L2 sequence of each HPV type with similar position within L2. In all of the 20 types analyzed the PTB domain was found around position aa 154-161 and aa 248-255. Additional PTB domains were found in differing localizations of the L2 protein sequence. Another motif which might be involved in several signal pathways and a probability value of 0.0002 was the Src homology (SH_2) domain. For example adaptor proteins, involved in signal transduction of the receptor tyrosine kinase pathway are known to contain SH_2 domains. The SH_2 domain was found at position aa 71-74 in the L2 sequence of each type analyzed by ELM.

Table 15: Examples of potential functional sites of L2 derived from ELM analysis

Motif	Description	Pattern	Probability Value	HPV types
Furin cleavage site[1]	Recognition site for furin protein convertase	R.[RK]R.*	0.0005	all
NLS[1]	Classical nuclear localization signal.	[^DE]((K[RK])|(RK))[KRP][KR][^DE]*	0.0002	HPV 6, 16, 18, 25, 31, 35, 39, 45, 51, 53, 59, 66, 68, 73, 82
Proprotein convertase 7 cleavage site	Recognition site for proprotein convertase 7	[R]...[KR]R.*	0.0005	HPV 6, 11, 16, 25, 33, 35, 51, 52, 53, 56, 58, 66 and 82
TRFH binding motif	Found in proteins recruited to the shelterin complex which recognizes telomere regions at the chromosomes	[FY].L.P*	0.0002	all
EVH1 domain	Protein-protein interaction module. EVH1 containing proteins are known to be associated with the actin cytoskeleton reorganization	[FILVY].{0,1}P.[PAILSK]P*	0.0001	HPV 6, 11, 16, 18, 31, 33, 51, 52, 53, 56, 58, 59, 66, 73 and 82
PDZ domain	Found in regulatory proteins, spending part of their time in membrane associated complexes. In combination with other signaling/regulatory domains involved in processes like transport and signal transduction	...[VLIFY].[ACVILF]$*	0.0001	HPV 6, 11, 16, 18, 31, 33, 35, 39, 45, 52, 53, 56, 58, 66
Fucosylation site	Attachment site for fucose residue to a serine.	C.{3,5}([ST])C	0.00004	all

[1] previously published functional sites within the HPV L2 protein sequence
*Nomenclature see table 116

However, the high number of potentially functional sites predicted by ELM and the lack of additional selection criteria prevented a significant selection of the most promising potential domains. Therefore, the ELM results were checked in context of previously identified interaction candidates from paragraph 5.1 to predict potential binding sites of the distinct proteins. For description of amino acid sequences ELM uses the nomenclature for peptide motifs described in the publication of Aasland and colleagues from 2002 [122].

Table 16: Nomenclature of ELM peptide motif description

Symbol	Description
[capital letters]	Distinct amino acids allowed
.	Unknown, other or any amino acid
[^..]	Listed amino acids are not allowed
[…]	Amino acid at this position can be any of the indicated amino acids
{ min, max }	Minimum required, maximum allowed amino acids
$	Matches the carboxy terminal
(...)	1. mark positions of, e.g. the amino acid covalently modified 2. Used to group parts of the expression
|	Matches either expression, separates two patterns

Identification of potential ligand binding site of IRS4

Literature research revealed an IRS-type PTB domain described in the sequence of the IRS4. IRS-type PTB domains are known to play a role in the interaction of IRS proteins and the IRS-receptor. The ELM describes a potential ligand binding site for proteins containing a Shc-like or an IRS-like PTB domain. According to the description, this domain complies one of two possible sequence patterns which are either (.[^P].NP.(Y)) or (.[ILVMFY].N..(Y)). The ELM analysis of L2 revealed corresponding sites within L2 sequences of different HPV types (Table 17). In the sequence of HPV16 L2, the described ligand binding site for IRS4 was identified at three different positions (aa 251-257, aa 261-267 and aa 360-366). Since IRS4 was previously identified in the TAP for the HPV16 full length and the HPV16 L2_Fr.3 (aa 262-473), the result of the ELM is in concordance with the TAP result. The ligand binding sites at position aa 261-267 and aa 360-366 are both included in the sequence of HPV16 L2_Fr3. However, the third potential domain (aa 251-257) was part of HPV16 L2_Fr.2 which did not reveal IRS4 as a potential interaction candidate, maybe due to unfavorable conformation or modification of HPV16 L2_Fr.2 in the TAP. Comparing the different HPV L2 sequences for the identification of the predicted IRS4 binding site, 12 out of 20 sequences showed one of the ELM described patterns.

Nine out of the 13 high risk HPV types (HPV16, 31, 33, 35, 39, 45, 51, 59 and 66) were observed to harbor at least one potential IRS4 binding domain. Furthermore, potential binding sites were identified in the low risk HPV types (HPV 6 and 11) and in one of the potential high risk types (HPV82). Seven of these HPV types showed a potential IRS4 binding site around position 246-252 and 251-257 (HPV6, 11, 16, 31, 35, 45 and 59), matching the same ELM pattern ((.[^P].NP.(Y))). The corresponding L2 domains were observed to be highly conserved, differing in a single amino acid located either at position two or six of the identified pattern. Additionally, for HPV 16 (aa 261-267), HPV 33 and HPV 39 an IRS4 binding site was predicted at a more C-terminal position around amino acid 350. In all three cases, the protein sequence complied with the ELM pattern (.[ILVMFY].N..(Y)).

The sequence of HPV16 (aa 360-366) and HPV39 (aa 355-361) were found to be highly similar whereas the HPV33 sequence (aa 337-343) showed strong differences.

Table 17: Overview of predicted IRS4 ligand sites in the different HPV L2 protein sequences

HPV type	Sequence	Position	Pattern	Probability
HPV 6	TYDNPVY	aa 248-254	(.[^P].NP.(Y))*	0.0001
HPV11	TYDNPVY	aa 247-253	(.[^P].NP.(Y))*	0.0001
HPV16	TYDNPAY	aa 251-257	(.[^P].NP.(Y))*	0.0001
	DVDNTLY	aa 261-267	(.[ILVMFY].N..(Y))*	0.0001
	SINNGLY	aa 360-366	(.[ILVMFY].N..(Y))*	0.0001
HPV18	-	not identified	-	-
HPV25	-	not identified	-	-
HPV31	TYENPAY	aa 246-252	(.[^P].NP.(Y))*	0.0001
HPV33	TVPNEQY	aa 337-343	(.[ILVMFY].N..(Y))*	0.0001
HPV35	TYDNPAY	aa 250-256	(.[^P].NP.(Y))*	0.0001
HPV39	DVDNNTY	aa 355-361	(.[ILVMFY].N..(Y))*	0.0001
HPV45	TFDNPAY	aa 250-256	(.[^P].NP.(Y))*	0.0001
HPV51	NIENPLY	aa 157-163	(.[^P].NP.(Y))*	0.0001
HPV52	-	not identified	-	-
HPV53	-	not identified	-	-
HPV56	-	not identified	-	-
HPV58	-	not identified	-	-
HPV59	TYDNPAY	aa 249-255	(.[^P].NP.(Y))*	0.0001
HPV66	TITNPLY	aa 156-162	(.[^P].NP.(Y))*	0.0001
HPV68	-	not identified	-	-
HPV73	-	not identified	-	-
HPV82	NIENPLY	aa 157-163	(.[^P].NP.(Y))*	0.0001

*Nomenclature see table 16

Identification of potential ligand binding site of YWHAZ

YWHAZ belongs to the family of 14-3-3 proteins, interacting with one of three patterns described by ELM (mode I binding motif, mode II binding motif or mode III binding motif). The three motifs are rather similar and differ only slightly with decreasing stringency from mode I (probability value: 0.008) to mode III (probability value: 0.0039) (Table 18). Thus, a mode I motif is more stringent than mode II or mode III. The ELM analysis of HPV16 L2 identified three potential 14-3-3 ligand sites, which were either mode II or mode III. One of the domains was found at the N-terminus of HPV16 L2 (aa 90-96). This domain confirmed the identification of YWHAZ in the TAP (5.1.1) with HPV16 L2 full length and HPV16 L2_Fr.1 (aa 1-193). The other ligand binding sites were located at aa 248-253 (mode III) and aa 315-321 (mode II). The corresponding positions match HPV16 L2_Fr.2 (aa 130-334) and HPV16 L2_Fr.3 (aa 262-473) of the TAP experiment, not revealing YWHAZ as a potential interaction candidate. Beside HPV16 L2, the L2 sequences of HPV 31, 33, 35, 52 and 58 were found to have a mode II ligand binding site at aa 89-95 (HPV 33, 35 and 52) or aa 90-96 (HPV 31).

Table 18: Overview of predicted YWHAZ ligand sites in the different HPV L2 protein sequences

HPV type	Sequence	Position	Pattern	Probability
HPV 6	HTTTSI [3] RLITYD [3]	aa 149-154 aa 245-250	[RHK][STALV].([ST]).[PESRDIF]*	0.0039
HPV11	RLVTYD [3] HSVTQS [3]	aa 244-249 aa 361-366	[RHK][STALV].([ST]).[PESRDIF] *	0.0039
HPV16	RPPLTVD [2] RSGKSIG [2]	aa 90-96 aa 315-321	R..[^P]([ST])[IVLM]. *	0.0016
	KLITYD [3]	aa 248-253	[RHK][STALV].([ST]).[PESRDIF] *	0.0039
HPV18	RKRASVT [2]	aa 9-15	R..[^P]([ST])[IVLM]. *	0.0016
	RSGTQI [3] RSTTSF [3]	aa 308-313 aa 364-369	[RHK][STALV].([ST]).[PESRDIF] *	0.0039
HPV25	RQSSTP [1]	aa 244-249	R.[^P]([ST])[^P]P*	0.0008
	RDLSSIN [2]	aa 365-371	R..[^P]([ST])[IVLM]. *	0.0016
	RVETTR [3]	aa 451-456	[RHK][STALV].([ST]).[PESRDIF] *	0.0039
HPV31	RPPVSID [2] RSGATIG [2]	aa 90-96 aa 308-314	R..[^P]([ST])[IVLM]. *	0.0016
HPV33	RPPVTVD [2]	aa 89-95	R..[^P]([ST])[IVLM]. *	0.0016
	KLITYD [3] HSYSTF [3]	aa 248-253 aa 379-384	[RHK][STALV].([ST]).[PESRDIF] *	0.0039
HPV35	RPPVTVE [2]	aa 89-95	R..[^P]([ST])[IVLM]. *	0.0016
	KLITYD [3]	aa 247-252	[RHK][STALV].([ST]).[PESRDIF] *	0.0039
HPV39	not identified	-	-	-
HPV45	KSFTYP [3]	aa 366-371	[RHK][STALV].([ST]).[PESRDIF] *	0.0039
HPV51	RKRASVT [2]	aa 9-15	R..[^P]([ST])[IVLM]. *	0.0016
	RLYSKS [3]	aa 226-231	[RHK][STALV].([ST]).[PESRDIF] *	0.0039
HPV52	RPPVTVE [2]	aa 89-95	R..[^P]([ST])[IVLM]. *	0.0016
HPV53	not identified	-	-	-
HPV56	not identified	-	-	-
HPV58	RPPVTVD [2]	aa 89-95	R..[^P]([ST])[IVLM]. *	0.0016
	RLVTYD [3] HSHTSF [3]	aa 248-253 aa 381-386	[RHK][STALV].([ST]).[PESRDIF] *	0.0039
HPV59	not identified	-	-	-
HPV66	not identified	-	-	-
HPV68	RSHISVP [2]	aa 375-381	R..[^P]([ST])[IVLM]. *	0.0016
HPV73	RLVTYD [3]	aa 253-258	[RHK][STALV].([ST]).[PESRDIF] *	0.0039
HPV82	RKRASVT [2]	aa 9-15	R..[^P]([ST])[IVLM]. *	0.0016

*Nomenclature see table 16
[1] mode I binding motif
[2] mode II binding motif
[3] mode III binding motif

All of the predicted YWHAZ ligand binding sites were highly similar, differing only in one of the variable amino acid positions. Furthermore, YWHAZ was identified in the PPD using the HPV16 L2 peptides aa 20-38 and aa 28-42 (5.1.6, Table 3). Though, the ELM did not determine a potential 14-3-3 interaction site at corresponding positions in the L2 sequence. However, each of the peptides contains a pattern similar to the ELM described 14-3-3 ligand binding site. In case of the aa 20-38 peptide, the pattern at aa 4-10 (KQAGTCP) is comparable to a mode III 14-3-3 motif ([RHK][STALV].([ST]).[PESRDIF]), except the additional glutamine at position 5. The peptide aa 28-42, harbors a pattern at position aa 9-15 (VEGKTIA) similar to a mode II pattern (R..[^P]([ST])[IVLM].). In this pattern, the arginine at position 9 was replaced by a valine. However, ELM did not provide any information if addition of an amino acid at position 2 of the pattern or a replacement by a hydrophobic amino acid is able to inhibit binding of 14-3-3 completely.

Comparing all of the tested L2 sequences, 15 out of 20 L2 sequences showed at least one of the described patterns. Four of the high risk HPV types (HPV 39, 56, 59 and 66) and one potentially high risk type (HPV 53) did not harbor a domain matching the 14-3-3 ligand binding site.

Identification of potential ligand binding site of CSE1L, CAPN2 and CAND1

An additional potential interaction candidate of HPV16 L2, identified in paragraph 5.1 was found to be the CSE1L. However, no binding motif has been described for CSE1L, yet. In contrast, literature research about the CAPN2 showed the presence of an EF-hand domain within the CAPN2 protein sequence contributing to protein-protein interactions. Additionally, HEAT repeats, representing important domains for protein interaction in the CAND1 protein are described in the literature. However the ELM analysis did not reveal any sites, potentially interacting with either of the described motif in CAPN2 or CAND1 within the L2 protein sequences tested. This might be due to the limitations of the ELM program, therefore not revealing any evidence about potential interactions of these proteins with L2.

5. Discussion

5.1. Identification and selection of HPV16 L2 interaction candidates

Tandem Affinity Purification

The tandem affinity purification is a two-step purification method which is supposed to result in specific co-purification of interacting candidates by reducing the number of contaminants. However, for identification of HPV16 L2 interaction candidates this method bears also some disadvantages. Since this method is based on the overexpression of the target protein in the cells, the protein is mainly limited to the nucleus and the cytosol of expressing cells. In this regard, L2 is only able to interact with a selection and not all of the proteins involved in viral infection. Compared to the capsid-incorporated L2, exposing only a limited number of epitopes [29-32], most interaction sites of the TAP fusion protein are supposed to be available for potential protein interaction. The availability of a high number of L2 epitopes makes the TAP method a promising system for the identification of potential interaction candidates involved in different steps of the viral infection pathway and life cycle.

Additional experiments were conducted with the aim to incorporate the Tap-tagged version of L2 into PsV bypassing the disadvantages of the TAP method. PsV produced with the TAP-tagged L2 were observed to be less efficient in transduction of infected cells, however showed a similar infectivity as L1-only PsV (data not shown). Incorporation of the L2-TAP, though, was confirmed to be successful, showing a comparable amount of L2-TAP and non-tagged L2 in the different PsV productions (data not shown). Further investigations on the L2-TAP PsV confirmed the PsV to be able to bind to the target cells but fail to be internalized (data not shown). Internalization was almost completely abolished and demonstrated to be much less efficient than L1 only PsV internalization. Infectious particles could only be generated by the production of chimeric PsV containing non-tagged and TAP-tagged L2 molecules whereas increasing amounts of non-tagged L2 correlated with increased transduction efficiency (data not shown). Fusion of L2 to the TAP tag might interfere with proper conformation of L2-TAP within the capsid. Little is known about the structure of L2 in general [43] and in context of viral capsids.

Immunoprecipitation of L2 from PsV infected cells

As described in the previous paragraph, infectious L2-TAP containing PsV could not be produced. In respect to overcome the disadvantages of the TAP method, IP of L2 was therefore performed from PsV infected cells using L2-specific antibodies. In contrast to the TAP method, based on the overexpression of the bait protein, PsV infection mimics the natural infection pathway, allowing co-purification of proteins directly involved in the infection process. Even though this method overcomes the limitations of L2 localization as described for the TAP method also the IP from infected cells bears some limitations. The viral capsid is predominately based on the assembly of L1 capsomers, representing the main structure [4]. L2, on the contrary, is finally incorporated and with around 12-36 molecules represents only a minor proportion of the capsid [27]. Only a limited number of L2 proteins enter the target cells via the PsV strongly reducing the availability of protein for precipitation. Furthermore, by incorporation of L2 into the viral capsid not all potentially functional sites of L2 are exposed for protein interaction, since L2 is mainly hidden within the L1 composed capsid. Several L2 epitopes, however, have been reported to be exposed even in the assembled HPV capsid [29-32]. The infection with PsV mimics the natural infection pathway of HPV, therefore allowing identification of interaction partners involved in different steps at different time points of HPV infection. Selection of a specific time point for IP represents another limiting factor for the identification of partners. Since at a specific time point only a distinct set of proteins can be identified and proteins interacting at earlier or later time points postinfection will be omitted due to the experimental set up.

Selection of suitable antibodies for IP of L2 from PsV infected cells

The limited availability of L2 epitopes made it indispensable to select for antibodies suitable for IP of PsV from infected cell extracts. Three L2-specific antibodies as well as two L1-directed antibodies were analyzed for their ability to precipitate L1/L2 from PsV infected cells. The two L1 antibodies confirmed precipitation of internalized PSV at all time points tested. PsV are entering the cell over a long period of time, indicated by constant increase of precipitated L1 signal intensity from 5-8h postinfection (Figure 4). Therefore, PsV-IP confirmed previous publications of papillomavirus entry kinetics, describing the half time of particle entry to be between 4-12h [94, 123, 124]. However, further analysis of the entry kinetics by Schelhaas and colleagues reported a dependence of entry kinetics on MOI used for infection [93]. While the half time of particles entering the cells using a low MOI was observed to be around 11h, the entry process gets faster with increasing the MOI (~4h). The data presented by Schelhaas et al. showed a constant increase of internalized PsV (MOI 10) until 8-9h postinfection before the detection by flow cytometry showed 100% internalization. This data correlates with the analyses of the performed PsV-IP. The specificity of the selected antibodies for

PsV-IP was confirmed by the negative controls. Progressing internalization to other compartments might lead to inaccessibility of PsV for precipitation by the applied IP protocol. The drop of L1 detection after 9h was probably caused by inefficient lysis of PsV containing compartments with the standard IP protocol.

The target regions of the L2 specific antibodies (K1L2 aa 64-81, K4L2 aa 20-38 and K18L2 aa 20-38) have previously been reported to be exposed at the surface of HPV capsid [29-31] therefore suggested to be available for IP of assembled HPV16 PsV. The results of the IP confirmed the availability of the corresponding L2 epitopes (aa 20-38 and aa 64-81) in the assembled PsV capsid by precipitation with K1L2 aa 64-81 and K4L2 aa 20-38. The epitopes are exposed even before the initial binding to HSPGs and the associated conformational changes confirmed by the precipitation of PsV only. However, precipitation targeting the epitope aa 20-38 was demonstrated to be restricted depending on the antibody used for the IP. While K4L2 aa 20-38 successfully precipitated L2, K18L2 aa 20-38 failed to purify PsV from the infected cells as well as from the PsV only. This indicates that inefficient L2 precipitation was rather due to modifications of the epitope than the exposure of the corresponding epitope. For K18L2 aa 20-38 binding, two cysteines within the corresponding epitope are essential for antibody binding [30]. Maybe these essential cysteines are modified somehow therefore preventing interaction with K18L2 aa 20-38. Although modification might be a possible explanation, also the structure of the PsV might be a limiting factor. In improperly assembled capsids, the L2 protein might be incorporated in an unnatural conformation, preventing interaction of K18L2 aa 20-38. However to make a final conclusion, the status of the corresponding cysteines and PsV assembly maybe inhibiting the IP of PsV by K18L2 aa 20-38 still need to be examined further.

Peptide pull down (PPD) of potential epitope interacting candidates from cell extracts

Rubio and colleagues identified several L2 epitopes targeted by neutralizing and cross-neutralizing antibodies (aa 20-38, aa 28-42 and aa 64-81) [30]. Since binding of these antibodies to the epitopes prevents infection in a PV-type specific or even type-independent manner, the epitopes are suggested to play an essential role during viral infection which is blocked by antibody binding. Potentially the epitopes are interaction sites for cellular proteins involved in internalization or trafficking of the virus necessary for the establishment of viral infection. As well as the other methods conducted for the identification of interaction partners, the PPD harbors several restrictions. Since only small epitopes are used for the identification of binding proteins, the co-purification is limited to a small set of cellular proteins potentially purified by this method. The limitation might probably be an advantage as well by identification of proteins at a restricted epitope, thus leading to a simultaneous identification of the corresponding interaction domain. However, it has not been shown that these epitopes are the actual target site of a protein interaction

inhibited by the neutralizing antibodies. It could also be possible that binding of the neutralizing antibody blocks interaction of a cellular protein close to the antibody site by covering only part of the interaction domain or by conformational terms. Therefore, proteins binding only part of the epitopes or even only close to these epitopes might not be identified due to the reduced number of available amino acids.

Shortlisting of potential interaction candidates of HPV16 L2 for further analysis

Since exclusion of generally known contaminants, like keratins and IgG, did not lead to a sufficient reduction of protein hits, additional criteria were necessary to select for the most promising interaction candidates. As an example, proteins were excluded based on the identification in non-overlapping fragments/peptides (TAP or PPD) or with HPV unrelated antibodies (PsV-IP). Not all of these criteria necessarily imply the excluded proteins to be unspecific protein hits, however were conducted for more stringent shortlisting of candidates. The exclusion of proteins from non-overlapping HPV16 L2 fragments, as an example, did not provide direct evidence to the contrary about the general existence of a specific protein interaction. Even though the existence of more than one protein interaction site might be rather unlikely, it cannot be excluded per se. This is also true, considering other criteria, like the elimination of protein hits appearing in a single screen within the same experimental set up. Even after selection based on the described criteria, a high number of potential candidates remained, thus proteins identified in more than one independent experiment were favored.

5.2. HPV16 L2 interaction with CSE1L/CAS protein

Identification of CSE1L (2 peptides) with two overlapping fragments in the TAP was confirmed by PsV-IP (1 peptide). Even though, identification of a single peptide (PsV-IP) is not a valid evidence for identification of proteins by MS, since a general agreement requires at least two independent peptides to be identified, repeated identification in three independent screens supported as true interaction candidate.

CSE1L is also known as exportin-2 or chromosome segregation-1 (yeast homolog) like protein. It was first reported as essential factor for importin α re-export to the cytoplasm after cargo release [125]. However, further investigation revealed additional functions in gene regulation by interaction with e.g. p53 [126] and CSE1L is supposed to play a role in apoptosis and proliferation [127, 128]. Additionally, CSE1L plays a role in viral infection e.g. in context of HIV [129]. Takeda et al. claimed CSE1L to have an essential role in nuclear import of the HIV Vpr protein. Even though there was no direct interaction of Vpr and CSE1L, CSE1L has been demonstrated to be important for the NPI-1 (importin α isotype) mediated nuclear transport of the protein [129]. It is known that HPV L2 protein contain two NLS sequences which might be involved in nuclear transport of the protein via importin α theoretically bridging HPV L2 with the CSE1L. The obtained data (Co-IP) on the interaction of CSE1L with HPV16 L2 validated interaction of the two proteins either directly or in a complex with importin α. Furthermore, the interaction with CSE1L in a importin α/importin β complex seems rather likely since for HPV11 and BPV1 L2 interaction with the importin complex has been reported already [58, 130]. There are several hypothesis on the mechanism of nuclear import, with some publications claiming nuclear envelope breakdown to be crucial for nuclear transport of the L2/viral DNA complex [119]. However, there are still many open questions on the nuclear transition of the L2/viral genome complex. Even though the described L2 NLS might not have a specific function during viral infection, the sequences might still be essential for establishment of a persistent infection or generation of new virions. A function of CSE1L in context of the importin complex might further be confirmed by the identification of importin 5 (note: also referred to as importin subunit β-3, member of the importin β family) in the TAP MS (HPV16 L2 full length). Importin was excluded for further analysis, however, based on the limited number of identified peptides. Members of the importin β family can either act to transport cargo proteins alone or in a heterodimeric complex with importin α subunits [131-133]. Maybe HPV16 L2 interaction with the heterodimeric importin complex leads to temporary interaction of CSE1L which be sufficient for co-purification of CSE1L with L2. This would indicate either direct interaction of L2 and CSE1L inducing release of the L2 from the importin complex or an indirect interaction of CSE1L with L2 via the interaction with importin α. After overexpression of CSE1L together with HPV16 L2, CSE1L shifted from an exclusive nuclear localization to an increased

cytoplasmic localization. This might indicate an increased transport through the nuclear envelope, thus an increase of importin α re-export to the cytoplasm. Maybe this is due to the overexpression of L2 and the involved high abundance of L2 to be transported. Also the co-localization of CSE1L with L2 mainly at the nuclear periphery and the lack of co-localization in the cytoplasm might support the hypothesis that CSE1L is involved in the transport of L2 to the nucleus. Transient interaction of the two proteins might for example induce the cargo release after passing the nuclear membrane. The role of CSE1L in HPV16 infection was additionally confirmed by a decreased transduction level of HPV16 PsV after downregulation of CSE1L. The impaired transduction might in this case not rely on reduced internalization or trafficking through endosome or TGN of the PsV but maybe due to improper release of the L2/DNA complex from the importin complex with the nucleus.

5.3. HPV16 L2 interaction with 14-3-3 zeta (YWHAZ)

YWHAZ was confirmed as potential interaction candidate by MS analysis of five independent experiments: the TAP analysis (HPV16 L2 full length → 1 peptide and HPV16 L2_Fr.1 → 2 peptides) as well as the PPD MS (HEK 293TT: aa 20-38 and aa 28-42 → both 2 peptides, HaCaT: aa 28-42 → 1 peptide). Even though in two samples the number of identified peptides did not fulfill general criteria, the repeated identification in several independent experiments indicated, YWHAZ is a true interaction partner of L2.

YWHAZ belongs to the 14-3-3 protein family representing the 14-3-3 zeta isoform (note: the phosphorylated from of 14-3-3 zeta is referred to as 14-3-3 delta). Proteins of this family represent adaptor proteins involved in a variety of signaling pathways, like apoptosis and cell cycle regulation [134, 135]. 14-3-3 proteins interact with a wide range of cellular proteins, including kinases, phosphatases and transmembrane receptors. Interaction of 14-3-3 proteins, with a specific protein, usually regulates the activity of the bound protein. The two major functions of YWHAZ have been described to be regulation of cell survival and cell cycle progression. In context of cell survival, YWHAZ has been reported to interact with a large number of apoptotic proteins [135, 136]. In addition, it is supposed to negatively regulate the G2-M phase checkpoint by modification of cyclin-dependent kinase activity [137-139]. In this context, 14-3-3 proteins and especially YWHAZ interact with phosphorylated regulators of the cell cycle, e.g. CDC25-B and C [137]. These phosphatases control G2-M transition by phosphorylation cyclin dependent kinases (CDK) [140]. Interaction of YWHAZ, CDC25-C prevents dephosphorylation of CDKs therefore impairing the assembly of e.g. the CDK1-cyclinB complex [140]. Additionally, YWHAZ is found in the cytoplasm where it has the ability to prevent nuclear import of NLS containing proteins [141] but also in the nucleus where it is expected to influence gene expression by regulating distinct transcription factors (e.g. p53) [142]. Several interactions with viral proteins have been reported e.g. with NS2 of MVM parvovirus and

HPV18 E6 [143, 144]. In context of HPV18 E6 interaction, YWHAZ is supposed to maintain the steady-state level of E6 expression [143]. In addition to an interaction of YWHAZ and L2 (IP), co-localization was demonstrated in the nuclei of overexpressing cells which was induced by a shift of the cytoplasmic YWHAZ to the nucleus. According to several publications, 14-3-3 proteins also contribute to the nuclear export of proteins as well as their retention in the cytoplasm [145-147]. Additionally, it has been demonstrated that 14-3-3 proteins regulate nuclear entry of cellular proteins [141, 148, 149]. In this regard it has been reported that 14-3-3 proteins mediate nuclear translocation by promoting the interaction of NLS containing proteins with importin α [149]. The efficiency of nuclear translocation strongly depends on the interaction affinity of the cargo protein to importin α [150], making the target sequence recognition a limiting factor [151]. Modifications of several proteins as the SV40 LT by phosphorylation have been demonstrated to increase the interaction with importin α/importin β complexes [152]. The deletion of the corresponding sites led to significantly lower translocation efficiency due to impaired recognition of the SV40 LT NLS sequence by the importin α [153]. Proteomic analyses suggested importin α to interact with 14-3-3 proteins [154], even though 14-3-3 proteins do not harbor an intrinsic NLS sequence. Further investigation demonstrated that the cellular proteins e.g. myopodin, binding both, 14-3-3 and importin α, mediating the interaction of the 14-3-3/myopodin/importin α complex [149]. The authors hypothesized that binding of myopodin to 14-3-3 might affect the conformation of myopodin, exposing the NLS and therefore making it available for binding to importin α [149]. Since the co-localization studies on YWHAZ and HPV16 L2 revealed an increase in nuclear localized YWHAZ, a function of YWHAZ in L2 nuclear translocation might be possible. The partial co-localization of the nuclear YWHAZ and L2 might therefore indicate the dissociation of the complex after successful import. Furthermore, the reduced transduction efficiency after YWHAZ knockdown indicates a beneficial effect of YWHAZ during the infection process, maybe in the translocation process of the L2/DNA complex to the nucleus. However, a different function of the interaction of YWHAZ and L2 might also be conceivable. In this regard L2 might impair a specific function of YWHAZ or recruit YWHAZ to modify the activity of cellular proteins by the interaction. Binding of 14-3-3 proteins with their interaction partners is mainly based on the recognition of phosphoserines and phosphothreonins [155, 156]. In HPV16 L2, three motifs, comply with the recognition criteria for 14-3-3 binding were identified of which the N-terminal binding motif (~90-96) was found to be conserved in several other types (HPV 31, 33, 35, 52 and 58).

5.4. HPV16 L2 interaction with insulin receptor substrate 4 (IRS4)

The insulin receptor substrate 4 was identified only by MS in TAP-tag purification, though the protein showed up in three independent approaches (both screens with HPV16 L2 full length and the screen eith HPV16 L2_Fr.3). In two of the three samples the protein was identified by 4 independent peptides, indicating a high likelihood for reliable identification. The third sample also provided two independent peptides complying general criteria for MS based protein identification.

IRS4 belongs to the family of insulin receptor substrates, consisting of IRS1, IRS2 and IRS4 in human cells. IRS3 is described to be expressed only in rodents and lacks a human equivalent. The human family members of IRS proteins represent a family of proteins strongly connected to signal transduction from activated growth factors. IRS members are phosphorylated upon receptor stimulation of e.g. the insulin receptor, IGF1R and FGFR [157]. After phosphorylation, IRS proteins bind to SH2 domain containing proteins, inducing a signal cascade, regulating cell metabolism and proliferation in several human cell lines [157-159]. Beside proliferation, interaction of IRS4 with distinct proteins, e.g. Brk was reported to have an influence on cell growth, survival and differentiation [160]. IRS4 also plays a role in the Akt signaling pathways through direct interaction with the p85 subunit of PI3K [157, 161]. According to the IRS4 activation by the IGF1 receptor, phosphorylated IRS4 has additionally been demonstrated to transduce the mitogenic signal derived from the activated IGF1R. Furthermore, for different viruses IRS4 was identified to function during infection. In this context, elevated IRS4 protein and mRNA level and activation of PI3K have been observed after infection with Adenovirus 5 (Ad5) [162, 163]. Interaction of IRS4 and Ad5E1A leads to constitutively activated IRS4 and association with PI3K. IRS4 might therefore enhance growth and proliferation of Ad5E1 expressing cells [163]. Additionally, a direct interaction of IRS4 and the AAV Rep protein was identified by TAP and validated, however the function of this interaction was not analyzed further [164]. It is generally known that PI3K/Akt/mTOR activation controls several cellular mechanisms, like metabolism growth and survival and proteins synthesis [165]. In viral infection Akt represents an essential factor for inhibition of apoptosis to extend the infection cycle. Therefore, several viruses acquired strategies to exploit Akt function to benefit in infection [166, 167]. Many DNA viruses so far have been reported to activate the PI3K pathway using different strategies. Members of the *Polyomaviridae*, as simian virus 40 (SV40) and mouse polyoma (Py) virus render PI3K and Akt constantly activated for transforming purposes [168-175]. One report described IRS1 to be required for SV40 transformation and claimed the large T (LT) antigen to IRS1 phosphorylation of Akt [176]. For HPV the activation of PI3K and Akt has primarily been described by functions of E6 and E7 inhibiting apoptosis by activation of the Akt pathway [177-179]. However, recent publication could demonstrate an early activation of the PI3K/Akt/mTOR pathway in HPV infection. In this context it

has been demonstrated that HPV activates the PI3K/Akt/mTOR pathway via interaction of HPV bound to heparan sulfate (HS) and growth factors (GF) with GF receptors [62, 82]. Probably the interaction prevents autophagy, playing an essential role in antiviral host cell response [180]. Since an activation of PI3K/Akt pathway seems to play a crucial role during viral infection through direct activation upon HPV binding, the constant regulation of this pathway during the initial infection might also be important. Since the IF data on the co-localization suggests a transient interaction of IRS4 and L2, this might indicate an activation of IRS4 function by L2 rather than a binding associated function of L2 and IRS4 in a complex. However, the link between L2 predominantly localized in the nucleus after overexpression and cytoplasmic IRS4 is still unclear similar to publication about SV40 LT and IRS1 [176]. IF analysis revealed an increase in nuclear localized IRS4 when co-expressed with HPV16 L2, however the mechanism of this recruitment is not revealed. Interaction domains of IRS4 have been identified at the C-terminal part of HPV16 L2 correlating with the identification in the TAP-tag purification. This potential interaction domain was observed to be conserved in seven of the tested HPV types (HPV 6, 11, 16, 31, 35, 45 and 59). However, even though HPV18 was not described to have a corresponding site for potential IRS4 interaction, transduction experiments using HPV18 PsV showed decreased transduction after IRS4 knockdown (data not shown). This might indicate the existence of an alternative interaction domain for IRS4 in HPV types lacking the described domain for HPV16.

5.5. HPV16 L2 interaction with calpain 4 (CAPN4)

Calpain 2 was identified in the MS analysis derived from the TAP co-purification using the HPV16 L2 full length (4 peptides) as well as the HPV16 L2_Fr.1 protein (3 peptides).

CAPN2 is a calcium-dependent non-lysosomal cysteine protease known to catalyze proteolysis of substrates in context of cytoskeletal reorganization and signal transduction. Calpains are involved in several processes, including signal transduction, cell proliferation, cell cycle progression, apoptosis and membrane fusion [181-183]. CAPN2 represents the catalytic subunit of m-calpain in which forms a heterodimer with the regulatory subunit CAPN4. Dissociation of the regulatory subunit from the catalytic subunit activates the proteolytic function of CAPN2 [184, 185]. In context of HPV, calpain has already been published to have distinct functions. In 2007 Darnell et al. described an interaction of HPV E7 with μ-calpain (CAPN1) to be essential for E7-mediated Rb degradation [186]. Calpain has also been demonstrated to be important for proteolytic processing of the E1^E4 protein of HPV16 and HPV18 for the formation of amyloid-like fibers and reorganization of the keratin network [187]. Furthermore calpains were identified to enhance herpes simplex virus 1 (HSV-1) intracellular trafficking and coxsackie virus B3 (CVB3) entry, trafficking and replication upon infection [188-190]. Regarding the function of calpain during viral trafficking, it has been reported that calpains are

activated by intracellular calcium (Ca^{2+}) release from the endoplasmatic reticulum (ER). The increase in intracellular Ca^{2+} concentration and calpain activation was demonstrated to facilitate infection with many viruses, like HIV, HSV, HCV and rotavirus [191-195]. For HSV-1, CAPN1 had been found to trigger entry and migration [189] whereas for CVB3 CAPN2 was found to be activated by Ca^{2+} release [190]. The confirmed interaction of CAPN2 with HPV16 L2 might correlation with a function during initial infection similar to other viruses. Instead of a calpain activation through increased intracellular Ca^{2+}, HPV16 L2 might bind CAPN2 directing CAPN2 to the actual site of function where CAPN4 is displaced. The obtained data on HPV16 PsV transduction after siRNA mediated CAPN2 knockdown do not correlate with this hypothesis, since no effect on PsV infectivity was observed. On the one hand this might either indicate CAPN2 to have a different role than the expected beneficial effect on initial virus infection. On the other hand it might also be possible, that experimental system was not suitable to detect a potential influence of CAPN2 on PsV transduction. First of all, Bozym et al. reported cell type specific differences of the function of CAPN2 in CVB3 infection, claiming a function of CAPN2 in endothelial but not in epithelial cell line [190]. Other reports also revealed a low level of calpain expression levels in HeLa cells, compared to e.g. other cancer cell lines, including e.g. a head and neck squamous carcinoma cell line [196]. The identification of CAPN2 (TAP) as well as the validation of the interaction with L2 by Co-IP, was both performed in HEK293TT cells whereas the IF as well as the knockdown experiments was performed in HeLa cells. The selection of a suitable cell line to analyze CAPN2 in context with HPV infection and L2 interaction might be crucial. Potentially there are differences in CAPN2 expression and function even in cell lines derived from the same organ but with different properties (e.g. cancer and non-cancer cell line).

5.6. HPV16 L2 interaction with cullin-associated and neddylation-dissociated 1 (CAND1)

Cullin-associated and neddylation-dissociated protein 1 (CAND1) was identified by MS analysis of the TAP co-purified proteins. In this experiment it was determined as potential interaction candidate in the HPV16 full length (3 peptides) and HPV16 L2_Fr.1 (2 peptides) TAP. Though there was no confirmation of a potential interaction by an additional experiment (e.g. PsV-IP or PPD), the number of peptides identified indicated a reliable detection of CAND1 as potential candidate.

CAND1 is known to directly interact with cullin1 in context of the SCF complex. This complex comprises four proteins, Cul1 and the RING domain protein Rbx1, forming the cullin-RING ubiquitin ligase, the adapter protein Skp1 and the substrate-binding F-box protein [197]. SCF complexes in general allow the recognition of substrates for ubiquitination, the cullin-RING ligases (CRL) function as E3 ubiquitin ligases [198]. Neddylation of Cul1 induces rearrangement of the SCF complex, specifically in the Cul1-Rbx binding which dissociates CAND1 and allows transfer of ubiquitin from the

associated E2 ligase to the substrate [199, 200]. *In vitro* and *in vivo* data about CAND1 are controversial. While the *in vitro* analyses of CAND1 suggest an inhibitory function on SCF complex assembly and ligase activity, in vivo data in *Arabidopsis* indicates a positive effect of CAND1 on the SCF complex [197, 201-204]. In this context CAND1 is supposed to have a regulatory function in the recycling process of substrate receptor modules maintaining proper CRL function. Regarding a potential association with viral infection, many viral proteins are reported to act on CRLs, mainly to initiate degradation of distinct cellular proteins. Examples are the adenovirus E4orf6 and E1B-55 [205] and the BZLF1 protein of EBV [206] inducing degradation of APOBEC3G (RNA-editing enzyme) and p53, respectively. Additionally, BPFL1, like other herpesvirus homologues of this protein has described to have NEDD8 specific deconjugase activity [207, 208]. Interaction of the catalytic site of BPLF1 with cullins prevents the binding of CAND1 and induces the proteasomal degradation of deneddylated cullins [209]. The inactivation of cullins is supposed to be beneficial for viral infection by inhibiting the innate immunity of the host [210-215] but also seems to be crucial for viral replication [208]. For HPV L2 proteins no protease activity has been described therefore a direct link between the EBV BPLF1 protein and L1 cannot be concluded. However, CAND1 is known to mediate the recycling of substrate receptor modules in context of the SCF complexes [198, 203, 204, 216, 217]. Recent publication reported the CAND1 protein to exchange F-box proteins therefore having an essential influence on verity of different SCF complexes. Specifically the promoting function of CAND1 in the F-box-cullin 1 assembly was described. Furthermore CAND1 was suggested to even favor specific F-box proteins depending on the availability of substrates [218]. Since CAND1 was found to bind different cullins, it is suggested that CAND1 similarly affects multiple CRLs [204, 219-222] and was suggested to function as substrate receptor exchange factor (SREF) for CRLs in general. Inhibition of CAND1 was observed to have a negative effect on some but not SCF complexes [204, 220-222] which might be explained by the differences in the exchange rates of the different SCF complexes [218]. Since an interaction of HPV16 L2 with CAND1 was validated (Co-IP and IF), HPV16 L2 might influence homeostasis of specific cellular proteins by deregulating CRLs through interaction with CAND1. The transduction rate of HP16 PsV was not affected by the downregulation of CAND1 therefore indicating that interaction of HPV16 L2 and CAND1 is not involved in any process of the initial infection. However, the deregulation of CRLs might play a role in steps of the viral life cycle occurring after the actual viral entry, like the viral assembly.

5.7. Conclusion

In the present study, several proteins have been identified as potential HPV16 L2 interaction partners by selection criteria from different MS analyses. The most promising candidates, IRS4, YWHAZ, CSE1L, CAPN2 and CAND1 were further validated for their binding capacity and the subcellular distribution in presence of HPV16 L2. In transduction experiments analyzing HPV16 PsV efficiency after downregulation of the corresponding candidates, the identified interactions were analyzed for their contribution in HPV infection. While downregulation of IRS4, YWHAZ and CSE1L inhibited PsV transduction, CAPN2 and CAND1 could not be demonstrated to play a role during the initial infection.

Based on the obtained data, IRS4 is suggested to play a role in maintaining the activation of the PI3K/Akt/mTOR pathway which was reported to be activated upon GFR stimulation by virus interaction with the host cell surface [62, 82]. Based on the results in this thesis, HPV16 L2 is hypothesized to recruit IRS4 to the nucleus where IRS4 gets activated to further supports constant PI3K activation and Akt signaling. However, the mechanisms underlying this hypothesis are not revealed and require further investigation. YWHAZ was also observed to reduce HPV16 PsV infectivity in the knockdown experiments and therefore suggesting YWHAZ either contributing to nuclear translocation of the L2/DNA complex or being regulated by L2. For IRS4 and YWHAZ, conservation of potential binding motifs in several HPV types could be identified in an *in silico* approach. Results from knockdown experiment including the transduction of HPV18, lacking the predicted IRS4 interaction domain led to the suggestion that an alternative binding site might exist in HPV18 L2. In addition, knockdown of CSE1L protein expression had also an inhibitory effect on the transduction with HPV16 PsV. Since this protein is known to be involved in cargo release from importin α/importin β complexes and the re-export of importin α, CSE1L is suggested to be an important factor contributing to the translocation of L2 to the nucleus upon initial infection. Downregulation of CAPN2 and CAND1 did have any influence on HPV16 PsV transduction in the performed experiments. While the interaction with CAND1 is supposed to have a function in CRL regulation at a later time point of the viral life cycle CAPN2 is still suggested to play a role in the infection pathway. Even though there are strong indications of functional interactions of the described proteins with HPV16 L2 further investigation of the mechanisms are indispensable. A closer look should be taken to the single steps of viral infection, including entry, trafficking and nuclear localization of the HPV16 L2/DNA complex to be able to distinguish the function of the proteins at different steps. In case of CAND1 further analysis should be conducted regarding later processes of the viral life cycle like the assembly of new virions under knockout conditions. The disclosure of the distinct functions of the described L2 interaction partners would maybe reveal further insight into the function of the minor capsid protein L2 during the viral life cycle.

6. References

1. Kovanda, A., et al., *Characterization of novel cutaneous human papillomavirus genotypes HPV-150 and HPV-151.* PLoS One, 2011. **6**(7): p. e22529.
2. Ghittoni, R., et al., *The biological properties of E6 and E7 oncoproteins from human papillomaviruses.* Virus Genes, 2010. **40**(1): p. 1-13.
3. de Villiers, E.M., et al., *Classification of papillomaviruses.* Virology, 2004. **324**(1): p. 17-27.
4. Kirnbauer, R., et al., *Papillomavirus L1 major capsid protein self-assembles into virus-like particles that are highly immunogenic.* Proc Natl Acad Sci U S A, 1992. **89**(24): p. 12180-4.
5. Accardi, R. and T. Gheit, *Cutaneous HPV and skin cancer.* Presse Med, 2014. **43**(12P2): p. e435-e443.
6. Munoz, N., et al., *Epidemiologic classification of human papillomavirus types associated with cervical cancer.* N Engl J Med, 2003. **348**(6): p. 518-27.
7. Schiffman, M.H., et al., *Biochemical epidemiology of cervical neoplasia: measuring cigarette smoke constituents in the cervix.* Cancer Res, 1987. **47**(14): p. 3886-8.
8. Denton, K.J., et al., *The sensitivity and specificity of p16(INK4a) cytology vs HPV testing for detecting high-grade cervical disease in the triage of ASC-US and LSIL pap cytology results.* Am J Clin Pathol, 2010. **134**(1): p. 12-21.
9. Munger, K. and P.M. Howley, *Human papillomavirus immortalization and transformation functions.* Virus Res, 2002. **89**(2): p. 213-28.
10. Kajitani, N., et al., *Productive Lifecycle of Human Papillomaviruses that Depends Upon Squamous Epithelial Differentiation.* Front Microbiol, 2012. **3**: p. 152.
11. Pett, M. and N. Coleman, *Integration of high-risk human papillomavirus: a key event in cervical carcinogenesis?* J Pathol, 2007. **212**(4): p. 356-67.
12. Werness, B.A., A.J. Levine, and P.M. Howley, *Association of human papillomavirus types 16 and 18 E6 proteins with p53.* Science, 1990. **248**(4951): p. 76-9.
13. Scheffner, M., et al., *The HPV-16 E6 and E6-AP complex functions as a ubiquitin-protein ligase in the ubiquitination of p53.* Cell, 1993. **75**(3): p. 495-505.
14. Munger, K., et al., *Complex formation of human papillomavirus E7 proteins with the retinoblastoma tumor suppressor gene product.* EMBO J, 1989. **8**(13): p. 4099-105.
15. Dyson, N., et al., *The human papilloma virus-16 E7 oncoprotein is able to bind to the retinoblastoma gene product.* Science, 1989. **243**(4893): p. 934-7.
16. Pagano, M., et al., *Binding of the human E2F transcription factor to the retinoblastoma protein but not to cyclin A is abolished in HPV-16-immortalized cells.* Oncogene, 1992. **7**(9): p. 1681-6.
17. White, E.A., et al., *Comprehensive analysis of host cellular interactions with human papillomavirus E6 proteins identifies new E6 binding partners and reflects viral diversity.* J Virol, 2012. **86**(24): p. 13174-86.
18. White, E.A., et al., *Systematic identification of interactions between host cell proteins and E7 oncoproteins from diverse human papillomaviruses.* Proc Natl Acad Sci U S A, 2012. **109**(5): p. E260-7.
19. Hagensee, M.E., N. Yaegashi, and D.A. Galloway, *Self-assembly of human papillomavirus type 1 capsids by expression of the L1 protein alone or by coexpression of the L1 and L2 capsid proteins.* J Virol, 1993. **67**(1): p. 315-22.
20. Buck, C.B. and B.L. Trus, *The papillomavirus virion: a machine built to hide molecular Achilles' heels.* Adv Exp Med Biol, 2012. **726**: p. 403-22.
21. Chen, X.S., et al., *Structure of small virus-like particles assembled from the L1 protein of human papillomavirus 16.* Mol Cell, 2000. **5**(3): p. 557-67.
22. Modis, Y., B.L. Trus, and S.C. Harrison, *Atomic model of the papillomavirus capsid.* EMBO J, 2002. **21**(18): p. 4754-62.

23. Wolf, M., et al., *Subunit interactions in bovine papillomavirus.* Proc Natl Acad Sci U S A, 2010. **107**(14): p. 6298-303.
24. Finnen, R.L., et al., *Interactions between papillomavirus L1 and L2 capsid proteins.* J Virol, 2003. **77**(8): p. 4818-26.
25. Day, P.M., et al., *Establishment of papillomavirus infection is enhanced by promyelocytic leukemia protein (PML) expression.* Proc Natl Acad Sci U S A, 2004. **101**(39): p. 14252-7.
26. Day, P.M., et al., *Mechanisms of human papillomavirus type 16 neutralization by l2 cross-neutralizing and l1 type-specific antibodies.* J Virol, 2008. **82**(9): p. 4638-46.
27. Buck, C.B., et al., *Arrangement of L2 within the papillomavirus capsid.* J Virol, 2008. **82**(11): p. 5190-7.
28. Sapp, M., et al., *Organization of the major and minor capsid proteins in human papillomavirus type 33 virus-like particles.* J Gen Virol, 1995. **76 (Pt 9)**: p. 2407-12.
29. Kawana, K., et al., *A surface immunodeterminant of human papillomavirus type 16 minor capsid protein L2.* Virology, 1998. **245**(2): p. 353-9.
30. Rubio, I., et al., *The N-terminal region of the human papillomavirus L2 protein contains overlapping binding sites for neutralizing, cross-neutralizing and non-neutralizing antibodies.* Virology, 2011. **409**(2): p. 348-59.
31. Yang, R., et al., *Cell surface-binding motifs of L2 that facilitate papillomavirus infection.* J Virol, 2003. **77**(6): p. 3531-41.
32. Gambhira, R., et al., *A protective and broadly cross-neutralizing epitope of human papillomavirus L2.* J Virol, 2007. **81**(24): p. 13927-31.
33. Kines, R.C., et al., *The initial steps leading to papillomavirus infection occur on the basement membrane prior to cell surface binding.* Proc Natl Acad Sci U S A, 2009. **106**(48): p. 20458-63.
34. Richards, R.M., et al., *Cleavage of the papillomavirus minor capsid protein, L2, at a furin consensus site is necessary for infection.* Proc Natl Acad Sci U S A, 2006. **103**(5): p. 1522-7.
35. Schiller, J.T. and D.R. Lowy, *Understanding and learning from the success of prophylactic human papillomavirus vaccines.* Nat Rev Microbiol, 2012. **10**(10): p. 681-92.
36. Campo, M.S., et al., *A peptide encoding a B-cell epitope from the N-terminus of the capsid protein L2 of bovine papillomavirus-4 prevents disease.* Virology, 1997. **234**(2): p. 261-6.
37. Kawana, Y., et al., *Human papillomavirus type 16 minor capsid protein l2 N-terminal region containing a common neutralization epitope binds to the cell surface and enters the cytoplasm.* J Virol, 2001. **75**(5): p. 2331-6.
38. Embers, M.E., et al., *Protective immunity to rabbit oral and cutaneous papillomaviruses by immunization with short peptides of L2, the minor capsid protein.* J Virol, 2002. **76**(19): p. 9798-805.
39. Gambhira, R., et al., *Protection of rabbits against challenge with rabbit papillomaviruses by immunization with the N terminus of human papillomavirus type 16 minor capsid antigen L2.* J Virol, 2007. **81**(21): p. 11585-92.
40. Marusic, M.B., et al., *Modification of human papillomavirus minor capsid protein L2 by sumoylation.* J Virol, 2010. **84**(21): p. 11585-9.
41. Doorbar, J. and P.H. Gallimore, *Identification of proteins encoded by the L1 and L2 open reading frames of human papillomavirus 1a.* J Virol, 1987. **61**(9): p. 2793-9.
42. Rippe, R.A. and W.J. Meinke, *Identification and characterization of the BPV-2 L2 protein.* Virology, 1989. **171**(1): p. 298-301.
43. Campos, S.K. and M.A. Ozbun, *Two highly conserved cysteine residues in HPV16 L2 form an intramolecular disulfide bond and are critical for infectivity in human keratinocytes.* PLoS One, 2009. **4**(2): p. e4463.
44. Gambhira, R., et al., *Role of L2 cysteines in papillomavirus infection and neutralization.* Virol J, 2009. **6**: p. 176.
45. Day, P.M., et al., *The papillomavirus minor capsid protein, L2, induces localization of the major capsid protein, L1, and the viral transcription/replication protein, E2, to PML oncogenic domains.* J Virol, 1998. **72**(1): p. 142-50.

46. Florin, L., et al., *Reorganization of nuclear domain 10 induced by papillomavirus capsid protein l2.* Virology, 2002. **295**(1): p. 97-107.
47. Becker, K.A., et al., *Dissection of human papillomavirus type 33 L2 domains involved in nuclear domains (ND) 10 homing and reorganization.* Virology, 2003. **314**(1): p. 161-7.
48. Becker, K.A., et al., *Nuclear localization but not PML protein is required for incorporation of the papillomavirus minor capsid protein L2 into virus-like particles.* J Virol, 2004. **78**(3): p. 1121-8.
49. Heino, P., J. Zhou, and P.F. Lambert, *Interaction of the papillomavirus transcription/replication factor, E2, and the viral capsid protein, L2.* Virology, 2000. **276**(2): p. 304-14.
50. Gornemann, J., et al., *Interaction of human papillomavirus type 16 L2 with cellular proteins: identification of novel nuclear body-associated proteins.* Virology, 2002. **303**(1): p. 69-78.
51. Schneider, M.A., et al., *The transcription factors TBX2 and TBX3 interact with human papillomavirus 16 (HPV16) L2 and repress the long control region of HPVs.* J Virol, 2013. **87**(8): p. 4461-74.
52. Florin, L., et al., *Assembly and translocation of papillomavirus capsid proteins.* J Virol, 2002. **76**(19): p. 10009-14.
53. Schafer, F., L. Florin, and M. Sapp, *DNA binding of L1 is required for human papillomavirus morphogenesis in vivo.* Virology, 2002. **295**(1): p. 172-81.
54. Mallon, R.G., D. Wojciechowicz, and V. Defendi, *DNA-binding activity of papillomavirus proteins.* J Virol, 1987. **61**(5): p. 1655-60.
55. Zhao, K.N., et al., *DNA packaging by L1 and L2 capsid proteins of bovine papillomavirus type 1.* Virology, 1998. **243**(2): p. 482-91.
56. Buck, C.B., et al., *Efficient intracellular assembly of papillomaviral vectors.* J Virol, 2004. **78**(2): p. 751-7.
57. Holmgren, S.C., et al., *The minor capsid protein L2 contributes to two steps in the human papillomavirus type 31 life cycle.* J Virol, 2005. **79**(7): p. 3938-48.
58. Bordeaux, J., et al., *The l2 minor capsid protein of low-risk human papillomavirus type 11 interacts with host nuclear import receptors and viral DNA.* J Virol, 2006. **80**(16): p. 8259-62.
59. Klucevsek, K., et al., *Nuclear import strategies of high-risk HPV18 L2 minor capsid protein.* Virology, 2006. **352**(1): p. 200-8.
60. Doorbar, J., et al., *The biology and life-cycle of human papillomaviruses.* Vaccine, 2012. **30 Suppl 5**: p. F55-70.
61. Zhou, J., et al., *Interaction of human papillomavirus (HPV) type 16 capsid proteins with HPV DNA requires an intact L2 N-terminal sequence.* J Virol, 1994. **68**(2): p. 619-25.
62. Surviladze, Z., A. Dziduszko, and M.A. Ozbun, *Essential roles for soluble virion-associated heparan sulfonated proteoglycans and growth factors in human papillomavirus infections.* PLoS Pathog, 2012. **8**(2): p. e1002519.
63. Johnson, K.M., et al., *Role of heparan sulfate in attachment to and infection of the murine female genital tract by human papillomavirus.* J Virol, 2009. **83**(5): p. 2067-74.
64. Abban, C.Y. and P.I. Meneses, *Usage of heparan sulfate, integrins, and FAK in HPV16 infection.* Virology, 2010. **403**(1): p. 1-16.
65. Liu, J. and S.C. Thorp, *Cell surface heparan sulfate and its roles in assisting viral infections.* Med Res Rev, 2002. **22**(1): p. 1-25.
66. Bernfield, M., et al., *Functions of cell surface heparan sulfate proteoglycans.* Annu Rev Biochem, 1999. **68**: p. 729-77.
67. Elenius, K., et al., *Induced expression of syndecan in healing wounds.* J Cell Biol, 1991. **114**(3): p. 585-95.
68. Shafti-Keramat, S., et al., *Different heparan sulfate proteoglycans serve as cellular receptors for human papillomaviruses.* J Virol, 2003. **77**(24): p. 13125-35.

69. Huang, H.S. and P.F. Lambert, *Use of an in vivo animal model for assessing the role of integrin alpha(6)beta(4) and syndecan-1 in early steps in papillomavirus infection.* Virology, 2012. **433**(2): p. 395-400.
70. Knappe, M., et al., *Surface-exposed amino acid residues of HPV16 L1 protein mediating interaction with cell surface heparan sulfate.* J Biol Chem, 2007. **282**(38): p. 27913-22.
71. Dasgupta, J., et al., *Structural basis of oligosaccharide receptor recognition by human papillomavirus.* J Biol Chem, 2011. **286**(4): p. 2617-24.
72. Schowalter, R.M., D.V. Pastrana, and C.B. Buck, *Glycosaminoglycans and sialylated glycans sequentially facilitate Merkel cell polyomavirus infectious entry.* PLoS Pathog, 2011. **7**(7): p. e1002161.
73. Selinka, H.C., et al., *Further evidence that papillomavirus capsids exist in two distinct conformations.* J Virol, 2003. **77**(24): p. 12961-7.
74. Day, P.M., D.R. Lowy, and J.T. Schiller, *Heparan sulfate-independent cell binding and infection with furin-precleaved papillomavirus capsids.* J Virol, 2008. **82**(24): p. 12565-8.
75. Bienkowska-Haba, M., H.D. Patel, and M. Sapp, *Target cell cyclophilins facilitate human papillomavirus type 16 infection.* PLoS Pathog, 2009. **5**(7): p. e1000524.
76. Pakula, R., et al., *Syndecan-1/CD147 association is essential for cyclophilin B-induced activation of p44/42 mitogen-activated protein kinases and promotion of cell adhesion and chemotaxis.* Glycobiology, 2007. **17**(5): p. 492-503.
77. Fischer, G., et al., *Cyclophilin and peptidyl-prolyl cis-trans isomerase are probably identical proteins.* Nature, 1989. **337**(6206): p. 476-8.
78. Schiller, J.T., P.M. Day, and R.C. Kines, *Current understanding of the mechanism of HPV infection.* Gynecol Oncol, 2010. **118**(1 Suppl): p. S12-7.
79. Bienkowska-Haba, M., et al., *Cyclophilins facilitate dissociation of the human papillomavirus type 16 capsid protein L1 from the L2/DNA complex following virus entry.* J Virol, 2012. **86**(18): p. 9875-87.
80. Selinka, H.C., et al., *Inhibition of transfer to secondary receptors by heparan sulfate-binding drug or antibody induces noninfectious uptake of human papillomavirus.* J Virol, 2007. **81**(20): p. 10970-80.
81. Roper, J.A., R.C. Williamson, and M.D. Bass, *Syndecan and integrin interactomes: large complexes in small spaces.* Curr Opin Struct Biol, 2012. **22**(5): p. 583-90.
82. Surviladze, Z., et al., *Cellular entry of human papillomavirus type 16 involves activation of the phosphatidylinositol 3-kinase/Akt/mTOR pathway and inhibition of autophagy.* J Virol, 2013. **87**(5): p. 2508-17.
83. Roden, R.B., et al., *Interaction of papillomaviruses with the cell surface.* J Virol, 1994. **68**(11): p. 7260-6.
84. Volpers, C., et al., *Binding and internalization of human papillomavirus type 33 virus-like particles by eukaryotic cells.* J Virol, 1995. **69**(6): p. 3258-64.
85. Woodham, A.W., et al., *The S100A10 subunit of the annexin A2 heterotetramer facilitates L2-mediated human papillomavirus infection.* PLoS One, 2012. **7**(8): p. e43519.
86. Waisman, D.M., *Annexin II tetramer: structure and function.* Mol Cell Biochem, 1995. **149-150**: p. 301-22.
87. Ma, G., et al., *Secretory leukocyte protease inhibitor binds to annexin II, a cofactor for macrophage HIV-1 infection.* J Exp Med, 2004. **200**(10): p. 1337-46.
88. Gerke, V., C.E. Creutz, and S.E. Moss, *Annexins: linking Ca2+ signalling to membrane dynamics.* Nat Rev Mol Cell Biol, 2005. **6**(6): p. 449-61.
89. Compton, T., *Receptors and immune sensors: the complex entry path of human cytomegalovirus.* Trends Cell Biol, 2004. **14**(1): p. 5-8.
90. Feire, A.L., H. Koss, and T. Compton, *Cellular integrins function as entry receptors for human cytomegalovirus via a highly conserved disintegrin-like domain.* Proc Natl Acad Sci U S A, 2004. **101**(43): p. 15470-5.

91. Giroglou, T., et al., *Human papillomavirus infection requires cell surface heparan sulfate.* J Virol, 2001. **75**(3): p. 1565-70.
92. Spoden, G., et al., *Clathrin- and caveolin-independent entry of human papillomavirus type 16--involvement of tetraspanin-enriched microdomains (TEMs).* PLoS One, 2008. **3**(10): p. e3313.
93. Schelhaas, M., et al., *Entry of human papillomavirus type 16 by actin-dependent, clathrin- and lipid raft-independent endocytosis.* PLoS Pathog, 2012. **8**(4): p. e1002657.
94. Selinka, H.C., T. Giroglou, and M. Sapp, *Analysis of the infectious entry pathway of human papillomavirus type 33 pseudovirions.* Virology, 2002. **299**(2): p. 279-287.
95. Smith, J.L., et al., *Caveolin-1-dependent infectious entry of human papillomavirus type 31 in human keratinocytes proceeds to the endosomal pathway for pH-dependent uncoating.* J Virol, 2008. **82**(19): p. 9505-12.
96. Bousarghin, L., et al., *Human papillomavirus 16 virus-like particles use heparan sulfates to bind dendritic cells and colocalize with langerin in Langerhans cells.* J Gen Virol, 2005. **86**(Pt 5): p. 1297-305.
97. Yan, M., et al., *Despite differences between dendritic cells and Langerhans cells in the mechanism of papillomavirus-like particle antigen uptake, both cells cross-prime T cells.* Virology, 2004. **324**(2): p. 297-310.
98. Fahey, L.M., et al., *A major role for the minor capsid protein of human papillomavirus type 16 in immune escape.* J Immunol, 2009. **183**(10): p. 6151-6.
99. Sapp, M.J., *HPV virions hitchhike a ride on retromer complexes.* Proc Natl Acad Sci U S A, 2013. **110**(18): p. 7116-7.
100. Ishii, Y., et al., *Inhibition of nuclear entry of HPV16 pseudovirus-packaged DNA by an anti-HPV16 L2 neutralizing antibody.* Virology, 2010. **406**(2): p. 181-8.
101. Yang, R., et al., *Interaction of L2 with beta-actin directs intracellular transport of papillomavirus and infection.* J Biol Chem, 2003. **278**(14): p. 12546-53.
102. Day, P.M., et al., *Identification of a role for the trans-Golgi network in human papillomavirus 16 pseudovirus infection.* J Virol, 2013. **87**(7): p. 3862-70.
103. Bonifacino, J.S. and R. Rojas, *Retrograde transport from endosomes to the trans-Golgi network.* Nat Rev Mol Cell Biol, 2006. **7**(8): p. 568-79.
104. Bossis, I., et al., *Interaction of tSNARE syntaxin 18 with the papillomavirus minor capsid protein mediates infection.* J Virol, 2005. **79**(11): p. 6723-31.
105. Dabydeen, S.A. and P.I. Meneses, *The role of NH4Cl and cysteine proteases in Human Papillomavirus type 16 infection.* Virol J, 2009. **6**: p. 109.
106. Laniosz, V., et al., *Human papillomavirus type 16 infection of human keratinocytes requires clathrin and caveolin-1 and is brefeldin a sensitive.* J Virol, 2009. **83**(16): p. 8221-32.
107. Kamper, N., et al., *A membrane-destabilizing peptide in capsid protein L2 is required for egress of papillomavirus genomes from endosomes.* J Virol, 2006. **80**(2): p. 759-68.
108. Bronnimann, M.P., et al., *A transmembrane domain and GxxxG motifs within L2 are essential for papillomavirus infection.* J Virol, 2013. **87**(1): p. 464-73.
109. Bergant Marusic, M., et al., *Human papillomavirus L2 facilitates viral escape from late endosomes via sorting nexin 17.* Traffic, 2012. **13**(3): p. 455-67.
110. Bergant, M. and L. Banks, *SNX17 facilitates infection with diverse papillomavirus types.* J Virol, 2013. **87**(2): p. 1270-3.
111. Bottcher, R.T., et al., *Sorting nexin 17 prevents lysosomal degradation of beta1 integrins by binding to the beta1-integrin tail.* Nat Cell Biol, 2012. **14**(6): p. 584-92.
112. Steinberg, F., et al., *SNX17 protects integrins from degradation by sorting between lysosomal and recycling pathways.* J Cell Biol, 2012. **197**(2): p. 219-30.
113. Pim, D., et al., *A Novel Pdz Domain Interaction Mediates the Binding between Hpv-16 L2 and Sorting Nexin 27 and Modulates Virion Trafficking.* J Virol, 2015.
114. Temkin, P., et al., *SNX27 mediates retromer tubule entry and endosome-to-plasma membrane trafficking of signalling receptors.* Nat Cell Biol, 2011. **13**(6): p. 715-21.

115. Popa, A., et al., *Direct binding of retromer to human papillomavirus type 16 minor capsid protein L2 mediates endosome exit during viral infection.* PLoS Pathog, 2015. **11**(2): p. e1004699.
116. Schneider, M.A., et al., *Identification of the dynein light chains required for human papillomavirus infection.* Cell Microbiol, 2011. **13**(1): p. 32-46.
117. Tai, A.W., J.Z. Chuang, and C.H. Sung, *Localization of Tctex-1, a cytoplasmic dynein light chain, to the Golgi apparatus and evidence for dynein complex heterogeneity.* J Biol Chem, 1998. **273**(31): p. 19639-49.
118. Herzig, R.P., U. Andersson, and R.C. Scarpulla, *Dynein light chain interacts with NRF-1 and EWG, structurally and functionally related transcription factors from humans and drosophila.* J Cell Sci, 2000. **113 Pt 23**: p. 4263-73.
119. Pyeon, D., et al., *Establishment of human papillomavirus infection requires cell cycle progression.* PLoS Pathog, 2009. **5**(2): p. e1000318.
120. Mamoor, S., et al., *The high risk HPV16 L2 minor capsid protein has multiple transport signals that mediate its nucleocytoplasmic traffic.* Virology, 2012. **422**(2): p. 413-24.
121. Wang, J.W. and R.B. Roden, *L2, the minor capsid protein of papillomavirus.* Virology, 2013. **445**(1-2): p. 175-86.
122. Aasland, R., et al., *Normalization of nomenclature for peptide motifs as ligands of modular protein domains.* FEBS Lett, 2002. **513**(1): p. 141-4.
123. Day, P.M., D.R. Lowy, and J.T. Schiller, *Papillomaviruses infect cells via a clathrin-dependent pathway.* Virology, 2003. **307**(1): p. 1-11.
124. Culp, T.D. and N.D. Christensen, *Kinetics of in vitro adsorption and entry of papillomavirus virions.* Virology, 2004. **319**(1): p. 152-61.
125. Kutay, U., et al., *Export of importin alpha from the nucleus is mediated by a specific nuclear transport factor.* Cell, 1997. **90**(6): p. 1061-71.
126. Tanaka, T., et al., *hCAS/CSE1L associates with chromatin and regulates expression of select p53 target genes.* Cell, 2007. **130**(4): p. 638-50.
127. Behrens, P., et al., *Implication of the proliferation and apoptosis associated CSE1L/CAS gene for breast cancer development.* Anticancer Res, 2001. **21**(4A): p. 2413-7.
128. Behrens, P., U. Brinkmann, and A. Wellmann, *CSE1L/CAS: its role in proliferation and apoptosis.* Apoptosis, 2003. **8**(1): p. 39-44.
129. Takeda, E., et al., *Nuclear exportin receptor CAS regulates the NPI-1-mediated nuclear import of HIV-1 Vpr.* PLoS One, 2011. **6**(11): p. e27815.
130. Fay, A., et al., *The positively charged termini of L2 minor capsid protein required for bovine papillomavirus infection function separately in nuclear import and DNA binding.* J Virol, 2004. **78**(24): p. 13447-54.
131. Gorlich, D., et al., *Two different subunits of importin cooperate to recognize nuclear localization signals and bind them to the nuclear envelope.* Curr Biol, 1995. **5**(4): p. 383-92.
132. Gorlich, D., et al., *Distinct functions for the two importin subunits in nuclear protein import.* Nature, 1995. **377**(6546): p. 246-8.
133. Moroianu, J., G. Blobel, and A. Radu, *Previously identified protein of uncertain function is karyopherin alpha and together with karyopherin beta docks import substrate at nuclear pore complexes.* Proc Natl Acad Sci U S A, 1995. **92**(6): p. 2008-11.
134. Nishimura, Y., et al., *Overexpression of YWHAZ relates to tumor cell proliferation and malignant outcome of gastric carcinoma.* Br J Cancer, 2013. **108**(6): p. 1324-31.
135. Weerasekara, V.K., et al., *Metabolic-stress-induced rearrangement of the 14-3-3zeta interactome promotes autophagy via a ULK1- and AMPK-regulated 14-3-3zeta interaction with phosphorylated Atg9.* Mol Cell Biol, 2014. **34**(24): p. 4379-88.
136. Liang, R., et al., *[Inhibitory effect of 14-3-3zeta on the proliferation of HL-60 cells and HL-60/VCR cells].* Zhongguo Shi Yan Xue Ye Xue Za Zhi, 2013. **21**(4): p. 866-71.
137. Mils, V., et al., *Specific interaction between 14-3-3 isoforms and the human CDC25B phosphatase.* Oncogene, 2000. **19**(10): p. 1257-65.

138. Jiang, K., et al., *Regulation of Chk1 includes chromatin association and 14-3-3 binding following phosphorylation on Ser-345.* J Biol Chem, 2003. **278**(27): p. 25207-17.
139. Lammer, C., et al., *The cdc25B phosphatase is essential for the G2/M phase transition in human cells.* J Cell Sci, 1998. **111 (Pt 16)**: p. 2445-53.
140. Timofeev, O., et al., *Cdc25 phosphatases are required for timely assembly of CDK1-cyclin B at the G2/M transition.* J Biol Chem, 2010. **285**(22): p. 16978-90.
141. Jerome, M. and H.K. Paudel, *14-3-3zeta regulates nuclear trafficking of protein phosphatase 1alpha (PP1alpha) in HEK-293 cells.* Arch Biochem Biophys, 2014. **558**: p. 28-35.
142. Stavridi, E.S., et al., *Substitutions that compromise the ionizing radiation-induced association of p53 with 14-3-3 proteins also compromise the ability of p53 to induce cell cycle arrest.* Cancer Res, 2001. **61**(19): p. 7030-3.
143. Boon, S.S. and L. Banks, *High-risk human papillomavirus E6 oncoproteins interact with 14-3-3zeta in a PDZ binding motif-dependent manner.* J Virol, 2013. **87**(3): p. 1586-95.
144. Brockhaus, K., et al., *Nonstructural proteins NS2 of minute virus of mice associate in vivo with 14-3-3 protein family members.* J Virol, 1996. **70**(11): p. 7527-34.
145. Mahalakshmi, R.N., et al., *Nuclear transport of Kir/Gem requires specific signals and importin alpha5 and is regulated by calmodulin and predicted serine phosphorylations.* Traffic, 2007. **8**(9): p. 1150-63.
146. Mahalakshmi, R.N., et al., *Nuclear localization of endogenous RGK proteins and modulation of cell shape remodeling by regulated nuclear transport.* Traffic, 2007. **8**(9): p. 1164-78.
147. Li, F.Q., et al., *Nuclear-cytoplasmic shuttling of Chibby controls beta-catenin signaling.* Mol Biol Cell, 2010. **21**(2): p. 311-22.
148. Agassandian, M., et al., *Calcium-calmodulin kinase I cooperatively regulates nucleocytoplasmic shuttling of CCTalpha by accessing a nuclear export signal.* Mol Biol Cell, 2012. **23**(14): p. 2755-69.
149. Faul, C., et al., *Promotion of importin alpha-mediated nuclear import by the phosphorylation-dependent binding of cargo protein to 14-3-3.* J Cell Biol, 2005. **169**(3): p. 415-24.
150. Weis, K., *Regulating access to the genome: nucleocytoplasmic transport throughout the cell cycle.* Cell, 2003. **112**(4): p. 441-51.
151. Jans, D.A., C.Y. Xiao, and M.H. Lam, *Nuclear targeting signal recognition: a key control point in nuclear transport?* Bioessays, 2000. **22**(6): p. 532-44.
152. Hubner, S., C.Y. Xiao, and D.A. Jans, *The protein kinase CK2 site (Ser111/112) enhances recognition of the simian virus 40 large T-antigen nuclear localization sequence by importin.* J Biol Chem, 1997. **272**(27): p. 17191-5.
153. Harreman, M.T., et al., *Regulation of nuclear import by phosphorylation adjacent to nuclear localization signals.* J Biol Chem, 2004. **279**(20): p. 20613-21.
154. Brunet, A., et al., *14-3-3 transits to the nucleus and participates in dynamic nucleocytoplasmic transport.* J Cell Biol, 2002. **156**(5): p. 817-28.
155. Yaffe, M.B., et al., *A motif-based profile scanning approach for genome-wide prediction of signaling pathways.* Nat Biotechnol, 2001. **19**(4): p. 348-53.
156. Muslin, A.J., et al., *Interaction of 14-3-3 with signaling proteins is mediated by the recognition of phosphoserine.* Cell, 1996. **84**(6): p. 889-97.
157. Fantin, V.R., et al., *Characterization of insulin receptor substrate 4 in human embryonic kidney 293 cells.* J Biol Chem, 1998. **273**(17): p. 10726-32.
158. Cuevas, E.P., et al., *Role of insulin receptor substrate-4 in IGF-I-stimulated HEPG2 proliferation.* J Hepatol, 2007. **46**(6): p. 1089-98.
159. Fantin, V.R., et al., *Insulin receptor substrate 4 supports insulin- and interleukin 4-stimulated proliferation of hematopoietic cells.* Biochem Biophys Res Commun, 1999. **260**(3): p. 718-23.
160. Qiu, H., et al., *Interaction between Brk kinase and insulin receptor substrate-4.* Oncogene, 2005. **24**(36): p. 5656-64.
161. Hoxhaj, G., K. Dissanayake, and C. MacKintosh, *Effect of IRS4 levels on PI 3-kinase signalling.* PLoS One, 2013. **8**(9): p. e73327.

162. O'Shea, C., et al., *Adenoviral proteins mimic nutrient/growth signals to activate the mTOR pathway for viral replication.* EMBO J, 2005. **24**(6): p. 1211-21.
163. Shimwell, N.J., et al., *Adenovirus 5 E1A is responsible for increased expression of insulin receptor substrate 4 in established adenovirus 5-transformed cell lines and interacts with IRS components activating the PI3 kinase/Akt signalling pathway.* Oncogene, 2009. **28**(5): p. 686-97.
164. Nash, K., et al., *Identification of cellular proteins that interact with the adeno-associated virus rep protein.* J Virol, 2009. **83**(1): p. 454-69.
165. Andjelkovic, M., et al., *Role of translocation in the activation and function of protein kinase B.* J Biol Chem, 1997. **272**(50): p. 31515-24.
166. Buchkovich, N.J., et al., *The TORrid affairs of viruses: effects of mammalian DNA viruses on the PI3K-Akt-mTOR signalling pathway.* Nat Rev Microbiol, 2008. **6**(4): p. 266-75.
167. Cooray, S., *The pivotal role of phosphatidylinositol 3-kinase-Akt signal transduction in virus survival.* J Gen Virol, 2004. **85**(Pt 5): p. 1065-76.
168. Ichaso, N. and S.M. Dilworth, *Cell transformation by the middle T-antigen of polyoma virus.* Oncogene, 2001. **20**(54): p. 7908-16.
169. Summers, S.A., L. Lipfert, and M.J. Birnbaum, *Polyoma middle T antigen activates the Ser/Thr kinase Akt in a PI3-kinase-dependent manner.* Biochem Biophys Res Commun, 1998. **246**(1): p. 76-81.
170. Kaplan, D.R., et al., *Common elements in growth factor stimulation and oncogenic transformation: 85 kd phosphoprotein and phosphatidylinositol kinase activity.* Cell, 1987. **50**(7): p. 1021-9.
171. Kaplan, D.R., et al., *Phosphatidylinositol metabolism and polyoma-mediated transformation.* Proc Natl Acad Sci U S A, 1986. **83**(11): p. 3624-8.
172. Utermark, T., et al., *The p110alpha isoform of phosphatidylinositol 3-kinase is essential for polyomavirus middle T antigen-mediated transformation.* J Virol, 2007. **81**(13): p. 7069-76.
173. Whitman, M., et al., *Association of phosphatidylinositol kinase activity with polyoma middle-T competent for transformation.* Nature, 1985. **315**(6016): p. 239-42.
174. Simmons, D.T., *SV40 large T antigen functions in DNA replication and transformation.* Adv Virus Res, 2000. **55**: p. 75-134.
175. Rundell, K. and R. Parakati, *The role of the SV40 ST antigen in cell growth promotion and transformation.* Semin Cancer Biol, 2001. **11**(1): p. 5-13.
176. DeAngelis, T., et al., *Transformation by the simian virus 40 T antigen is regulated by IGF-I receptor and IRS-1 signaling.* Oncogene, 2006. **25**(1): p. 32-42.
177. Spangle, J.M. and K. Munger, *The human papillomavirus type 16 E6 oncoprotein activates mTORC1 signaling and increases protein synthesis.* J Virol, 2010. **84**(18): p. 9398-407.
178. Pim, D., et al., *Activation of the protein kinase B pathway by the HPV-16 E7 oncoprotein occurs through a mechanism involving interaction with PP2A.* Oncogene, 2005. **24**(53): p. 7830-8.
179. Menges, C.W., et al., *Human papillomavirus type 16 E7 up-regulates AKT activity through the retinoblastoma protein.* Cancer Res, 2006. **66**(11): p. 5555-9.
180. Deretic, V. and B. Levine, *Autophagy, immunity, and microbial adaptations.* Cell Host Microbe, 2009. **5**(6): p. 527-49.
181. Saido, T.C., H. Sorimachi, and K. Suzuki, *Calpain: new perspectives in molecular diversity and physiological-pathological involvement.* FASEB J, 1994. **8**(11): p. 814-22.
182. Huang, Y. and K.K. Wang, *The calpain family and human disease.* Trends Mol Med, 2001. **7**(8): p. 355-62.
183. Carafoli, E. and M. Molinari, *Calpain: a protease in search of a function?* Biochem Biophys Res Commun, 1998. **247**(2): p. 193-203.
184. Yoshizawa, T., et al., *Calpain dissociates into subunits in the presence of calcium ions.* Biochem Biophys Res Commun, 1995. **208**(1): p. 376-83.

185. Pal, G.P., J.S. Elce, and Z. Jia, *Dissociation and aggregation of calpain in the presence of calcium.* J Biol Chem, 2001. **276**(50): p. 47233-8.
186. Darnell, G.A., et al., *Human papillomavirus E7 requires the protease calpain to degrade the retinoblastoma protein.* J Biol Chem, 2007. **282**(52): p. 37492-500.
187. Khan, J., et al., *Role of calpain in the formation of human papillomavirus type 16 E1^E4 amyloid fibers and reorganization of the keratin network.* J Virol, 2011. **85**(19): p. 9984-97.
188. Li, M., et al., *Coxsackievirus B3-induced calpain activation facilitates the progeny virus replication via a likely mechanism related with both autophagy enhancement and apoptosis inhibition in the early phase of infection: an in vitro study in H9c2 cells.* Virus Res, 2014. **179**: p. 177-86.
189. Zheng, K., et al., *Calcium-signal facilitates herpes simplex virus type 1 nuclear transport through slingshot 1 and calpain-1 activation.* Virus Res, 2014. **188**: p. 32-7.
190. Bozym, R.A., et al., *Release of intracellular calcium stores facilitates coxsackievirus entry into polarized endothelial cells.* PLoS Pathog, 2010. **6**(10): p. e1001135.
191. Benali-Furet, N.L., et al., *Hepatitis C virus core triggers apoptosis in liver cells by inducing ER stress and ER calcium depletion.* Oncogene, 2005. **24**(31): p. 4921-33.
192. Manninen, A. and K. Saksela, *HIV-1 Nef interacts with inositol trisphosphate receptor to activate calcium signaling in T cells.* J Exp Med, 2002. **195**(8): p. 1023-32.
193. Foti, M., et al., *The HIV Nef protein alters Ca(2+) signaling in myelomonocytic cells through SH3-mediated protein-protein interactions.* J Biol Chem, 1999. **274**(49): p. 34765-72.
194. Tian, P., et al., *The rotavirus nonstructural glycoprotein NSP4 mobilizes Ca2+ from the endoplasmic reticulum.* J Virol, 1995. **69**(9): p. 5763-72.
195. Cheshenko, N., et al., *Herpes simplex virus triggers activation of calcium-signaling pathways.* J Cell Biol, 2003. **163**(2): p. 283-93.
196. Zhu, D.M. and F.M. Uckun, *Calpain inhibitor II induces caspase-dependent apoptosis in human acute lymphoblastic leukemia and non-Hodgkin's lymphoma cells as well as some solid tumor cells.* Clin Cancer Res, 2000. **6**(6): p. 2456-63.
197. Zheng, J., et al., *CAND1 binds to unneddylated CUL1 and regulates the formation of SCF ubiquitin E3 ligase complex.* Mol Cell, 2002. **10**(6): p. 1519-26.
198. Dye, B.T. and B.A. Schulman, *Structural mechanisms underlying posttranslational modification by ubiquitin-like proteins.* Annu Rev Biophys Biomol Struct, 2007. **36**: p. 131-50.
199. Duda, D.M., et al., *Structural insights into NEDD8 activation of cullin-RING ligases: conformational control of conjugation.* Cell, 2008. **134**(6): p. 995-1006.
200. Saha, A. and R.J. Deshaies, *Multimodal activation of the ubiquitin ligase SCF by Nedd8 conjugation.* Mol Cell, 2008. **32**(1): p. 21-31.
201. Bornstein, G., D. Ganoth, and A. Hershko, *Regulation of neddylation and deneddylation of cullin1 in SCFSkp2 ubiquitin ligase by F-box protein and substrate.* Proc Natl Acad Sci U S A, 2006. **103**(31): p. 11515-20.
202. Goldenberg, S.J., et al., *Structure of the Cand1-Cul1-Roc1 complex reveals regulatory mechanisms for the assembly of the multisubunit cullin-dependent ubiquitin ligases.* Cell, 2004. **119**(4): p. 517-28.
203. Schmidt, M.W., et al., *F-box-directed CRL complex assembly and regulation by the CSN and CAND1.* Mol Cell, 2009. **35**(5): p. 586-97.
204. Zhang, W., et al., *Genetic analysis of CAND1-CUL1 interactions in Arabidopsis supports a role for CAND1-mediated cycling of the SCFTIR1 complex.* Proc Natl Acad Sci U S A, 2008. **105**(24): p. 8470-5.
205. Luo, K., et al., *Adenovirus E4orf6 assembles with Cullin5-ElonginB-ElonginC E3 ubiquitin ligase through an HIV/SIV Vif-like BC-box to regulate p53.* FASEB J, 2007. **21**(8): p. 1742-50.
206. Sato, Y., et al., *Expression of Epstein-Barr virus BZLF1 immediate-early protein induces p53 degradation independent of MDM2, leading to repression of p53-mediated transcription.* Virology, 2009. **388**(1): p. 204-11.

207. Soucy, T.A., et al., *An inhibitor of NEDD8-activating enzyme as a new approach to treat cancer.* Nature, 2009. **458**(7239): p. 732-6.
208. Gastaldello, S., et al., *A deneddylase encoded by Epstein-Barr virus promotes viral DNA replication by regulating the activity of cullin-RING ligases.* Nat Cell Biol, 2010. **12**(4): p. 351-61.
209. Gastaldello, S., et al., *Herpes virus deneddylases interrupt the cullin-RING ligase neddylation cycle by inhibiting the binding of CAND1.* J Mol Cell Biol, 2012. **4**(4): p. 242-51.
210. Qu, Z., et al., *Tax deregulation of NF-kappaB2 p100 processing involves both beta-TrCP-dependent and -independent mechanisms.* J Biol Chem, 2004. **279**(43): p. 44563-72.
211. Chang, S.J., et al., *Poxvirus host range protein CP77 contains an F-box-like domain that is necessary to suppress NF-kappaB activation by tumor necrosis factor alpha but is independent of its host range function.* J Virol, 2009. **83**(9): p. 4140-52.
212. Garcin, D., et al., *All four Sendai Virus C proteins bind Stat1, but only the larger forms also induce its mono-ubiquitination and degradation.* Virology, 2002. **295**(2): p. 256-65.
213. Ulane, C.M. and C.M. Horvath, *Paramyxoviruses SV5 and HPIV2 assemble STAT protein ubiquitin ligase complexes from cellular components.* Virology, 2002. **304**(2): p. 160-6.
214. Lin, W., et al., *Hepatitis C virus expression suppresses interferon signaling by degrading STAT1.* Gastroenterology, 2005. **128**(4): p. 1034-41.
215. Precious, B., et al., *Simian virus 5 V protein acts as an adaptor, linking DDB1 to STAT2, to facilitate the ubiquitination of STAT1.* J Virol, 2005. **79**(21): p. 13434-41.
216. Liu, J., et al., *NEDD8 modification of CUL1 dissociates p120(CAND1), an inhibitor of CUL1-SKP1 binding and SCF ligases.* Mol Cell, 2002. **10**(6): p. 1511-8.
217. Cope, G.A. and R.J. Deshaies, *COP9 signalosome: a multifunctional regulator of SCF and other cullin-based ubiquitin ligases.* Cell, 2003. **114**(6): p. 663-71.
218. Pierce, N.W., et al., *Cand1 promotes assembly of new SCF complexes through dynamic exchange of F box proteins.* Cell, 2013. **153**(1): p. 206-15.
219. Lo, S.C. and M. Hannink, *CAND1-mediated substrate adaptor recycling is required for efficient repression of Nrf2 by Keap1.* Mol Cell Biol, 2006. **26**(4): p. 1235-44.
220. Bosu, D.R., et al., *C. elegans CAND-1 regulates cullin neddylation, cell proliferation and morphogenesis in specific tissues.* Dev Biol, 2010. **346**(1): p. 113-26.
221. Kim, S.H., et al., *Drosophila Cand1 regulates Cullin3-dependent E3 ligases by affecting the neddylation of Cullin3 and by controlling the stability of Cullin3 and adaptor protein.* Dev Biol, 2010. **346**(2): p. 247-57.
222. Feng, S., et al., *Arabidopsis CAND1, an unmodified CUL1-interacting protein, is involved in multiple developmental pathways controlled by ubiquitin/proteasome-mediated protein Degradation.* Plant Cell, 2004. **16**(7): p. 1870-82.

7. Appendix

7.1. Supplementary data MS analysis

Table 19: Overlapping protein hits from L2 full length TAP #1 and #2

Protein
complement component 1 Q subcomponent-binding protein, mitochondrial
DnaJ protein homolog 2
ruvB-like 1 [Homo sapiens]
Chain A, Human Mitochondrial Single-Stranded Dna Binding Protein
ruvB-like 2
tubulin beta-4B chain
elongation factor 1-alpha 1
importin 5 (Importin subunit beta-3)

7.2. Amino Acids

Table 20: Amino acid one letter code

A	**Alanine**	**M**	**Methionine**
C	**Cysteine**	**N**	**Asparagine**
D	**Aspartate**	**P**	**Proline**
E	**Glutamate**	**Q**	**Glutamine**
F	**Phenylalanine**	**R**	**Arginine**
G	**Glycine**	**S**	**Serine**
H	**Histidine**	**T**	**Threonine**
I	**Isoleucine**	**V**	**Valine**
K	**Lysine**	**W**	**Tryptophan**
L	**Leucine**	**Y**	**Tyrosine**

7.3. Table of figures

7.4. Abbreviations

A

aa	amino acid
AAV	Adeno-associated virus
Ad	Adenovirus
Akt	Protein kinase B
al.	alteres
APS	Ammonium persulfate

B

bp	base pairs
BPV	Bovine papillomavirus
BSA	Bovine serum albumin

C

^{o}C	Degree Celsius
CAND1	Cullin-associated and neddylation dissociated protein 1
CAPN2	Calpain 2
CBP	Calmodulin binding peptide
CDK	cyclin-dependent kinase
CIA	Chloroform isoamylalcohol
CIN	Cervical intraepithelial neoplasia
CIP	Calf intestinal alkaline phosphatase
CMV	Cytomegalovirus
Co-IP	Co-immunoprecipitation
CRL	Cullin-RING ligase
CSE1L	exportin-2 or chromosome segregation-1 (yeast homolog) like protein
C-terminus	Carboxyl-terminus
CV	coxsackievirus

D

DAPI	4´,6´-diamidino-2-phenylindol
DAXX	Death-associated protein
DMEM	Dulbecco´s modified Eagles medium
DMSO	Dimethyl sulfoxide
DNA	Deoxyribonucleic acid
dNTP	Deoxyribonucleotide triphosphate
ds	Double stranded
DTT	Dithiothreitol

E

E6	Human papillomavirus early protein 6

E7	Human papillomavirus early protein 7
EBV	Epstein-Barr virus
ECL	Enhanced luminescence
ECM	Extracellular matrix
E.coli	*Escherichia coli*
EDTA	Ethylen-di-amino-tetra-acetate
e.g.	Example given
	EGF Epidermal growth factor
ELISA	Enzyme-linked immunosorbent assay
ER	Endoplasmatic reticulum
EtOH	Ethanol

F

FCS	Fetal calf serum
fwd.	Forward

G

GAMPO	goat anti mouse peroxidase
GARPO	goat anti rabbit peroxidase
GF	Growth factor
GFR	Growth factor receptor
GLuc	Gaussia luciferase
GPCF	Genomic & Proteomics Core Facility

H

h	Hours
HCV	Hepatitis C virus
HEK	Human embryonic kidney cells
HeLa	Henrietta Lack´s cells
HEPES	4-(2-hydroxyethylen)-1-piperazineethanesulfonic acid
HIV	Human immunodeficiency virus
HPV	Human papillomavirus
HRP	Horseradish peroxidase
HSPG	Heparan sulfate proteoglycan
HSV	Herpes simplex virus

I

Ig	Immunglobulin
IgG	Immunglobulin G
IGF1	Insulin-like growth factor 1
IP	Immunoprecipitation
IRS4	Insulin receptor substrate 4

K

kb	Kilo base pair
kDa	Kilo Dalton
kV	Kilo Volt

L

l	Liter
L1	Human papillomavirus major capsid protein
L2	Human papillomavirus minor capsid protein
LB	Luria Broth

M

M	Molar
mA	milli Ampère
MeOH	Methanol
µg	Microgram
µl	Microliter
µM	Micromolar
µm	Micrometer
min	minutes
ml	Milliliter
mM	Millimolar
MOI	Multiplicity of infection
mRNA	Messenger RNA
MS	Mass-spectrometry
mTOR	mammalian target of rapamycin complex 1
MVM	Parvovirus minute virus of mice

N

NAc	Sodium acetate
NES	Nuclear export signal
NLS	Nuclear localization signal
nM	Nanomolar
NPC	Nuclear pore complex
NS2	MVM nonstructural protein
nt	Nucleotide
N-terminus	Amino-terminus

O

OD	Optical density
ORF	Open reading frame
Ori	Origin of replication

P

PAGE	Polyacrylamid gel electrophoresis
PBS	Phosphate buffered saline
PBS-T	Phosphate buffered saline-tween
PCR	Polymerase chain reaction
PFA	Paraformaldehyd

PI3K	Phosphatidylinositol-4,5-bisphosphate 3-kinase
P/S	Penicillin/Streptavidine
PsV	Pseudovirion
PV	Papillomavirus

R

Rb	Retinoblastoma protein
rev.	Reverse
RNA	Ribonucleic acid
rpm	Revolutions per minute
RT	Room temperature

S

SCF	Skp, cullin, F-box containing complex
SDS	Sodium dodecyl sulfate
sec	Second
siRNA	Short interference RNA
shRNA	Short hairpin RNA
snt	Supernatant
SPOP	Speckle-type POZ protein
SREF	Substrate receptor exchange factor
ss	Single stranded
SV40	Simian virus 40
SV40 LT	Simian virus 40 large T-antigen

T

TAE	Tris-acetate-EDTA buffer
TAP	Tandem affinity purification
TE	Tris-EDTA buffer
TEMED	N,N,N´,N´-tetra-methylethylendiamin
TEV	Tobacco etch virus
TGN	Trans-Golgi network
TGS	Tris-glycin-SDS buffer
Tris	Tris(hydroxymethyl)-aminomethan

U

U	International units for enzyme activity
UV	Ultra violet

V

Vif	HIV-1 virion infectivity factor
Vpr	HIV viral protein R
VLP	Virus-like particle
v/v	Volume per volume

W

w/v	Weight per volume

Y

YWHAZ	14-3-3 zeta